

Alma Mater Studiorum – Università di Bologna

**DOTTORATO DI RICERCA IN
INGEGNERIA CHIMICA DELL'AMBIENTE E DELLA
SICUREZZA**

Ciclo XXVIII

**Settore Concorsuale di afferenza: 09/D3 (Impianti e Processi Industriali
Chimici)**

Settore Scientifico disciplinare: ING-IND/25 (Impianti Chimici)

**OLIVE MILL WASTEWATER VALORISATION THROUGH
POLYPHENOL ADSORPTION**

Presentata da: AURORA ESTHER MOLINA BACCA

Coordinatore Dottorato

PROF. ING. SERENA BANDINI

Relatore

ING. DARIO FRASCARI

Correlatore

PROF. DOTT. DAVIDE PINELLI

Esame finale anno 2016

INDEX

ACKNOWLEDGMENTS.....	8
ABSTRACT.....	9
KEYWORDS.....	10
OBJECTIVES.....	11
PROJECT ACKNOWLEDGMENTS.....	12

CHAPTER 1

INTRODUCTION

1.1 World production of olive oil and European Union directives for the agro industrial wastes treatment.....	14
1.2 Olive oil production process.....	16
1.2.1 Extraction methods.....	16
1.2.2 Olive oil Subproducts, Applications and Recovery.....	20
1.3 Olive Mill Wastewaters.....	23
1.3.1 Olive Mill Wastewaters Characteristics.....	23
1.3.2 Olive Mill Wastewaters Environmental Impact.....	25
1.3.3 Olive Mill Wastewaters Recovery.....	26
1.4 Phenolic Compounds.....	28
1.4.1 Phenolic Compounds Characteristics, Properties and Applications.....	28
1.4.2 Phenolic Compounds in the Olive Mill Wastewaters and their Recovery.....	29
1.4.3 Tyrosol and Hydroxytyrosol.....	31

CHAPTER 2

THEORETICAL CONTENTS

2.1 Adsorption Process.....	33
2.1.1 Types of Adsorption.....	33
2.1.2 Types of Adsorbents.....	33
2.1.2.1 Ion exchange resins.....	34
2.1.2.2 Affinity ligands.....	34
2.1.2.3 Silica resins.....	34
2.1.2.4 Polymeric resins.....	34
2.1.2.5 Molecular Sieves.....	35
2.1.2.6 Cyclodextrin-based polymers.....	35
2.1.2.6.1 Cyclodextrin-based Polyurethanes (CDP).....	35
2.2 Mass Transport.....	36
2.3 Adsorption Kinetics and Equilibrium.....	40
2.3.1 Adsorption Kinetics.....	40
2.3.2 Adsorption Equilibrium.....	40
2.4 Adsorption Bed Design.....	44
2.5 Column Adsorption.....	46
2.5.1 Adsorption Breakthrough Curves.....	47
2.5.2 Mass Transfer Units (N) and Length of Unused Bed (LUB).....	49
2.6 Fixed Bed Column Packing.....	52

2.6.1 The Dynamic Axial Compression (DAC).....	52
2.6.2 The Flow Packing.....	52
2.6.3 The Pack-in-Place.....	53
2.6.4 Dry Packing.....	53
2.7 Fluid Dynamic Characterization.....	53

CHAPTER 3

MATERIALS AND METHODS

3.1 Olive Mill Wastewaters (OMW), resins, Cyclodextrin-based polyurethane (CDP) and chemicals.....	59
3.2 Cyclodextrin-based polyurethane Synthesis.....	62
3.3 Analytical methods.....	62
3.3.1 Total Phenols.....	62
3.3.2 Tyrosol (Ty) and Hydroxytyrosol (HTy) Quantification.....	63
3.3.3 Total Solids.....	63
3.3.4 COD.....	64
3.3.5 Total carbohydrates.....	64
3.3.6 Total lipids.....	64
3.3.7 Total proteins.....	64
3.3.8 Density and pH.....	68
3.3.9 Antioxidant Activity (ABTS Assay).....	64
3.3.10 Volatile Fat Acids (VFA) Content.....	65

3.4	<i>Adsorption Columns System</i>	66
3.4.1	<i>Adsorption Columns System for Phenolic Mixture Recovery</i>	66
3.4.2	<i>Adsorption Column System for Tyrosol and Hydroxytyrosol Recovery</i>	67
3.5	<i>Adsorption Kinetics</i>	69
3.5.1	<i>Adsorption Kinetics for Amberlite XAD 16</i>	69
3.5.2	<i>Adsorption Kinetics for CDP</i>	70
3.6	<i>Adsorption Isotherms</i>	70
3.6.1	<i>Adsorption Isotherms for Amberlite Resins (Phenolic Mixture)</i>	70
3.6.2	<i>Adsorption Isotherms for CDP (Tyrosol and Hydroxytyrosol)</i>	71
3.7	<i>OMW pre-treatment</i>	72
3.8	<i>Adsorption column packing</i>	72
3.8.1	<i>Adsorption Column packing Amberlite Resins</i>	72
3.8.2	<i>Adsorption Column Packing for CDP</i>	73
3.9	<i>Fluid dynamic tests</i>	74
3.9.1	<i>Fluid dynamic test Amberlite Resins Packed Bed</i>	74
3.9.2	<i>Fluid dynamic test CDP Packed Bed</i>	76
3.10	<i>Adsorption Process</i>	76
3.10.1	<i>Breakthrough tests and simulations for Amberlite Resins</i>	76
3.10.2	<i>Breakthrough test for CDP</i>	80
3.11	<i>Desorption-regeneration tests</i>	81
3.11.1	<i>Desorption-regeneration tests for Phenolic Mixture Recovery</i>	81
3.11.2	<i>Desorption-regeneration tests for Tyrosol and Hydroxytyrosol Recovery</i>	82
3.12	<i>Preliminary Economic Analysis for Phenolic Mixture Recovery with Amberlite XAD 16</i>	83

3.13 Amberlite IRA 958Cl and Amberlite IRA 67Cl resin Screening.....	83
----------------------------------------------------------------------	----

CHAPTER 4

RESULTS AND DISCUSSION: RECOVERY OF PHENOLIC MIXTURES

4.1 Ancillary results: PCs analytical method selection	85
4.2 Olive Mill Wastewaters (OMW) Characterization.....	87
4.3 Adsorption Kinetics for Amberlite XAD 16.....	88
4.4 Adsorption Isotherms for Amberlite XAD 16.....	90
4.4.1 OMW Imperia 2012.....	90
4.4.2 OMW Imperia 2013.....	91
4.5 Fluid Dynamic Characterization for Amberlite XAD 16.....	92
4.6 OMW pre-treatment.....	97
4.7 Phenolic compounds and COD Breakthrough tests for Amberlite XAD 16.....	97
4.8 Desorption step and Antioxidant Activity of the Obtained Product (Amberlite XAD 16).....	113
4.9 Preliminary Cost Evaluation for Amberlite XAD 16.....	116
4.10 Amberlite IRA 958Cl and Amberlite IRA 67Cl Screening.....	118
4.11 Adsorption Kinetics for Amberlite IRA 958Cl.....	123
4.12 Adsorption Isotherms for Amberlite IRA 958Cl.....	123
4.13 Fluid dynamic Characterization for Amberlite IRA 958Cl Bed.....	124
4.14 Phenolic compounds and COD Breakthrough tests for Amberlite IRA 958Cl	126

4.15 Desorption-regeneration tests and productivity for Amberlite IRA 958Cl.....	130
----------------------------------------------------------------------------------	-----

CHAPTER 5

RESULTS AND DISCUSSION: RECOVERY OF PURE POLYPHENOLS

5.1 Cyclodextrin based Polymers (CDP) for single phenolic compounds Recovery: Tyrosol (Ty) and Hydroxytyrosol (HTy).....	132
5.2 Adsorption Kinetics for CDP.....	132
5.3 Adsorption Isotherms for Tyrosol and Hydroxytyrosol with CDP.....	133
5.4 Fluid Dynamic Characterization of the CDP Bed.....	135
5.5 Tyrosol and Hydroxytyrosol Breakthrough tests for CDP.....	136
5.6 Desorption Solvent Selection: Batch tests.....	138
5.7 Desorption-regeneration tests for CDP.....	139

CHAPTER 6

CONCLUSIONS	142
--------------------------	-----

LIST OF SYMBOLS.....	145
----------------------	-----

INDEX OF TABLES.....	147
----------------------	-----

INDEX OF FIGURES.....	149
-----------------------	-----

BIBLIOGRAPHY.....	154
-------------------	-----

ACKNOWLEDGMENTS

The development of this work has been a very interesting experience from which I have learnt many different things, not only from the technical point of view, also from the personal one.

I want to thank to my parents and my sister, the best I have. Be far for so many time has not been easy, although this situation, they have given me all their love, help and support always.

Also I want to thank Cristian, my special partner. Thanks for all the shared moments, all the support, force, help and patience, and for all the love.

Thanks to all the persons at DICAM, for your friendship and your valuable help during this work.

Dario Frascari e Davide Pinelli, thank you very much for everything, for your advices and teachings, for trusting on my job, and for making easier for me my permanence in the Department.

I also want to thank to the FHNW Molecular Nanotechnology research group and their team leader for the important contributions to this work and for the nice job experience.

Finally, I want to thank to all the people that in one way or another have given support and help to this work.

ABSTRACT

Due to the negative environmental impact of the Olive Mill Wastewaters (OMW), research is done in order to treat and valorize them. In this work, different OMW from different Italian regions (Liguria and Puglia) and harvests (from 2012 to 2014) were tested in order to recover polyphenols (PCs), molecules with a high added value because of their beneficial properties. The solid phase used for PCs recovery was the resin Amberlite XAD16; the desorption solvent was acidified ethanol. An HPLC method for total PCs content quantification was developed using a C18 column.

A new, repeatable and reliable column packing method was developed. The packing quality was evaluated with step-change fluid dynamic analysis tests using NaCl 0.04M as tracer. Also, to avoid clogging problems in the packed columns an OMW pre-treatment was designed, capable to remove 98% of the solids.

Several breakthrough tests were performed to evaluate the influence of linear velocity and column length (0.52m and 2.0m). A repeatability test was performed in order to evaluate the stability of the process. The process was modeled using a plug flow with axial dispersion model with solid-liquid mass transfer; implemented in COMSOL3.5a.

The desorption curves were obtained with subsequent solvent regeneration. Antioxidant activity tests were performed with the desorption product using the ABTS method.

On the basis of economic considerations, two new ion-exchange resins were tested (IRA958Cl and IRA 67Cl). IRA958Cl showed the best performance. Two breakthrough tests at different linear velocities were conducted with this resin.

In order to recover specific high added value molecules (tyrosol and hydroxytyrosol) from the actual OMW, experiments were performed in collaboration with the Fachhochschule Nordwestschweiz (FHNW) using a Cyclodextrin-based polyurethane

polymer, synthesized by the FHNW research group. Then, in order to increase the purity of tyrosol in the desorption fractions several organic solvents were tested.

KEYWORDS: adsorption, olive mill wastewater, phenolic compounds, tyrosol, hydroxytyrosol, Amberlite resins, cyclodextrin-based polymers, mass-transfer, modeling.

OBJECTIVES

The first goal of this thesis was the development of a reliable and cost-effective process for the continuous-flow extraction of a phenolic mixture from olive mill wastewaters (OMW), characterized by the possibility of recycling both the adsorbing phase and the extraction solvent.

The second objective was the development of a reliable process for the continuous-flow extraction of specific high added value molecules (tyrosol and hydroxytyrosol) from olive mill wastewaters (OMW) using a Cyclodextrin-based Polyurethane (CDP).

PROJECT ACKNOWLEDGMENTS

This research was conducted in the framework of the UE FP7 research project “Integrating biotreated wastewater reuse and valorization with enhanced water use efficiency to support the Green Economy in EU and India” (Water4Crops). Project co-funding by the European Commission under Grant Agreement n. 311933 (Water4Crops project) is acknowledged.

CHAPTER 1

INTRODUCTION

1.1 World production of Olive Oil and European Union directives for the agro industrial wastes treatment

According to the International Olive Council (IOC) [1], the international organism for the responsible and sustainable development of the olives cultivation and their products elaboration, there are 47 countries in which the olive oil is produced, and 160 countries in which it is consumed. The 98% of the producers are located in the Mediterranean zone, and the 80% of them work with the three phases method for the oil elaboration [1].

In the European Union, in the last five years has been produced the 69.9% of the world olive oil, being the most important producers Spain, Greece and Italy (See table 1.1).

Country	Production (Tonnes per year 2014/2015)	% Production (2014/215)
World	2,988,500	100%
Spain	841,200	62.7%
Greece	300,000	19.0%
Italy	222,000	14.0%
Portugal	61,000	3.4%
Tunisia	340,000	6.2%
Turkey	170,000	5.7%
Morocco	120,000	5.6%
Syria	105,000	4.2%

Table 1.1 Olive Oil Production in the year 2014/2015 [1].

Italy is the country with the highest olive oil consumption, near the 40% for the year 2014/2015. The health properties of the olive oil have been known worldwide and the consumption is increasing, thus, also the cultivation areas.

The European Union is the most important producer and consumer, the quantity of olive oil produced is around 1,731,100 tonnes/year (2014/2015) [1], so, also the quantity of Olive Mill Wastewaters (OMW) associated (7-8 m³OMW/tonne of olive oil [2]). This is becoming an important problem in the Mediterranean Sea Basin, during the collection period (November to March) 10-12 x 10⁶ tonnes of OMW are produced [3], and a considerable part of this is discharged in the Mediterranean aquatic body. Because of these, there are some laws that regulates the OMW treatment. The OMW are included in the Urban Wastewater Treatment Directive 91/271/EEC, which concerns the collection, treatment and discharge of the wastes, in order to protect the environment from adverse effects from their inadequate discharge [4]. This directive is part of the Waste Framework Directive (2008/98/EC) in which the EU Member States were requested to reuse between 50%-70% of their household and general wastes by the 2020 [3, 5].

Each government of the olive oil producers has implemented national regulations for the OMW treatment, like Spain, where is not allowed to discharge the OMW in receiving waters, and some technical improvements are being considered in order to produce a lower volume of OMW during olive oil obtaining. In some other cases like Italy and Greece, there are not specific regulations, but all the EU Member States has to adopt a management and prevention plan for the wastes [5].

As it is evident, there are environmental pollution problems associated with the disposal of the OMW, because it is not possible to use them directly as irrigation waters because of their polyphenolic content (phytotoxicity), so, in this project has been proposed the polyphenols separation by an adsorption-desorption process, in a suitable cost-effective system which besides permit the wastewaters decontamination and valorization, lets the recycling of the adsorption solid phase and the desorption solvent.

1.2 Olive oil production process

For the olive oil production all the process phases are very important, from the olives harvest and storage to the bottling, influencing the final quality of the product. The oil, besides a great flavour, has to keep the healthy properties of the olive fruit [6-10].

The olive oil production is composed by five important steps: harvest, mill, shake, extraction and refinement.

1.2.1 Extraction Methods

The *harvest* is very important, the period and the kind of olive (taken from the tree or from the soil) affect directly the quality of the oil. Usually, the fruit harvest is done when the concentration of fat acids in the pomace and the fruit polyphenols content are in the maximum. This influences the sensorial characteristics of the final oil.

The harvest method has to be chosen in order to produce the minor possible damage to the fruit and to the tree, to avoid problems during the washing and storage of the olives and for the growing of new fruits (i.e. damaged branches).

After the harvest, the olives are screened to separate them from leaves, stones and dust, and then they are washed with cold water, to remove the remaining dust and herbicides. Later, they are stored. To produce an olive oil of very high quality the olives have to be processed in the 24 hours after their harvest, longer times lead to lower quality.

After this, the olives are subjected to the *mill*, where they are broken and a paste is formed [7,8].

Until the 60's the main mill method was the stone mill, but the productivity and the quality were low. Nowadays, the most used methodology is the hammermill, in this type of mill the olives are fed automatically, and the system includes a sieve, when the olive particles have the right size they pass if not they pass through the mill again [6].

Once the paste is ready, the *shake* process starts. The objective of this step is to take out the oil from the olive paste by using rotatory blades with a very slow movement inside semicylindrical containers, which are jacketed, so that water at 25°C-30°C can heat the olives paste facilitating the oil extraction, reducing its viscosity and helping the formation of the oil phase. Higher temperatures can damage the properties of the paste and the obtained oil.

From the paste, drops of oil come out forming bigger drops by aggregation. If later the extraction is done with the press system, the shake process takes maximum 20 minutes, otherwise, the process is a longer. The shaking time is important, because if it is very long the oil is going to be in contact with the wastewaters for more time, changing the oil characteristics, its phenolic content and in its stability, thus, lowering its quality.

The next step is the *extraction*, where the oil is separated from the other olive components, water, seeds, husk, etc.

Until the decade of 60's the most used method was the press system . With this methodology, the product of the shaker is wrapped in woven baskets and pressed, the liquid phase passes while the solids are retained in the baskets. All the liquid is collected and decanted in order to separate the suspended solids that contaminate the oil. This is discontinuous process, so nowadays is not very applied [6,7].

The need of a continuous cycle production, led to some technological research, thus, the two and three phases systems were adopted, enhancing the weaknesses of the previous press process, also reducing the workforce and the economical expenses. Also, this kind of process helps to minimize the time that the olives have to be stored, improving the quality of the oil obtained.

In the two and three phases systems, the oil is extracted with the centrifugal force of the rotatory machines of high speed, known as *decanters*. The two phases technology has two outlet sites, one for the oil-rich one and the other for the solid waste, but it is very hard to separate the emulsion made of oil and olive mill waste water, and also the solid waste is very hard to handle, it is composed by 75% of

water, to dehydrate it, temperatures about 1200°C are required. For this reason, the three phases system is proposed, so the decanters has three outlets, thus, the oil, the water and the solid part are separated. The disadvantage of this process is the addition of water, so the volume of produced olive mill waste water is high, leading to environmental problems because of its discharge.

A scheme of the olive oil production with the two and three phases system is presented in figure 1.1.

In the continuous processes the olive paste coming from the shaker is fed continuously to the decanter and the wastes come out also in a continuous way.

The solid part that is still rich in oil passes again (3 times maximum) through the decanters. The oil coming from the first extraction is the most valuable and is known as virgin olive oil, while the product of the later centrifugations has different qualities, lower respect to the virgin oil.

The last step is the *refinement* [9]. This part is done only if the oil is not adequate for consumption because of its organoleptic characteristics or its acidity. If this process is applied to a virgin oil, it loses its virginity because of the loss of antioxidants and vitamins, and for this, it is usually rectified by the addition of virgin oil of good quality (this part is done also with refined non-virgin oil).

The refinement process can be applied in its totality or just partially, depending on how defective and the kind of defects of the oil that has to be refined.

The refinement process is composed by the following stages: wintering, mucilage separation, neutralization and deodorizing.

The *wintering* consists in the cooling of the oil, in order to avoid the glycerides of high fusion point and all the components that solidify with cold. Then the not wanted solid substances are filtered. In the past this step was done leaving the containers with the oil to cool with the cold air of the environment, nowadays, this is done by cooling the containers until 5°C rapidly, and keeping this temperature for 24 hours.

The *mucilage separation* is done by adding water and phosphoric acid, in this way the rubbery compounds are eliminated, but also some desirable proteins of the oil.

The *discoloration* or *whitening* is done using active carbon or bentonite. In this way the oil colour is adjusted.

The *neutralization* needs the treatment with alkalis. The esters obtained, are easily removed because of their insolubility on the oil.

The *deodorizing* is done with water at 160°C-180°C and high vacuum, eliminating aldehydes. This process is not done where the oil is produced but in specialized refineries.

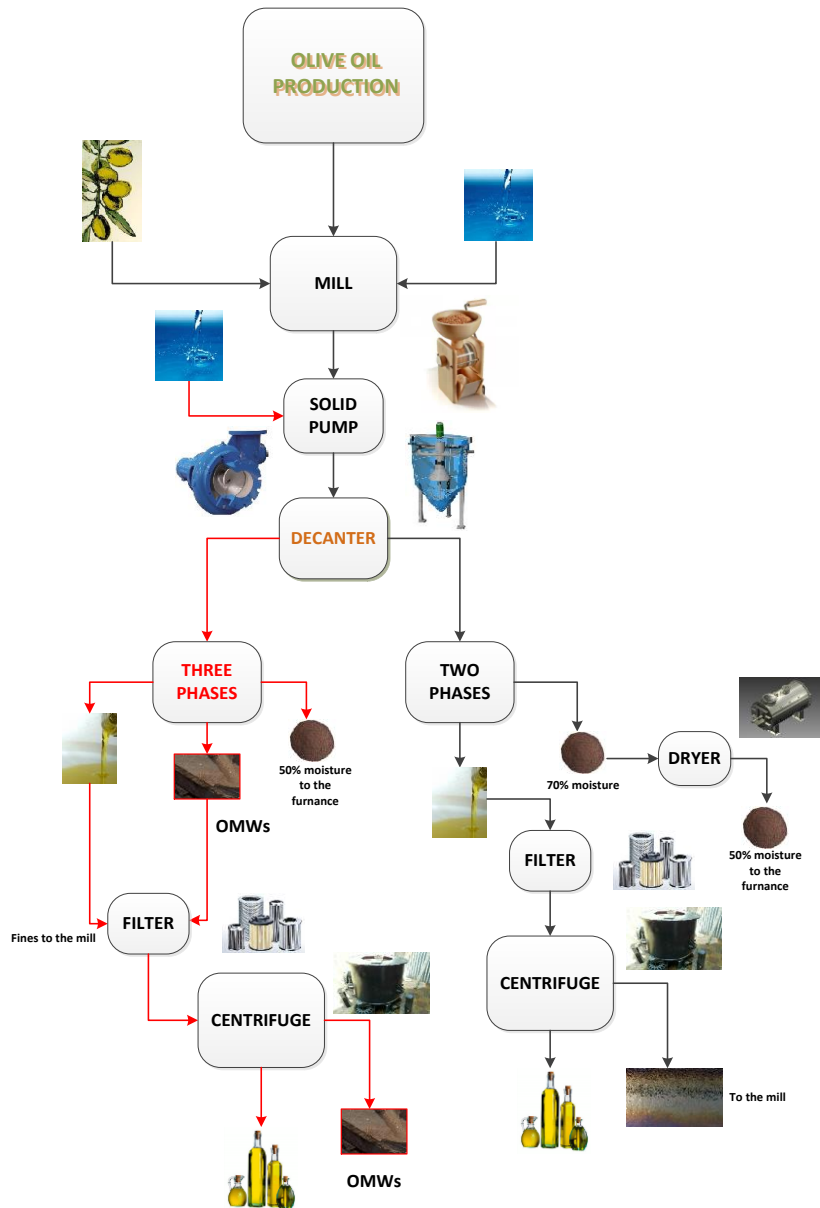


Figure 1.1 Olive oil production with the two and three phases systems based on [6].

1.2.2 Olive Oil Subproducts, Applications and Recovery

All the steps of the olive oil production lead to different wastes and/or subproducts. Nowadays, with the higher interest in the environmental care, almost all the wastes are reutilized.

The residue of leaves and fine branches, produced after olives cleaning and before their processing. This type of waste is mainly used to feed animals, and recently, also to produce compost with other organic residues. In other cases, although the high moisture content of this waste, it is used for energy generation from biomass [10].

An important residue from the olive oil production is the *marc*. Once the oil has been extracted from the olives, the paste formed by the pomace and the seeds is a waste. The marc is used to extract marc oil, the rest is used for energy production after drying, and for composting. It can be used also to feed pigs and poultry, by milling it, in order that the seeds do not hurt the animals, and mixing it with other milled cereals [10].

If the marc is used to obtain oil, after the extraction and drying there is a waste composed by 15%-30% of pomace, 30%-40% of seed and 30%-50% of other pomace solids. Its moisture is around 10% and it has a high combustible value, because of its high calorific power (4100 kcal/kg dry base [10]), thus, it is usually used to dry the marc before its oil extraction, or to generate energy for other part of the plant [10,11] .

Another waste from the olive oil production is the *alperujo*, it is obtained only with the two phases extraction system. It is composed by different olive parts and residual oil, it has a solid (marc) and a liquid part (olive mill wastewaters). It is difficult to handle, it has been proposed to use it to feed won, but it is necessary to know the food shortages of the feeding the food that the alperujo can help to complete. Some studies have been done in order to valorise this subproduct. One solution is to use it as fertilizer. The direct use of *alperujo* in the soil can affect negatively seed germination, microbial activity and the plat growing, because of its organic matter, phenolic and fat acids content, although, it is rich in minerals like potassium that can help the soil, it is has also organic nitrogen, but it is poor in phosphorous and micronutrients, so, it is suitable for composting.

Fernández-Hernández et al (2014) [12], have studied the effects of a compost made with sheep or horse manure or olive pruning (used as nitrogen source or bulking agent) mixed with alperujo. The application of this fertilizer was evaluated in terms of soil characteristics, plant growing, fruit content and oil quality. This study showed that the soil had a significant increase of available nitrogen, phosphorous, potassium and organic matter content, after the compost use. Also the fruit had 15% more of oil than fruit obtained from a tree treated with inorganic fertilization. The quality of the oil was the same in both cases (compost and inorganic fertilizer).

It has been suggested that can be used for mannitol obtaining, also to produce polysaccharides like xanthan and pullulan (food additives), for bioplastics, with the polyhydroxybutyrates (PHB) by microbial treatment, for pectin obtaining, colorants and antioxidants (for its phenolic content) [10].

Other proposal for alperujo valorisation is the biodiesel production. According to Hernández et al (2014) [13], the alperujo has around 4% of oil, this oil can be converted in biodiesel (94.7%, crops and products) and glycerine (5.3%. crops and products), by transesterification in presence of basic catalyst. The biodiesel obtained fulfil the ASTM specifications, so this approach is promising for alperujo valorisation. Also Lama-Muñoz et al (2014) [14] use the alperujo oil for biodiesel obtaining, with a yield production very similar to that obtained for Hernández et al (2014). Lama-Muñoz et al (2014) [14] applied a two-step process, an acidic esterification to remove free fatty acids from the oil and a basic transesterification for the biodiesel and glycerol obtaining.

Another use of alperujo is the pectin production. Rubio-Senent et al (2015) [15] obtained different pectins from alperujo treated with water steam (160°C), they found that the properties of the produced pectins are similar to that of the apple pectin, so they could be use as emulsifiers in the food industry. The biological properties of the studied pectins are similar to the citrus pectin, so they could have biomedical applications, for example, to reduce serum cholesterol levels and the risk of bowel cancer, and the cancer metastasis. The obtained pectins have a low molecular weight, so they can be easily absorbed by the intestinal track.

The *olive seeds or stones* are other residue. It is usually used for thermic energy obtaining because of its low moisture content (around 13%) and high calorific power (4400 kcal/kg dry base [10]). Some olive oil plants use it to generate the heat for the shake step or to dry the marc. Another usage is in the cosmetic field, where some exfoliant products use them to remove dead cell from the skin [10].

Finally, if the oil is extracted with the three phases system, one of the wastes are the olive mill wastewaters (OMW). It represents an important environmental issue because of its bad smell, low biodegradability, high organic, fatty acids and phenolic contents. It is composed by the olive water, the water added during the extraction process and of the olives cleaning, and it also has a certain quantity of solids. An important research job is being done to valorise this residue and to minimize its environmental impact, as it is going to be explained in the next section.

1.3 Olive Mill Wastewaters (OMW)

The olive mill wastewaters are one of the largest produced residues of the olive oil extraction. It has become an important environmental problem because of its physic-chemical characteristics that make of it a very dangerous contaminant for aquatic bodies and for agriculture.

1.3.1 Olive Mill Wastewaters Characteristics

The OMW are red-to black colored liquid, with high conductivity and mildly acidity. The OMW properties vary with the type of olive, the growing practices, the weather conditions, the olives storage time and the olive oil extraction process.

Their main component is water (83%-92% [16]), followed by a high concentration of phenolic compounds (mainly phenolic acids, secoiridoids and flavonoids), sugars and different organic acids. They also contain a high quantity of potassium and some calcium and sodium, so the OMW could have potential as fertilizers.

The main characteristics of the OMW according to Dermeche et al (2013) [16] are listed in table 1.2.

Property	Value
Dry Matter	6.33 – 7.19
Ash (%)	1
pH	2.24 – 5.9
Electrical Conductivity (dS/m)	5.5 – 10
Total Carbon (%)	2 – 3.3
Organic Matter (%)	57.2 – 62.1
Total organic Carbon (g/L)	20.19 – 39.8
Total Suspended Solids (g/L)	25 – 30
Mineral Suspended Solids (g/L)	1.5 – 1.9
Volatile Suspended Solids (g/L)	13.5 – 22.9
Volatile Solids (g/L)	41.9
Mineral Solids (g/L)	6.7
Volatile Acidity (g/L)	0.64
Inorganic Carbon (g/L)	0.2
Total Nitrogen (%)	0.63
P (%)	0.19
Na (%)	0.15
Ca (%)	0.42 – 1.15
Mg (%)	0.11 – 0.18
Fe (%)	0.26 ± 0.03
Cu (%)	0.0021
Mn (%)	0.0015
Zn (%)	0.0057
Lipids (%)	0.03 – 4.25
Total Phenols (%)	0.63 – 5.45
Total Sugars (%)	1.5 – 12.22
Chemical Oxygen Demand (g/L)	30 – 320

Table 1.2 Chemical Characteristics of the Olive Mill Wastewaters [16].

1.3.2 Olive Mill Wastewaters Environmental Impact

As it has been said before, the OMW are a very important environmental concern, their discharge without treatment can led to several problems, they can contaminate much more than urban wastewaters [10].

The OMW have a high organic load, low pH, high COD and BOD which make them very toxic for aquatic life. Also their high phenolic content, the bad smell and the dark colour can damage not only the natural aquatic bodies, they can also change soil quality and its microbial activity, and properties and can be phytotoxic for plant growing and seed germination.

Talking about soil pollution, it is important to say that the use of OMW as irrigation water is not possible, some compounds which come from the oil that can increase the soil hydrophobicity, decreasing water retention and infiltration rates.

Some experiments have been done to evaluate the effect of direct irrigation with non-treated OMW and the results in e long term are negative, however, the OMW have also fertilization potential, so a pre-treatment or a rigid control in the volumes used for irrigation [16].

Considering the disposal of the OMW into aquatic bodies, the can change the ecosystem balance because of the reduction of the available oxygen. Also, the high concentration of reduced sugars stimulates microbial respiration, so the level of dissolved oxygen reduces. Euthopication can appear as result of phosphorous or other OMW mineral addition, motivating plant growing and decreasing other aquatic species development, which can induce an important change in the aquatic ecosystem affected. Also, it has been demonstrated in some marine studies [16], that the OMW discharge in natural water bodies deteriorate the aquatic community,

as it has been said, which besides the other mentioned problems, can reduce or change the self-purification mechanisms of the rivers, lakes, etc.

In the surface water the OMW dark colour can lead to not sunlight reception for the vegetal water species, also the OMW lipids can block also block the oxygen exchange, damaging the ecosystem. Their use as irrigation waters can also lead to a high groundwater pollution.

The OMW are also disposed in big containers for evaporation, this practice is not very good from the engineering point of view, because of the low stability and safety of the liquid accommodation. The OMW overflow is possible, contributing to the pollution of agricultural soil, r surface waters. Also, the OMW led to evaporation or discharged into surface waters lead to their fermentation, which produces methane, hydrogen sulphide and other pungent gases. This, can have a negative effect on the normal and touristic lives of the zones near to the OMW production or disposal.

1.3.3 Olive Mill Wastewaters Recovery

Due to the important environmental concern that the olive mill wastewaters are, and because of their content of molecules of pharmaceutical interest, during the last 20 years different detoxification, valorisation and recovery techniques have been studied and developed for their treatment [17].

The most applied treatments include decolouration, solid filtration, COD reduction and recovery of phenolic compounds and other high added value molecules.

Nogueira et al (2014) [18] have applied a photocatalytic oxidation followed by the biological biodegradation of funghi *Pleurotussajorcaju* and *Phanerochaetechrysosporium*. According to their results an important reduction in colour, ecotoxicity, COD and total phenols content was achieved.

Another treatment for the OMW has been proposed by Gebreyohannes et al (2015) [19] with the forward osmosis. With this process the OMW are de-hydrate, the volume reduction achieved was of 71% with a complete decolouration and a 98% rejection of the phenols and ions. From the concentrate obtained in the membranes

were fractionated and recovered some phenolic compounds. From the phenolic concentrate it is also possible to obtain syngas for the production of methane, synthetic fuel and ammonia [19].

The OMW can be also used for hydrogen production. Casanovas et al (2014) [20] have used a steam reforming process of distilled OMW for the H₂ obtaining. The catalytic honeycombs functionalized with lanthanum-stabilized ceria with Pt and Rh produces 40 STP mL of pure hydrogen per mL of distilled OMW, and after the reaction, also an important reduction in the COD load (90%-96%) was observed. Also, Tosti et al (2015) [21] studied this application. They also work with distilled OMW and a catalytic process with a Pt-Ag membrane. They were able to achieve the production of hydrogen-rich mixture with a poor coke and methane formation. The hydrogen production is a new and very interesting approach for OMW re-utilization.

Another interesting work was conducted by Masi et al (2015) [22]. The OMW were evaporated leading to the obtaining of a concentrate rich in phenolic compounds and a condensate with just 2.4 gL⁻¹ of COD (98.7% of removal after evaporation), which made it easily degradable biologically. The treated condensate had a pH near to neutrality without alkalinity dosing. The total removal of COD after complete processing was 99.8%.

Scoma et al (2015) [23] used electro dialysis for the separation-concentration of volatile fat acids (VFA) from OMW, for the production of polyhydroxyalkanoates. It was possible to remove between 30%-35% of the VFA present originally in the OMW studied.

Martinez-Gonzalez et al (2015) [24] used dephenolized -fermented OMW for the polyhydroxyalkanoates (PHAs) obtaining using *Cupriavidus necator* pure culture as biocatalyst. The accumulation of PHAs achieved is the range of 46%-55%, depending on single or double sequential processing.

The OMW also can be used for feed supplementation in animals food. Gerasopoulos et al (2015) [25] have studied the OMW effect in the broiler chickens

plasma and tissues antioxidant activity, which showed to be higher than the activity observed into the control (non-treated group).

Different approaches are studied in order to valorise and recover the OMW, to avoid or at least to reduce their environmental impact.

1.4 Phenolic Compounds

The olives are fruits rich in antioxidants like phenolic compounds, that can be found in the oil after extraction, and in all extraction by-products, including the olive mill wastewaters, distributed in different proportions according to their polarity.

1.4.1 Phenolic Compounds Characteristics, Properties and Applications

They are molecules characterized by the presence of one or more phenol groups, they are biosynthesized as secondary metabolites in plants. They are found in fruits, vegetables, berries, peanuts, cocoa, wine, beer and olive oil. The plants produce them in response to environmental pressure, like pathogen and insect attack, UV radiation and wounding [26].

As general classification they are separated in simple (hydrolysable tannins) and complex phenols (condensed tannins or flavonoids, and lignins). Also, they can be divided according to the type and number of phenolic subcomponents. i.e. hydroquinones and catechins [26].

Industrially they are used in the leather tannery (tannic acid) and nowadays in the cosmetics and pharmaceutical fields, because of their chelating, antiaging, antioxidant, anticarcinogenic, antibacterial and thermogenic properties. They also help in the reduction of cardiovascular disease risk. Some phenols are also used as pesticides, acaricides and insecticides. They can also be used in the food industry as additives, especially for the wine flavor, and some are sold as dietary supplements [26].

1.4.2 Phenolic Compounds in the Olive Mill Wastewaters and their Recovery

Talking about the polyphenolic compounds, it is important to say that due to their amphiphilic nature, i.e. their polarity, they distribute between the olive oil and its extraction by-products [16, 27]. Most of the phenolics contained in the olives products have showed to be more soluble in the aqueous phase than in the oily one, which explains, why the polyphenols content in the olive oil is less than 5% while in the wastewaters is about 50% (depending on the olive type and the extraction system) [27].

Because of the high polyphenolic content of the Oil Mill Wastewaters (OMW), between 100 mgL⁻¹ and 17500 mgL⁻¹ [16, 28-30], they are associated with a negative environmental impact, since the direct discharge, in soil, of the untreated waters inhibits seed germination and plant growing, changes the physicochemical soil properties and its normal microbial activity [16]. Their disposal in aqueous bodies, can cause eutrophication, which can be translated into a plant growing decay, the development of new species in the ecosystem and the reduction in the population of other vegetable and animal species. Also, the phenols that give the dark OMW color, can contaminate water, becoming it darker, that, together to the OMW lipids, which for a layer in the water surface, the natural exchange of oxygen and sun light could be changed, leading to all the negative effects mentioned above. Also their bad odor is a fact to consider [16].

As it was said before, the phenolic compounds have important health properties, being very interesting the antioxidant activity presented by oleuropein, tyrosol and hydroxytyrosol. The last one of these phenols, has showed one of the highest antioxidant, antibacterial anti-inflammatory and antiangiogenic activities, for name just some of its valuable health properties [31-34], which make of it one of the most expensive phenolic compounds, besides to oleuropein and tyrosol. However its high market price, its powerful antioxidant activity, makes that hydroxytyrosol, have an important demand in the pharmaceutical, food and cosmetics fields [32]. Nowadays, there are some chemical and biotechnical ways developed for its production, being

all of them expensive because of the high price of some of the narrow matters [33]. The hydroxytyrosol recovery from OMW is a much more economical manner to produce it [33], because it is the most abundant polyphenol in the olive mill wastewaters [16, 28, 32].

Because of the OMW phenols content, that in a way or another, has to be extracted, different authors have propose diverse recovery methodologies. The most know method is the liquid-liquid extraction, using ethyl acetate as solvent [16], because of its high efficiency. Also, some optimization studies have been done with ethanol at pH2 [16]. Because of the solvent toxicity and flammability, this type of procedure is being replaced by the use of supercritical fluids, as CO₂ [16]. However, for the OMW, in some cases, the polyphenols recovery yield continues to be better with the traditional liquid-liquid extraction separation [16].

Otherwise, the membrane technology offers some alternatives by ultrafiltration processes [35]. Nowadays, optimization procedures are being developed, in order to reduce the membranes fouling, an important problem in the OMWs treatment, because of their high content of suspended solids [35]. However, a filtration process (filtration, ultrafiltration, microfiltration, etc.) is recommended as a pretreatment step for the OMW dephenolization [35].

Other recent initiative, is the Cloud Point Extraction technique (CPE), initially investigated by Gortzi et al 2010 [36], for the polyphenols recovery from wine sludge, using Genapol X-080 and PEG-8000 as surfactants, achieving very good results (75.8% and 95.8% of recovery, respectively). With this technique, an aqueous solution of a non-ionic surfactant is carried to a higher temperature of which it stars to form micelles, so higher than its cloud point temperature, so the formed micelles aggregate, and a two phases separation occurs, obtaining a surfactant-rich phase or coacervate, and a diluted phase. The solute present in the initial aqueous solution, is then, distributed between both phases, so there is an extraction.

There is another way to recover phenolic compounds from OMW, the solid-liquid extraction. This, is an excellent manner to treat OMW, because it suitable to handle the large wastewaters production volumes [37], besides, it is easily adaptable to industrial production lines, with a semi-continuous operation [38].

In the present work has been proposed the OMW polyphenols by an adsorption-desorption process, in a suitable cost-effective system which permits the wastewaters decontamination and valorization, and the recycling of the adsorption solid phase and the desorption solvent, in order to develop a more environmentally friendly process.

1.4.3 Tyrosol and Hydroxytyrosol

Tyrosol is a phenolic substance present in different organic sources. It is one of the most concentrated phenols in the olive oil, in the argan oil and in the white wine. Tyrosol is known for its antioxidant capacity. Recently, its cardio-protection properties were discovered and have been studied [39].

Hydroxytyrosol is a phenolic phytochemical compound. After gallic acid hydroxytyrosol is the phenol with the highest antioxidant capacity. It is known for its antiinflammatory and antiviral properties, it also helps in the reduction of the risk of heart diseases and of some cancer types (skin and colon). One of the most important source is the olive tree, where it is a immunostimulator and antibiotic , it is present mainly in the leaves, also in the extra virgin olive oil [40].

As it was said before, pure tyrosol and hydroxytyrosol are usually produced by biological and or enzymatic pathways using different bacterial and fungal species [41], but this procedures require expensive reagents for the growth media.

Knowing that olive oil, and so its by-products, the olive mill wastewaters are considered an important source of valuable phenolics, for this reason, research is done for selective recovery of antioxidants like gallic acid, tyrosol and

hydroxytyrosol. Some studies have been done by Sannino et al (2012) [42], they have proposed a small- scale process for pure hydroxytyrosol obtaining from olive mill wastewaters using a soxhlet continuous liquid-liquid extraction followed by two chromatographic stages consistent with the silica gel middle pressure and percolation on C-18 phase chromatography.

Also the used of molecular imprinted polymers has been evaluated for the selective extraction of high added value phenols from olive mill wastewaters [31, 43, 44].

New approaches are studied, one of this is the cyclodextrin-based polymers for selective solid-liquid extraction of tyrosol and hydroxytyrosol from the olive mill wastewaters. This technology is going to be tested and discussed in the present work.

CHAPTER 2

THEORETICAL CONTENTS

2.1 Adsorption Process

The adsorption is a separation process based on the capacity of some types of solids to retain selectively target molecules (sorbate) on their surfaces. The affinity between the solid and the sorbate is a key parameter to develop an appropriate adsorption process. The sorbate transport from the liquid phase to the surface of solid phase and from there to binding sites, has also to be studied deeply to properly take advantage of this separation operation.

2.1.1 Types of Adsorption

There are two kinds of adsorption phenomena, the first one is the *physisorption*, or *Van der Waals sorption* which is completely reversible, it is due to intermolecular attractive forces between the molecules of the sorbate and the solid phase [45]. The second one is *chemisorption* or *activated adsorption*, in which there are chemical bonds formation between the sorbed substance and the stationary phase. In general, in the desorption the adsorbed substance is recovered but with some chemical changes, for this reason, this type of adsorption is so important in heterogeneous catalysis. It is also possible that both phenomenon be present simultaneously in the same adsorption process [45].

2.1.2 Types of Adsorbents

The adsorbents are granular solids from different particles sizes and with a big surface area. They have to be chemically inert with the fluid which they are in contact with. It is essential that the particles do not reduce their size during the adsorption process, and they have to offer a low pressure drop in the packed bed. It is imperative to understand the adsorption capacity of the sorbent according to the nature of the substance we want to separate.

2.1.2.1 Ion exchange resins

They are used in the chemisorption. Their operating principle is the chemical substitution reaction between two electrolytes, one in the solution of the mobile phase and the other in the solid one.

In the other hand, in the physical adsorption there are two main kinds of interaction: affinity ligands and hydrophobicity [46].

2.1.2.2 Affinity ligands

The affinity ligands are biochemical molecules chemically attached to an inert solid. According, to their molecular weight and their selectivity, there are two important kinds of ligands, the *specific* and the *general* ones.

As it is expected, the specific ligands have a very big selectivity, they attach just one composite, but they are of difficult obtaining, and are usually used for repetitive separations of the same compound.

The general ligands link a group of biochemical substances, so we can separate a group of compounds from a solution, and in some cases we are able to do a separation between the group compounds.

2.1.2.3 Silica resins

There are of two types, coated and not coated ones. The last ones can act really well in water and in organic solvents, so they are widely used for the separation of hydrophilic substances. The covered ones are coated with long-chain alkanes, becoming suitable for hydrophobic compounds adsorption.

2.1.2.4 Polymeric resins

They have two important characteristics, their high stability and their low cost. In general, they are bigger than silica resins, and are suitable for process behind 4 bar of pressure. There are two types of polymeric resins, natural and synthetic. The

natural resins (dextran and agarose) are very hydrophilic and are suitable for separate proteins and biomaterials [46].

Then, for the synthetic polymers, there are two widely used in the industry, polyacrylamide and styrene divinylbenzene. The first ones are found as hydrogel, and are mainly used in the size exclusion chromatography [46]. The styrene divinylbenzene polymers are widely used for the adsorption of non-polar substances from aqueous solutions.

2.1.2.5 Molecular Sieves

They are synthetic zeolites crystals. The sorbate is trapped in the crystal cells, according to the cell diameter, but the sieves can separate substances not only by size exclusion also by adsorption having into account the polarity of the sorbate molecule and the sieve insaturation. They are mainly used for dehydration processes and for gas hydrocarbons separation. They regenerate with the elution solvent but also by heating [46].

2.1.2.6 Cyclodextrin-based polymers

The cyclodextrins are cyclic oligosaccharides composed by α -1,4-coupled D-glucose units. They are characterized by a high solubility in water, even if they have an apolar internal cavity.

They can form inclusion or «Host-Guest» complexes with hydrophobic molecules. One of their most important characteristics is that there is not covalent bonds formation with the «Guest» molecule, so there is not chemical modification of it. They are widely used for drug delivery purposes [84].

2.1.2.6.1 Cyclodextrin-based Polyurethanes (CDP)

Because of cyclodextrin high solubility in water, it was necessary to support them in a polymeric matrix, for this task polyurethanes have been chosen.

Polyurethanes are polymeric materials obtained by the reaction of a diisocyanate and a poly-ol. According to the reactants couple selected, the polyurethane

produced has different properties. In this case, in order to enhance the CDP selectivity for Tyrosol and Hydroxytyrosol, different diisocyanates and poly-oles were tested, until the best combination was found: 4,4'-methylene diphenyl diisocyanate and β -cyclodextrin [85].

2.2 Mass Transport

The adsorption is a separation operation, and as in all separation processes the mass transport is very important. The sorbate transport from the liquid to the solid phase occurs through a stagnant mass transfer layer at the surface of the solid particle and the adsorbate diffuse through pores to an active site [46] So, there are different transport mechanisms that are involved. The first one is the transport by *diffusion*, in which the solute moves from the point of greater concentration to the point of less concentration, so the solute transport is due to concentration gradients, the *diffusion* will occur until the concentration gradient exists, even if there is not fluid movement. This transport mechanism is described by *Fick's first law*, which says that the mass of fluid that is diffusing is proportional to the concentration gradient [47].

$$F = -D_{iff} \left(\frac{dC}{dx} \right) \quad (2.1)$$

Here,

F is the solute mass flux per unit area per unit time

D_{iff} is the diffusion coefficient

C is the solute concentration

dC/dx is the concentration gradient

When there is a solute carried by a moving flow, there is the solute transport by *convection*. The quantity of transported solute depends on its concentration and on the amount of fluid that is moving [47].

If we talk about the *convective transport* in a porous media, for a normal flow to a unit cross-sectional area, the amount of flow moving is equal to the *average liquid linear velocity* (v_i) multiplied by the *effective porosity* of the media (ϵ) [47].

The *average liquid linear velocity* is the rate at which the flux of fluid across the unit cross-sectional area of pore space passes [47], and the *effective porosity* is the porosity in which the fluid can flow, excluding non-interconnected and dead-end pores [47].

$$F_x = v_x \epsilon C \quad (2.2)$$

$$\rightarrow \frac{\partial C}{\partial t} = -v_x \frac{\partial C}{\partial x} \quad (2.3)$$

Equation 3 is the expression for the *convective transport* in one dimension [47]. The solution of this equation leads to a sharp concentration front, in which the advancing side has the concentration of the invading fluid, while in the other side the concentration is the background value, and it does not change. This situation is called *plug flow*, and in it all the pore fluid is replaced by the invading solute front [47].

The solute in a porous media flows at velocities higher and lower than the *average linear velocity*, this is due to:

1. When the fluid is moving through the pores, it moves faster in the center than in the edges of the pores.
2. To do the same linear distance, a portion of the fluid can take longer paths than other fluid portion.
3. Pores are not equal between them, so the longer ones let the fluid flows faster.

Thank to this different velocities, mixing is occurring along the flowpath, so that there is a solute dilution in the advancing flow edge. This mixing is known as *mechanical dispersion*. If it occurs in the direction of the flowpath, it called *longitudinal dispersion* and if it occurs in a direction normal to the flowpath then it is named *transversal dispersion* [47].

Assuming that dispersion can be described with the *Fick's first law* and that the quantity of *mechanical dispersion* is a function of the *liquid linear average velocity* there is possible to talk about the coefficient of mechanical dispersion, that is equal to the multiplication of the *dispersivity* (α), which is a property of the medium, and the *liquid linear average velocity*.

$$\mathbf{Longitudinal\ mech.\ dispersion\ coeff. = \alpha_L v_L \quad (2.4)}$$

$$\mathbf{Transversal\ mech.\ dispersion\ coeff. = \alpha_T v_T \quad (2.5)}$$

The *diffusion* cannot be separated from the *mechanical dispersion* for the flow in a porous media, so combining them it is possible to define a parameter called *hydrodynamic dispersion coefficient* (D), which can be calculated, for parallel and normal direction of flow, as:

$$\mathbf{D_L = \alpha_L v_L + D_{iff} \quad (2.6)}$$

$$\mathbf{D_T = \alpha_T v_T + D_{iff} \quad (2.7)}$$

With these parameters defined it is possible to write the *Convection-Dispersion Equation* for solute transport (Fetter 2.) This expression is based on a mass balance in a small representative volume of the porous media. Some assumptions have been done [47]:

1. The porous medium is homogeneous, isotropic and it is saturated with the fluid.
2. The flow conditions let the application of Darcy's law.

The equation for the *convective transport* is:

$$\mathbf{Convective\ transport = v_i \epsilon C \, dA \quad (2.8)}$$

While for the *dispersive transport* we have:

$$\mathbf{Dispersive\ transport = \epsilon D_i \frac{\partial C}{\partial i} \, dA \quad (2.9)}$$

Where dA is the cross-sectional area and the subscript i is the direction which is normal to the cross-sectional area.

So the mass flux per unit cross-sectional area per unit time is:

$$F_i = v_i \varepsilon C - \varepsilon D_i \frac{\partial C}{\partial i} \quad (2.10)$$

So, the mass of sorbate entering to the representative elementary volume is:

$$F_x dz dy + F_y dx dz + F_z dx dy \quad (2.11)$$

The sorbate mass coming out from the representative elementary volume is:

$$\left(F_x + \frac{\delta F_x}{\delta x} dx\right) dy dz + \left(F_y + \frac{\delta F_y}{\delta y} dy\right) dx dz + \left(F_z + \frac{\delta F_z}{\delta z} dz\right) dx dy \quad (2.12)$$

The mass change rate inside the representative elementary volume is:

$$\varepsilon \frac{\partial C}{\partial t} dx dy dz \quad (2.13)$$

So doing the mass balance for the elementary volume chosen we have:

$$\frac{\partial F_x}{\partial x} + \frac{\partial F_y}{\partial y} + \frac{\partial F_z}{\partial z} = -\varepsilon \frac{\partial C}{\partial t} \quad (2.14)$$

Then replacing F_i for equation 10 and after some mathematical treatment, we obtain:

$$\left[\frac{\partial}{\partial x} \left(D_x \frac{\partial C}{\partial x}\right) + \frac{\partial}{\partial y} \left(D_y \frac{\partial C}{\partial y}\right) + \frac{\partial}{\partial z} \left(D_z \frac{\partial C}{\partial z}\right)\right] - \left[\frac{\partial}{\partial x} (v_x C) + \frac{\partial}{\partial y} (v_y C) + \frac{\partial}{\partial z} (v_z C)\right] = \frac{\partial C}{\partial t} \quad (2.15)$$

For the longitudinal direction respect to the fluid flow, for a *conservative solute*, i.e. a sorbate that does not interact with the porous media, and considering the *average liquid linear velocity* v_x is uniform in the space, the mass balance equation is [47]:

$$D_L \frac{\partial^2 C}{\partial x^2} - v_x \frac{\partial C}{\partial x} = \frac{\partial C}{\partial t} \quad (2.16)$$

2.3 Adsorption Kinetics and Equilibrium

2.3.1 Adsorption Kinetics

The adsorption kinetics can be expressed in the same way as convectional reaction kinetics [48].

$$R_{ads} = k' C^n \quad (2.17)$$

Where R_{ads} is the adsorption rate, C is the sorbate concentration and n is the kinetic order.

The adsorption rate can be written in an Arrhenius form:

$$R_{ads} = A e^{(-E_a/RT)} C^n \quad (2.18)$$

It is important to have into account that the key controlling parameters that govern the adsorption rate are [48]:

1. The arrival rate of the sorbate molecules to the solid phase surface.
2. The proportion of incident sorbate molecules that are adsorbed.

Knowing the adsorption kinetics for a determined couple of solid and mobile phases is very helpful to estimate the time in which the equilibrium of the system is reached.

2.3.2 Adsorption Equilibrium

The adsorption equilibrium is a dynamic state, reached when the net rate of adsorption in the solid phase is equal to the rate of desorption [47].



C_L is the sorbate concentration in the liquid, S represents the adsorption sites (that is equivalent to the sorbate concentration in the solid phase C_S , so the amount of the sorbate that is occupying the adsorption sites) and $C_L S$ is the bound to the site, with K_{eq} as the equilibrium constant governing the reaction [46].

In this dynamic process the most important parameter is the adsorption phase capacity for a particular sorbate, and as it is evident, in this characterization there are three important factors: the concentration of the sorbate in the liquid phase C_L , the sorbate concentration in the solid phase C_s and the temperature. Keeping one of this factors constant it is possible to represent the equilibrium of the system graphically. Usually the temperature is kept constant and the graph obtained is called *adsorption isotherm*.

The gas-solid systems have been studied deeper than the liquid-solid ones, so the adsorption equilibrium is based on the theories investigated for gas-solid processes, but these models are also applied to the liquid-solid systems.

The *linear isotherm* is the first of these theories, in which it is postulated that at low concentrations of the sorbate, molecules are sufficiently separate to not influence on another, so it is possible to say that the concentration of the sorbate in the solid phase is proportional (equilibrium constant K_{eq}) to the sorbate concentration in the liquid phase, supposing a mono-layer formation. This model can be applied just to a few systems.

$$C_s = K_{eq}C_L \quad (2.20)$$

Where C_s is the sorbate concentration in the solid phase, C_L is the sorbate concentration in the liquid phase, and K_{eq} is the equilibrium constant.

One of the most used isotherm theories is the *Langmuir isotherm*, this equilibrium model supposes a mono-layer formation until saturation of the active sites of the solid surface, and it is based on the following assumptions [49]:

1. Between adjacent molecules in the solid surface there are not interactions
2. In all over the solid surface the energy of adsorption is the same
3. Once the molecules are adsorbed, they are at fixed places and they cannot migrate over the solid surface

$$C_s = \frac{K_{eq}C_L}{1+K_{eq}} \quad (2.21)$$

Another well-known model is the *Freundlich isotherm*, it is an empirical theory which says that the adsorbed concentration of the sorbate in the solid phase increases as its concentration is higher in the media, following an exponential trend (Bergmann and Machado). It also proposes a multi-layer formation.

$$C_S = \beta C_L^{1/n} \quad (2.22)$$

Here, β is the Freundlich equilibrium constant and n is the Freundlich exponent [50].

If $1/n < 1$ the isotherm is considered to have a favorable shape, meaning that there is affinity between the solid phase and the sorbate molecules. If $1/n > 1$ the isotherm has unfavorable shape, so the solid phase could not be suitable for the sorbate adsorption.

Another important model is the *BET isotherm* (*Brunauer, Emmet and Teller and Emmet and De Witt isotherm*), it assumes that there are not interaction between adjacent adsorbed molecules, and that the retained molecules cannot migrate through the solid phase, as the *Langmuir* model. It also contemplates the formation of multi-layers of adsorbed sorbate and that the net amount of surface that is empty or has a mono, bi, tri-layer and so on, is constant for any specific equilibrium condition [49]. It applies the *Langmuir theory* to each layer, so it is the extension of the *Langmuir model* to the multi-layer case [51]. It is also applied for the measurement of the surface area of a material [51].

$$\frac{1}{v[(p_0/p)-1]} = \frac{c-1}{v_m c} \left(\frac{p}{p_0}\right) + \frac{1}{v_m c} \quad (2.23)$$

With,

$$c = e^{\left(\frac{E_1 - E_L}{RT}\right)} \quad (2.24)$$

p and p_0 are equilibrium and saturation pressures respectively, of the sorbate gas at the adsorption temperature, v is the quantity of adsorbed gas, usually defined as volume, v_m is the quantity of gas adsorbed in the monolayer, c is the *BET constant*,

E_1 is the energy of adsorption for the monolayer, and E_L is the energy to the next and higher layers, and it is equal to the heat of liquefaction [51].

The *BET equation* can fit all the shapes known for an adsorption isotherm. The shapes that are presented in the following figure and that are taken from a classification proposed in an article of *Brunauer, Deming, Deming and Teller* [49].

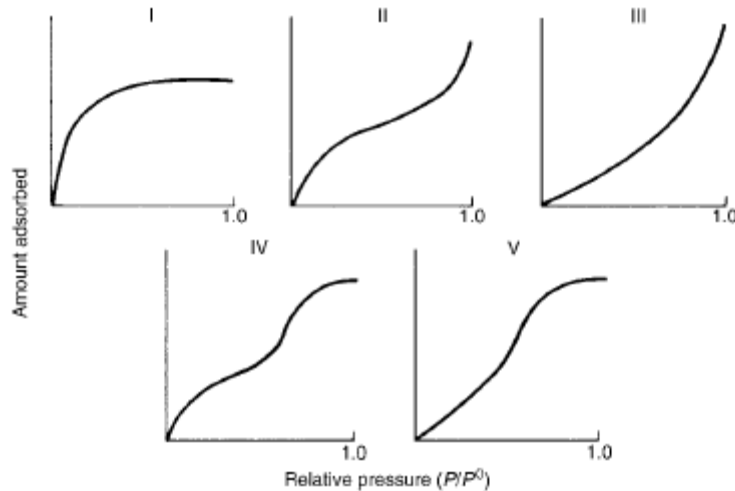


Figure 2.1 Isotherms shape classification according to *Brunauer, Deming, Deming and Teller* [49].

Another isotherm theory with a very different point of view is known as the *Gibbs isotherm*, in it it is assumed that all the adsorbed layers behave as liquid films and that the adsorbed molecule can move through the solid surface. According to this it is possible to apply the mathematical relations of classical thermodynamics [49].

With this approach the properties that determine the free energy of the "film" are temperature, pressure, area available to the film (A_s) and the number of molecules contained (n_s) [49], so the Gibbs free energy is written as:

$$G = F(P, T, n_s, A_s) \quad (2.25)$$

At constant pressure and temperature, and after some mathematical treatment the equation for the *Gibbs isotherm* is:

$$dG = \frac{n_s}{A_s} RT d(\ln P) \quad (2.261)$$

Where Γ is a spreading or two-dimensional pressure.

2.4 Adsorption Bed Design

To design an adsorption bed for a specific system the mandatory information needed are the volumetric flow rate to treat, the concentration of the target substance (the one to be adsorbed) in the column inlet and the maximum concentration accepted of the solute at the column outlet [52].

Once the project information is known the steps for the adsorption bed design are:

1. *Adsorbent Material Selection:* To choose the adsorbent solid phase it is necessary to evaluate its adsorption capacity (the maximum saturation capacity) and the type of equilibrium relation of the system, through the elaboration of the adsorption isotherms, and the easiness of regeneration. It is also important to consider all the solid chemical and physical properties and its cost.

Another important concern is the solid particle size, because as smaller they are, smaller is going to be the occupied volume, so the porosity of the bed, and the volume of the apparatus, but the pressure drop is going to be bigger.

2. *Temperature and Pressure of Operation:* These parameters have to be estimated from the equilibrium isotherms and from the process economic analysis.
3. *Solid Phase Regeneration Frequency:* If the regeneration frequency is low, the bed has a higher useful life, it also means, higher quantities of solid for each useful life period. If the regeneration frequency is high the cost of this step can be very high. The selection of the regeneration frequency has to be done according to the economic analysis of this stage.

4. *Determination of the Effective Volume of Adsorption Bed:* The minimum quantity of solid can be calculated from the adsorption capacity of the adsorbent at saturation, which can be estimated using the inlet solute concentration in the equilibrium isotherm expression, assuming an adsorption yield of 100% and a utilized bed fraction of 1. With this information and knowing the solid bulk density, the theoretical volume of the bed can be determined. The effective bed volume is calculated by increasing the theoretical bed volume the 20%-40%, which means an adsorption yield less than 100% and an utilized bed fraction minor than 1.

5. *Determination of the transversal area of the column:* To obtain the right transversal area it is necessary to work with values of liquid superficial velocities which let non very high pressure drops. Usually, the values of superficial velocity are in the range of 0.25 m/s to 0.50 m/s [52].

6. *Determination of the column length:* The column length is calculated by dividing the column volume by the optimal transversal section.

There is also the empirical approach to design the adsorption bed. For this method the pilot tests are the starting point. Usually, the liquid superficial velocity is fixed, transversal area is calculated as well as the total volume of the column (and the quantity of solid to be packed), the breakthrough time and the adsorption cycle time can be determined from the test [52].

With the empirical method the adsorption yield is known a priori, but the cycle time could not be the optimum value, and the opposite situation is present with the first approach [52].

2.5 Column Adsorption

To optimize and design a large-scale adsorption process it is important to understand the adsorption dynamics. For this it is necessary to performance a mass balance of the process.

The mass balance equation, excluding the reaction term is:

$$\frac{\partial C_{L,i}}{\partial t} = -v_{int} \cdot \frac{\partial C_{L,i}}{\partial z} + D_L \cdot \frac{\partial^2 C_{L,i}}{\partial z^2} - \frac{\rho_b}{\varepsilon} \frac{\partial C_{S,i}}{\partial t} \quad (2.27)$$

The left side of the mass balance corresponds to the accumulation term, while in the right side we have the convection, dispersion and adsorption terms, respectively.

Here,

$C_{L,i}$ is the sorbate i concentration in the liquid phase

z is the longitudinal distance

D_L is the coefficient of longitudinal dispersion

V_{int} is the liquid phase interstitial velocity ($Q/A\varepsilon$)

ε is the packed bed porosity

$C_{S,i}$ is the sorbate i concentration in the solid phase.

ρ_b is the density of the packed solid phase

t is the time

If we consider that the driving force is linear, the adsorption term can be written as:

$$\frac{\rho_b}{\varepsilon} \frac{\partial C_{S,i}}{\partial t} = k_L a (C_{L,i} - C_{L,i}^{eq}) \quad (2.28)$$

Where,

$k_L a$ is an overall mass transfer coefficient, which includes the internal and external mass transfer resistance [46].

$C_{L,i}^{eq}$ is the sorbate i concentration in the liquid phase that is in equilibrium with the sorbate concentration in the solid phase ($C_{S,i}$).

If the equilibrium can be described by a linear isotherm, equation 28 can be written as:

$$\frac{\rho_b}{\varepsilon} \frac{\partial C_{S,i}}{\partial t} = k_L a \left(C_{L,i} - \frac{C_{S,i}}{K_{eq}} \right) \quad (2.29)$$

For a Langmuir isotherm the expression would be:

$$\frac{\rho_b}{\varepsilon} \frac{\partial C_{S,i}}{\partial t} = k_L a \left(C_{L,i} - \frac{C_{S,i}(1+K_{eq})}{K_{eq}} \right) \quad (2.30)$$

And for a Freundlich isotherm it is:

$$\frac{\rho_b}{\varepsilon} \frac{\partial C_{S,i}}{\partial t} = k_L a \left(C_{L,i} - \left(\frac{1}{\sqrt[n]{\beta}} \sqrt[n]{C_{S,i}} \right) \right) \quad (2.31)$$

For equations 2.29 and 2.30 K_{eq} is the equilibrium constant, and for equation 2.31 β is the Freundlich equilibrium constant and n is the Freundlich exponent, as it was mentioned in section 2.3.2.

2.5.1 Adsorption Breakthrough Curves

The adsorption breakthrough curves are plots of the ratio of the sorbate outlet concentration and its inlet concentration in the liquid phase, as function of time (or the volume) [53].

The figure 2.2 shows an adsorption breakthrough curve [54].

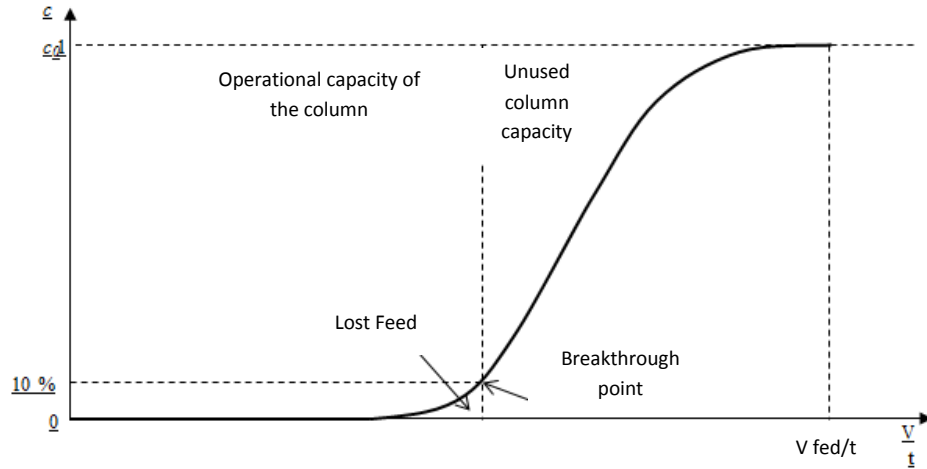


Figure 2.2 Adsorption breakthrough curve [54].

The shape of the breakthrough curve depends also on the adsorption isotherm of the studied system, and its steepness determines the extent of the column capacity that can be used. So, the curve shape is important to establish the column length [53].

Usually, the adsorption is performed until the breakthrough point which is the moment in which the outlet fluid concentration is between the 5%-10% of the inlet concentration value. After that point, the outlet concentration increase rapidly until be the same as in the column fed, which means that the packed bed is saturated.

From the breakthrough curve it is possible to obtain different information of the adsorption process that is occurring, by using the following equations:

$$m_{fed}(t) = Q \cdot C_{L0} \cdot t \quad (2.32)$$

$$m_{out}(t) = Q \cdot \int C \cdot dt \quad (2.33)$$

$$m_{sorbed}(t) = m_{fed}(t) - m_{out}(t) \quad (2.34)$$

$$m_{sorbed}(t) = Q \cdot C_{L0} \cdot t - Q \cdot \int C \cdot dt = Q \cdot [C_{L0} \cdot t - \int C \cdot dt] \quad (2.35)$$

$$m_{sorbed}(t) = W \cdot C_S \quad (2.36)$$

$$m_{sat}(t) = Q \cdot \int_0^{t_{sat}} C \cdot dt \quad (2.37)$$

m_{fed} is the solute mass fed at the column inlet, C_{L0} is the feed concentration, t is the adsorption test total time, Q is the liquid phase flow rate, m_{out} is the sorbate mass that is coming out from the column, $m_{sorbate}$ is the sorbate mass that has been adsorbed, W is the packed resin weight, C_S is the sorbate concentration in the solid phase, m_{sat} is the sorbate mass theoretically adsorbed when the packed bed is saturated, and t_{sat} is the time to reach saturation.

With this information the packed bed efficiency η_{resin} , which is the fraction of the packed bed that has been utilized, is calculated as:

$$\eta_{resin} = \frac{m_{sorbate}(t)}{m_{sat}(t)} \quad (2.38)$$

2.5.2 Mass Transfer Units (N) and Length of Unused Bed (LUB)

The *mass transfer units* (N) methodology is a method for the analysis of packed bed separation processes. The quantity of *mass transfer units* is a way to understand the difficulty of the studied separation, analogously at the trays of a plate column, so higher is the number of units, the final product has a higher purity.

The *mass transfer units* can be calculated as:

$$N = k_L a \cdot \frac{L}{v_s} = k_L a \cdot \frac{L}{\varepsilon \cdot v_{int}} = \left[\frac{L \cdot \varepsilon}{v_s} \right] / \left[\frac{\varepsilon}{k_L a} \right] = k_L a \cdot \frac{\tau}{\varepsilon} = \frac{t_{convection}}{t_{mass\ transport}} \quad (2.39)$$

Where,

v_s is the liquid superficial velocity.

If N is higher the breakthrough curve is steeper. In the case of a system with a linear isotherm if the column length increases, also the *mass transfer zone* (that is the length of bed over which the sorbate concentration from a higher value C_{L1} to a lower one C_{L2} [55] does, so the dimensionless breakthrough curve becomes steeper, so, η_{resin} grows. With a favorable shape isotherm this effect is much more marked [52,56].

This shows that the *mass transfer units* are a key parameter for adsorption optimization. N depends only on the *mass transfer coefficient* $k_L a$ and the system residence time τ , which means that depends on *column length* (L) and the *liquid superficial velocity* (v_s).

Thus, in order to increase the *column efficiency*, lowering the packed resin costs, $k_L a$ and τ have to increase, and this can be done by lowering v_s or by increasing the *column length*.

If v_s is reduced, $k_L a$ will behave in the same way (because the interstitial velocity decreases, which is directly related with the liquid phase superficial velocity), lowering, so there is a minor effect in the *column efficiency* improvement, so, it is more convenient to increase the *column length* [52].

This can be explained by the following expressions:

$$k_L a \propto v_{int}^\beta \quad (2.40)$$

$$N = k_L a \cdot \frac{\tau}{\varepsilon} = k_L a \cdot \frac{L}{\varepsilon \cdot v_{int}} = K_T \cdot \frac{v_{int}^\beta \cdot L}{\varepsilon \cdot v_{int}} = K_T \cdot \frac{L}{\varepsilon \cdot v_{int}^{(1-\beta)}} \quad (2.41)$$

Where K_T is a proportionality constant.

Once the optimum column length is found for the small or pilot scale, the process can be scaled up, for this the most used procedure is the *length of unused bed (LUB)*, the procedure will be explained below.

The *LUB* of the adsorption column can be estimated as:

$$LUB = Total\ bed\ length - Used\ bed\ length \quad (2.42)$$

$$Used\ bed\ length = Total\ bed\ length \cdot \eta_{resin} \quad (2.43)$$

The *LUB* depends on the breakthrough curve shape; it means that it depends on the equilibrium isotherm of the system, and not on the column length. According to this, also in the larger column the *LUB* is going to be the same, and the packed bed efficiency will increase.

$$\eta_{large} = \frac{L_{large} - LUB}{L_{large}} \quad (2.44)$$

With the *larger column efficiency* (t_B) the breakthrough time for the larger column can be calculated as:

$$t_B = \eta_{large} \cdot t^* \quad (2.45)$$

t^* is the *adsorption ideal time*:

$$t^* = \frac{m_{fed}(t^*)}{Q \cdot C_{L0}} = \frac{m_{sorbate}(t^*) + m_L(t^*)}{Q \cdot C_{L0}} \quad (2.46)$$

$$m_L(t) = C_{L0} \cdot V_L \quad (2.47)$$

With V_L is the liquid volume used in the test.

If the equilibrium can be described by a *linear isotherm* for $m_{sorbate}$ calculation, t^* is estimated as:

$$t^* = \frac{W \cdot K_{eq} + V_L}{Q} = \tau \cdot \left(K_{eq} \cdot \frac{\rho_{bulk}}{\varepsilon} + 1 \right) = \tau \cdot f_{delay} \quad (2.48)$$

Where f_{delay} is the *delay factor*, which measures the delay of the fluid front because of adsorption and τ is the *column residence time*, which obtaining will be explained in the section 2.7.

Coming back to the *LUB* scaling up procedure, it is important to say that if the isotherm which describes the system equilibrium is of *favorable shape* (convex curve) the breakthrough curve shape keeps constant, so the length of the *mass transfer zone (MTZ)*, is also constant, thus, the proportion of adsorbent mass and unused bed length, too [52].

If the isotherm is linear, the *MTZ* is not constant over the column length, so if the length is increased also the *LUB* grow. This means that if the *LUB* procedure is used for the adsorption column scale up, η_{resin} will be overestimated, so, also the adsorbent mass will have to be overestimated [52].

In general, for the optimization of an adsorption process it is important to consider parameters like the *column efficiency*, *resin regeneration cost*, *pressure drop* and so on, which depend simultaneously different factors as *column length and diameter*, *liquid phase superficial velocity (volumetric flow)* and the *mass of packed resin*. For this reason, once the optimum values for the *column length* and the *liquid superficial velocity* are found in small scale, the most applied practice for scaling up to the industrial process is to keep these values by increasing the *column diameter*.

2.6 Fixed Bed Column Packing

The column packing is a critical step, because the packing yield affects directly the column performance and, obviously, the adsorption efficiency. For medium, large and industrial scales, there are two ways of adding the resin beads into a column, in their dry form (dry packing), or as a slurry (slurry packing). These are the techniques applied also for chromatography columns.

Industrially, there are three used methods, *dynamic axial compression (DAC)*, *flow packing* and *pack-in-place*.

2.6.1 The Dynamic Axial Compression (DAC):

It is very popular because provides a constant compression to the packed bed, which helps to reduce the particle size segregation, and most important, minimizes channel formation, so the packing quality is really good. Besides, it is a one-step process, making it easier.

2.6.2 The Flow Packing:

This process can be made in two ways, constant pressure or constant flow. In each case, it is necessary to use a flow rate at least 30% bigger than the process real volumetric flow [57]. It is suitable for packing soft gel media or not very small particles, otherwise, channeling probability is very high, because a not really dense bed is formed.

2.6.3 The Pack-in-Place:

This methodology is very similar to the flow packing one, it is used in case of preset column high, and does not need to remove the adjuster cell of the column.

2.6.4 Dry Packing:

This method has an important advantage, it minimizes the column washing up, but it has a clear disadvantage, it is very hard to have a well-packed column [58].

The base support (sand, ecc.) is poured inside and then washed with a solvent (usually the actual mobile phase) in order to remove trapped bubbles. Then the solid phase is poured inside. Once it is inside the solvent is passed through and the column is tapped to help the particles to settle with a better distribution. For this packing procedure, tapping demonstrated to produce beds of better quality [59].

The dry packing is widely used for non-spherical and low dense materials, with particle sizes down 50 μm , with smaller diameters the quality of the bed is worsened [60]. It is also used when the slurry methods cannot be applied, because of hardware limits of the column system or for the slurry transportation.

2.7 Fluid Dynamic Characterization

To evaluate the fluid dynamic behavior of a packed bed, usually it is applied the Retention Time Distribution Method or RTD method.

The residence time distribution gives the information about the mixing that is occurring inside a reactor or a packed bed, and it is one of the most important parameters in their characterization.

The RTD can be determined experimentally, by many different ways [61], but the most used methods are based in the injection of an inert tracer, which are the ones that we are going to explain here.

The tracer is injected at time $t = 0$, and the effluent concentration is measured at the outlet of the column or reactor, during time. There are two ways to inject the marker, the *pulse input* or the *step input* [61].

The first one consists in the injection of a certain amount of tracer in one shot in the shortest possible time (compared with the residence time). To apply this methodology, the dispersion between the injection point and the real column entrance has to be negligible, so it is necessary that the column/reactor hardware enables compliance with this condition, otherwise it is better to use the second listed approach for injecting the marker.

The tracer concentration is measured at the reactor outlet as function time. The graphic response obtained, named also as *C curve* [61], is showed in figure 2.3.

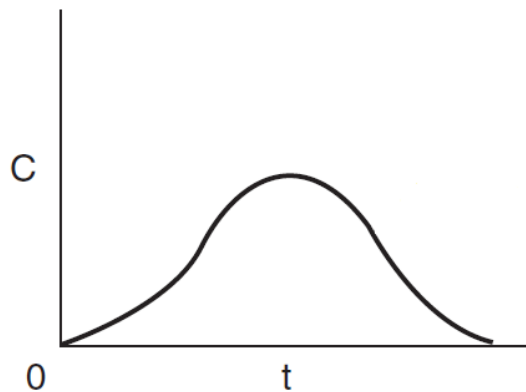


Figure 2.3 Response of a pulse injection test [61].

Where C is the tracer concentration at the reactor/column outlet. It can be measured as conductivity, radioactivity or by absorbance [61].

With the *C curve* it is possible to obtain the *Residence Time Distribution Function* or *E curve* which "describes in a quantitative manner how much time different fluid elements have spent in the reactor"¹.

The *E curve* is obtained from the experimental data with the following equation:

¹ S.H. Fogler & M.N. Gürmen, *Elements of Chemical Reaction Engineering*, forth ed., Pearson, Michigan, 2008.

$$E(t) = \frac{C(t)}{\int_0^{\infty} C(t) dt} \quad (2.49)$$

The denominator in equation 1 is the area below the *C curve*, so the integral can be estimated by numerical methods application.

Another important expression for the *RTD function* is:

$$\int_0^{\infty} E(t) dt = 1 \quad (2.50)$$

If we consider that $\int_{t_1}^{t_2} E(t) dt$ is the fraction of matter that is coming out from the reactor that has been inside it for a period of time between t_1 and t_2 , equation 2 results evident.

On the other hand, the *step input* method, considers a time-varying injection marker, usually in a system with a constant volumetric flow rate.

The response obtained at column/reactor outlet is showed in figure 2.4.

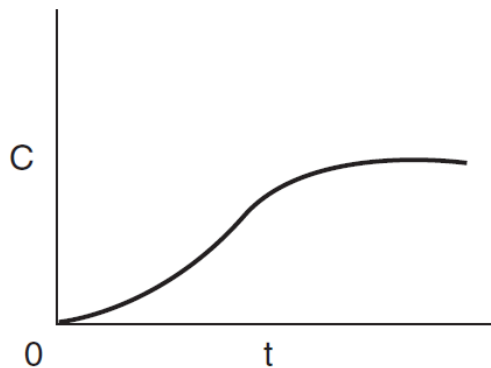


Figure 2.4 Response of a step injection test [61].

From this curve, it is possible to calculate the *Cumulative Retention Time Distribution Function* or *F curve*. The *F function* is defined as:

$$F(t) = \frac{C(t)_{out}}{C_o} \quad (2.51)$$

Then, from the *F curve RTD Function* can be estimated as:

$$E(t) = \frac{dF(t)}{dt} \quad (2.52)$$

Once the *E function* is found, the average residence time can be calculated with the following equation:

$$\bar{t} = \tau = \int_0^{\infty} t \times E(t) dt \quad (2.53)$$

The theoretical residence time (τ) is equal to the average residence time if there are not dead zones inside the column/reactor.

With this information is also possible to estimate the packed bed porosity (for a packed column or a packed bed reactor) by applying the following expressions:

$$\text{Liquid Volume} = \text{Volumetric Flow rate} \times \tau \quad (2.54)$$

$$\varepsilon = \frac{\text{Liquid Volume}}{\text{Total column/reactor Volume}} \quad (2.55)$$

With the *E curve* obtaining is very important to characterize a packed bed and to evaluate the packing quality and the column efficiency, which are very significant parameters, because the column/reactor performance and the reproducibility of the results obtained depend directly on them.

A high quality packing has to be homogeneous and stable, with no air bubbles of air trapped, with no channels or preferential paths formation.

To test the efficiency of the column and the quality of the packing the most used approach is the *theoretical plate model*, presented by Martin and Synge in 1941 [62]. This model proposes the column division in several discrete sections, called *theoretical plates*, in which the sorbate in the solid and in the mobile phases is in partition equilibrium, so it (sorbate) is moving through the column in an equilibrated liquid phase from one plate to another [63].

The *E curve* obtained can be used for calculating the numbers of *plates* of a column and to evaluate column packing, as follows:

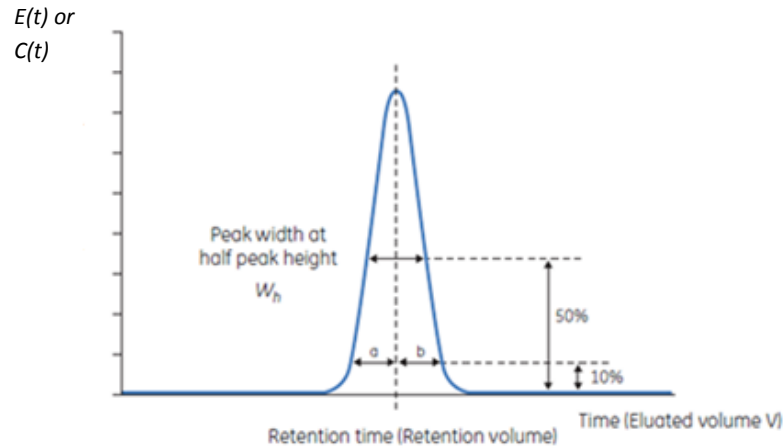


Figure 2.5 *E* curve(for pulse or step injection) or *C* curve (for pulse injection) analysis for packing quality and column efficiency testing. Modified from [64].

$$N = 5.54 \left(\frac{\tau}{W_h} \right)^2 \quad (2.56)$$

Where,

N is the number of plates

τ is the residence or retention time

W_h is the peak width at half height

With the number of plates the *height equivalent of a theoretical plate* or *HETP* can be estimated as:

$$HETP = \frac{L}{N} \quad (2.57)$$

L is the column length

Higher is the number of plates (N) or smaller is the value of *HETP*, the efficiency of the column is higher.

With these two parameters the *reduced plate height* or h can be calculated with the expression:

$$h = \frac{HETP}{d_p} \quad (2.58)$$

According to different analytical and process chromatographic column producers [64,65], application in which the packing quality and column performance are as significant as for an adsorption process, values of $h \leq 3$ are characteristic of a high efficiency column.

Another important parameter is the *asymmetry factor* or As of the peak, which measures the deviation of the obtained peak from an ideal Gaussian peak.

$$As = \frac{b}{a} \quad (2.59)$$

Where b is the right half of the *E curve* or *C curve*, and a is its left half.

If $0.8 \leq As \leq 1.8$ the packing can be considered of good quality and a good performance of the column can be expected [65].

As with values minor than 0.8 are present in peaks with fronting, which means that the packing was over-packed, and values superior than 1.8 (peaks with tailing) mean under-packed beds, and in both cases the column has to be re-packed [65].

Also, according to PALL Life Sciences [65] and GE Healthcare Bio-Sciences [64] technicians, although the values for N , HETP, h , and As , the most important is the repeatability of them not only after each packing procedure, also after several separation (adsorption) cycles, so it is important to do the fluid dynamic test not only after packing, but also after the different steps of the separation process itself.

CHAPTER 3

MATERIALS AND METHODS

3.1 Olive Mill Wastewaters (OMW), resins, Cyclodextrin-based polyurethane (CDP) and chemicals

The OMW used in this study, labeled “Imperia 2012”, “Imperia 2013” and “Imperia 2014” were provided by an olive mill located near Imperia, in the North-West of Italy. The OMW labeled as “Gallipoli 2012” produced in the Apulia Region in Southern Italy. The main characteristics of the tested OMW are reported in Table 4.2.

For the phenolics mixture recovery, the adsorption non-ionic solid phase is the styrene-divinylbenzene resin Amberlite XAD 16 (DOW Chemicals Europe GmbH, Horgen, Switzerland). Its main characteristics are described in the Table 3.1. The resin was activated as follows: i) resin soaking with acidified ethanol (0.5% HCl 0.1N), ii) overnight drying at 105°C, iii) second resin soaking with acidified ethanol, iv) washing with demineralized water (twice) [66]. Finally, the activation solvent was removed by siring aspiration and a mass of activated and hydrated resin (28.3% w/w resin, 71.7% w/w water) was obtained.

The adsorption ionic-exchange solid phases tested are the anionic resins Amberlite IRA958Cl and IRA 67Cl (DOW Chemicals Europe GmbH, Horgen, Switzerland). The first one is a strongly basic anion exchange resin, with quaternary ammonium functional group in a crosslinked acrylic polymer matrix, and the last one is a weakly basic anion exchange resin, with tertiary amine functional group in a crosslinked acrylic gel structure. The properties of both ionic resins are listed on tables 3.2a. and 3.2b.

The cyclodextrin-based polyurethane (CDP) used for tyrosol and hydroxytyrosol selective recovery was synthesized by the FHNW research group, as it is described in the section 2.2. The reagents for CDP synthesis, the solvents for Ty and HTy

elution, and the HPLC mobile phase components for the Ty and HTy method, were obtained from Sigma Aldrich (Buchs, Switzerland).

The desorption-regeneration solvent for phenols mixture recovery, the HPLC mobile phase components for total PCs content analysis, gallic acid, the Folin-Ciocalteu reagent, sodium carbonate, sodium chlorate, sulfuric acid, the ABTS reagent, the ascorbic acid and the solvents for resin activation were obtained from Sigma Aldrich (Milan, Italy). The COD Test Tubes were acquired from Aqualytic (Dortmund, Germany).

Matrix	Macroreticular aliphatic crosslinked polymer (styrene / divinylbenzene)
Physical form	White translucent beads
Specific density (kg/L)	1.039
Adsorption capacity at saturation (mg/gdry resin)^a	370
Surface area (m²/g)	800
Porosity (dry resin; L/L)	0.55
Average particle size (dry resin; mm)	0.63
Uniformity coefficient	2.0
Fines content (mm)	< 0.350: 2.0% max
Coarse content (mm)	> 1.18: 2.0% max
Maximum reversible swelling	25% (on p-xylene via methanol)

Table 3.1 Technical characteristics of adsorption resin Amberlite XAD 16.

Matrix	Crosslinked acrylic macroreticular structure
Functional groups	Quaternary ammonium
Physical form	White opaque beads
Ionic form as shipped	Chloride
Total exchange capacity (Cont. Value)	≥0.8eq/L (Cl ⁻ form)
Moisture holding capacity (Cont. Value)	66 to 72% (Cl ⁻ form)
Specific gravity	1.05 to 1.08 (Cl ⁻ form)
Shipping weight	720 g/L
Particle size	
Uniformity coefficient	≤1.8
Harmonic mean size	630 to 850 μm
Fine contents (Cont. Value)	<0.355 mm : 1.0% max
Coarse beads	>1.180 mm : 5.0% max

Table 3.2 a). Technical characteristics of adsorption ionic resin Amberlite IRA 958Cl.

Matrix	Crosslinked acrylic gel structure
Functional groups	Tertiary amine
Physical form	Translucent white spherical beads
Ionic form as shipped	Free Base (FB)
Total exchange capacity (Cont. Value)	≥1.60eq/L (FB form)
Moisture holding capacity (Cont. Value)	56 to 64% (FB form)
Shipping weight	700 g/L
Particle size	
Uniformity coefficient (Cont. Value)	≤1.8
Harmonic mean size (Cont. Value)	0.500 to 0.750 mm
<0.300 mm (Cont. Value)	3.0% max
Reversible swelling	FB → Cl ⁻ ≤ 30%

Table 3.2 b). Technical characteristics of adsorption ionic resin Amberlite IRA 67Cl.

3.2 Cyclodextrin-based Polyurethane Synthesis

To prepare 668g of CDP are needed 290g of methylated β -cyclodextrin (Me β CD) and 378g of 4,4'-methylene diphenyl diisocyanate (MDI). The polymerization reaction occurs in presence of dibutyltin dilaureate (DBTDL, 2mL) as catalyst. In one flask the Me β CD with 630mL of acetone. In a second flask put the MDI with 270mL of acetone. Both flasks were stirred at heated until 40°C. Once the temperature was reached, 2mL of DBTDL were added to the Me β CD suspension , and stirring continued for 10 minutes. Then, heating was stopped and the Me β CD flask was put in ice. The MDI suspension was added dropwise to the Me β CD flask, agitating vigorously for 30 seconds. A white polymer was obtained, it was scrapped to get a powder. The CDP was washed with acetone to remove residual DBTDL, and then with water to eliminate Me β CD not reacted. The polymer was dried under vacuum overnight, and grinded with a small kitchen crusher.

3.3 Analytical methods

3.3.1 Total Phenols

Two different approaches were applied and compared to measure total PCs: the conventional colorimetric test developed by Folin and Ciocalteu (FC) [67] and an in-house developed HPLC method. In the Foulin-Ciocalteu (FC) method, 25 mL flasks, carefully cleaned with sulfuric acid 25% and washed with de-ionized (DI) water, were filled with 12.5 mL of DI water, 125 μ L of sample (diluted as required, to avoid absorbance signal saturation) and 1.25 mL of FC reagent. After 2 minutes, the reaction was quenched by adding 3.75 mL of sodium carbonate (20% w/v). Finally, the flasks were diluted to the volume mark, and left at 75°C for two hours. Then, the absorbance was read at 765 nm with a Cary 100Scan UV spectrophotometer (Agilent, Santa Clara, California), using as reference a dephenolized OMW obtained by repeated adsorptions with the Amberlite XAD16 resin until the attainment of a

final PC content < 1% of the original PC level in the OMW, and then treated with FC reactants. The method was calibrated with acid gallic as external standard.

For the HPLC method, a Jasco 880 pump, a Jasco 875-UV Intelligent UV/vis detector (Easton, Maryland) set at 264 nm and a C18 Kinetex 2.6 μ m 100A Phenomenex column were utilized. The flow was set at 1.0 mL/min. The following mobile phase gradient was applied: 0-4 minutes, 100% phase A (HPLC water with 0.1% orthophosphoric acid); 4-6 minutes, 70% phase A and 30% phase B (acetonitrile); 6-15 minutes 70% phase A and 30% phase B. The mobile phase gradient was designed to merge all the phenolic peaks into a single broad peak. This approach makes the analysis faster and the method more sensitive, but it prevents the identification of the single compounds. An internal standard (gallic acid 50 mg/L) was added in each HPLC analysis.

3.3.2 Tyrosol (Ty) and Hydroxytyrosol (HTy) Quantification

A HPLC method was developed for quantifying Ty and HTy in the inlet OMW and in the adsorption and desorption samples. An Agilent 1100 Series G1311A Quat pump, an Agilent 1100 Series G1313A ALS UV/VIS detector set at 230 nm and a ZORBAX SB-C18 4.6 μ m 5-Micron column, were used. The flow rate was set at 1.0 mL/min, the column was thermostated at 15°C and the mobile phase was composed by 90% acidified water (0.1% H₃PO₄) and 10% pure acetonitrile. The time of each analysis was 70 minutes.

3.3.3 Total Solids

20 mL of OMW were dried overnight at 105°C in a porcelain crucible, cooled in a desiccator and weighted using a 4-digit analytical balance. The procedure was applied in triplicate. *Suspended Solids*. 20 mL of OMW were filtered with a 0.45 μ m ALBET cellulose nitrate membrane filter and placed in a Whatman vacuum filtration system. The filter was dried at 105°C for two hours, cooled in a desiccator and weighted. The procedure was applied in triplicate. *Dissolved solids* were calculated as the difference between total and suspended solids.

3.3.4 COD

The COD was measured spectrophotometrically using the Aqualytic COD Vario Tubes (range: 0-1500 mg_{O2}/L). Each tube contained potassium permanganate in an acid medium, to which 2 mL of diluted sample were added. The tubes were then left at 150°C for 2 hours in a ECO16 Velp Scientifica thermoreactor (Monza, Italy). After cooling the tubes for 30 minutes, the absorbance of each sample was measured at 610 nm. For COD of selected desorption samples, the ethanol (elution solvent) was stripped with nitrogen and the residual solid was re-suspended in water, in the same volume of ethanol that was stripped.

3.3.5 Total carbohydrates

The total carbohydrates were determined by a modified Dubois method [68]. The calibration curve was made with glucose as standard. All measurements were done in duplicate.

3.3.6 Total lipids

Lipids were evaluated as reported in [69] using as a standard the olive oil produced at the industrial plant to which the tested OMW belongs.

3.3.7 Total proteins

Proteins were determined with the Bradford method [70], by using the commercial protein assay dye reagent concentrate from BioRad (Milano, Italy).

3.3.8 Density and pH

A 100 mL ITI Tooling pycnometer was used for OMW density estimation, whereas pH was measured with an EUTECH Instruments pH 2700 Series pH-meter (Thermoscientific, Waltham, Massachusetts).

3.3.9 Antioxidant Activity (ABTS Assay)

From the ABTS (2,2'-azino-bis(3-ethylbenzothiazoline-6-sulphonic acid) stock solution (7mM in 2.5mM of K₂SO₇) was prepared one day before the assay and it

was left to incubation overnight without light at room temperature. Then, before the analysis, the ABTS work solution was prepared from the stock solution using the spectrophotometer at 734 nm, the final absorbance has to be 0.7+/-0.02. 1mL of the ABTS work solution reacted with maxim100µL of sample (already diluted).Then the analysed samples were incubated at 30°C for 30 minutes and read in the spectrophotometer at 734 nm, using water as blank. The calibration line was done with ascorbic acid as standard [71].

To calculate the antioxidant activity of the sample as µg of ascorbic acid equivalent/µL of sample, the following expression was applied:

$$\text{Antioxidant Activity } \left(\frac{\mu\text{g ascorbic acid eq.}}{\mu\text{L sample}} \right) = \frac{\text{Value calculated from calibration line (g ascorbic acid eq.)} \times \text{sample dilution factor}}{\text{Sample volume reacted with 1mL ABTS work solution } (\mu\text{L sample})}$$

(3.1)

3.3.10 Volatile Fat Acids (VFA) Content

For VFA quantification a HPLC method was applied. A Shimadzu pump, with a refraction index detector and a coregel H3 columnm thermostated at 40°C, were used. The mobile phase is H₂SO₄ 0.12N. The flow rate was set initially at 0.6 mL/min. In order to separate properly the VFA a ramp of flow rate was implemented, as it is shown in table 3.3.

Time	Flow Rate
0 min to 28.2 min	0.6 mL/min
28.2 min to 34.5min	0.9 mL/min
34.5 min to 62 min	1.3 mL/min
62 min to 64 min	0.6mL/min

Table 3.3 Flow rate ramp for HPLC method for VFA quantification.

3.4 Adsorption Columns System

3.4.1 Adsorption Columns System for Phenolic Mixture Recovery

The adsorption system for PCs recovery is composed by an in-line microfiltration system, in which a filter holder of 12.5 cm of diameter kept a Whatman paper filter of 25 μ m or a 11 μ m, according to the OMW pretreatment step (section 3.7), followed by four pyrex glass columns, each one of 52.5 cm of length and 2.44 cm of diameter. The columns were connected in series by Teflon pipes and steel fittings, but could also work separately. The total length of the adsorption zone is 2.00 m. Each column had one sampling point in the top and other one at the bottom, letting the change of the flow direction, and the sampling at different lengths of the adsorption zone when the columns worked connected. The top sampling point worked also as purge to remove the trapped air that could accumulate in the packing and rinsing operations, or for possible leakages in the system. Before the first, the second and the fourth columns, pressure indicator were put. The last column was connected to an auto sampling system composed by 15 electrovalves L321 (Sarai) with the respective timers, which let overnight programmed sampling.

A picture and a process flow diagram of the adsorption system is displayed in figures 3.1a. and 3.1b.

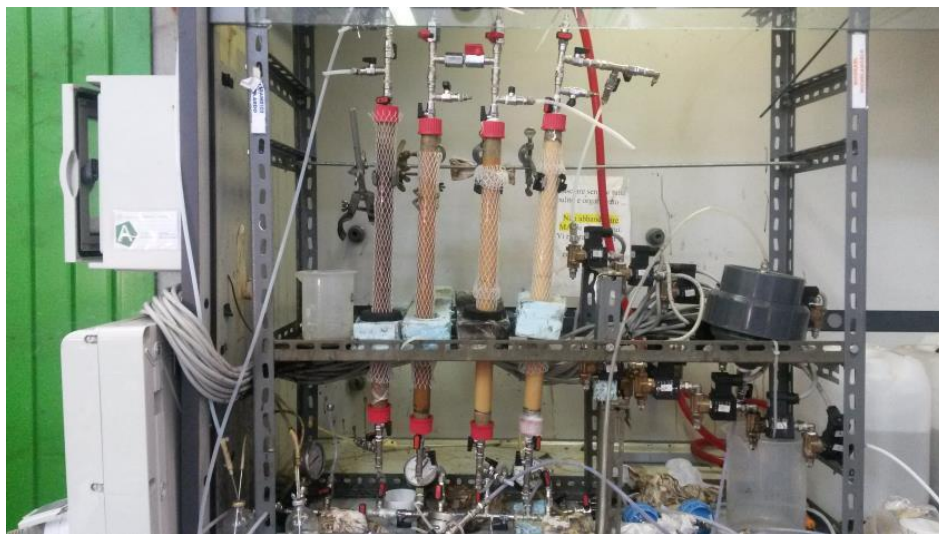


Figure 3.1 a). PCs adsorption system

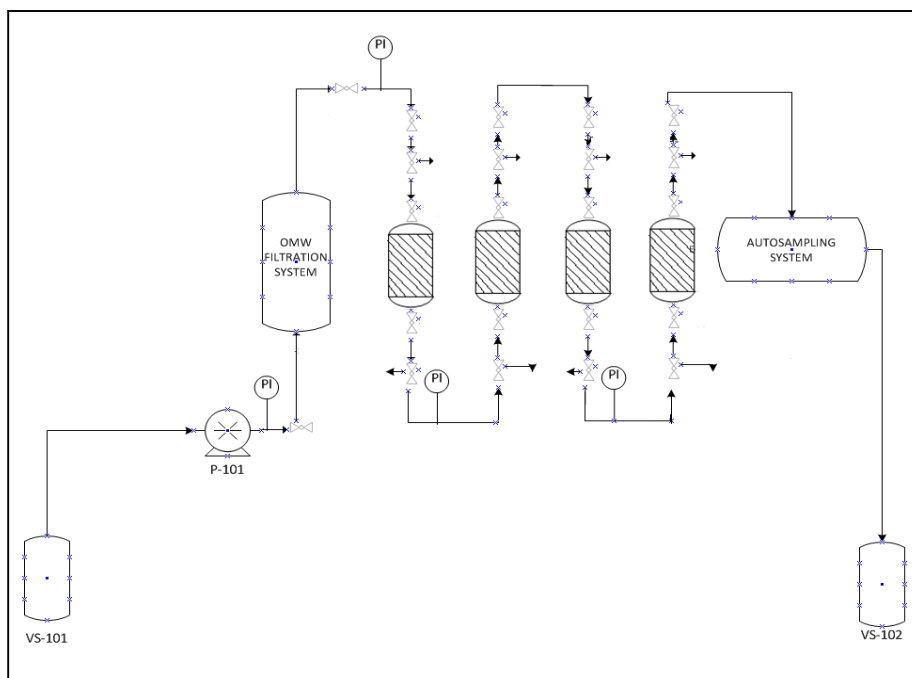


Figure 3.1 b). Process flow diagram of the PCs adsorption system

3.4.2 Adsorption Column System for Tyrosol and Hydroxytyrosol Recovery

For the Ty and HTy recovery system, the OMW pre-treatment was done separately, using the filter holder and the Whatman filter paper of 11 μ m used in the PCs adsorption system.

The adsorption pilot plant is made in stainless steel; it is composed by one storage tank of 25L for the OMW, connected to a feed tank of 2L. Between these tanks there was a Wolftechnik Filtersysteme Filtergehäuse F-10 cartridge filter of 5 μ m, that was not used because on the small pore size, to avoid pressure drop problems. The adsorption system had also one rinsing tank of 15L, and two elution vessels (for desorption solvents) of 2.0L, two columns of 13.0 cm of length and 6.0 cm of diameter connected in series by steel pipes and fittings. The columns could also work separately. There were also two reclaim tanks of 5L each, and a collecting tank for the dephenolized OMW of 30L. The feed, rinsing and elution tanks had EGE MFP 075 GA-LM030 filling level meters. Between the feed tank and the column there was a Bronkhorst mini CORI-Flow mass meter which gave the signal

of the mass flow rate passing to the software in which the process was programmed and controlled. Another equal device was located between the elution tanks (in the point in which the pipes of each tank became one pipe) and the column.

The columns were connected to a two auto sampling systems, one for collecting the adsorption samples, and the second for the desorption ones. Each auto sampling system let the collection of 46 fractions. WIKA A-10 pressure sensors were located between the feed, rinsing and elution tanks and the columns. Two WIKA TR-30 temperature sensors were located at the columns bottom. The system had 33 Gemü 0322, 0324, 0326 magnetic valves and a HOKE R6000 overflow valve.

The OMW were fed by a magnetic-diaphragm metering Prominent Delta pump at the bottom of the column, with a maximum velocity of 0.52 m/h. The desorption solvents were fed at the column bottom with two Bram hose pumps at 0.44 m/h, and the rinsing water was fed at the column bottom by a Verder Verdergear motor VEM pump. The process settings were fixed with the software SIMENS S7-1200, and all the control parameters of the pilot plant. The control system worked with compressed air at 5 bars. The complete adsorption system and the program software belong to SIMA-tech GmbH (Schwalmtal, Germany).



Figure 3.2 a). "Laboratory-Phenols-Adsorption-Reactor" of SIMA-tec GmbH (Schwalmtal, Germany), fot Ty and HTy adsorption (SIMA-tec).

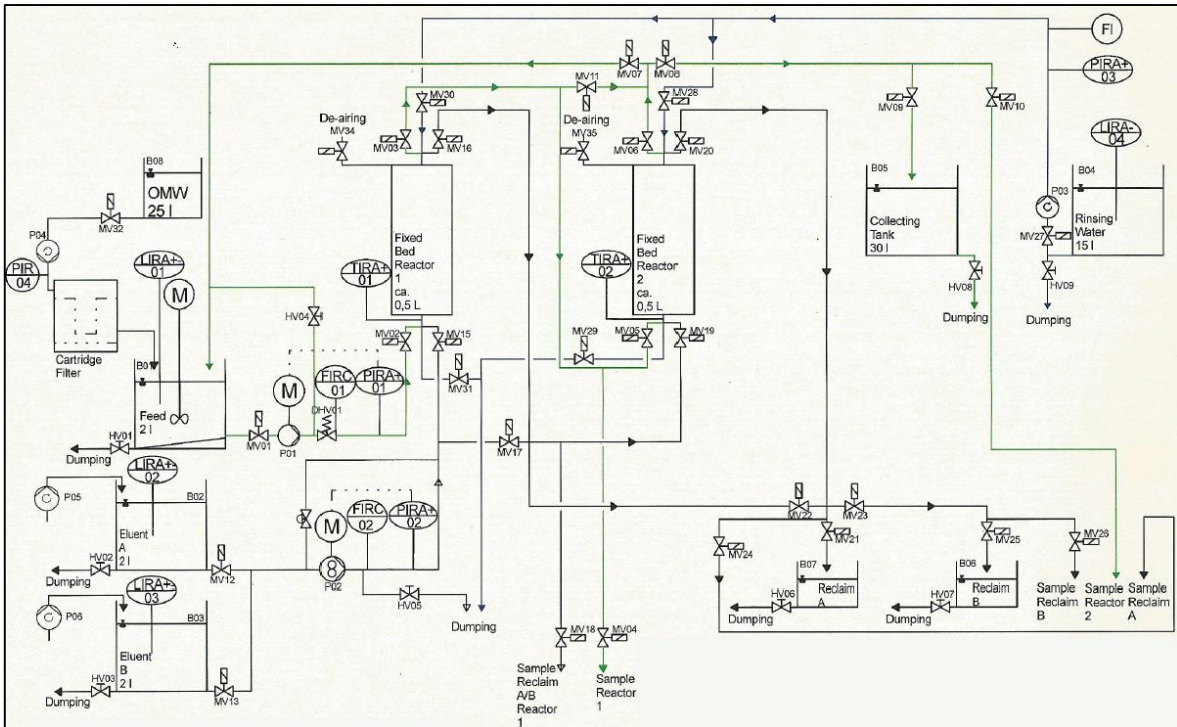


Figure 3.2 b). Process flow diagram of the "Laboratory-Phenols-Adsorption-Reactor" of SIMA-tec GmbH (Schwalmtal, Germany), for Ty and HTy adsorption (SIMA-tec).

3.5 Adsorption Kinetics

3.5.1 Adsorption Kinetics for Amberlite XAD 16

To know the time that takes to the system resin-OMW, to 1.5L of OMW was added the equivalent of 93.5g of dry Amberlite XAD 16 (previously activated, section 3.1). The volume of liquid phase was chosen in order that with sampling the total volume did not change more than 5%, otherwise, the thermodynamical properties of the system could change and the data obtained would not be representative of the initial system.

The mixed phases are then located in a shaker at 140 rpm. A sample of 2mL was taken every 4 minutes until 20 minutes, then every 10 minutes until 60 minutes,

then at 90 minutes and finally at 120 minutes. The samples were analyzed with the total phenols HPLC method.

Then, with the concentrations obtained in the liquid phase samples, it was possible to know how was changing the concentration of the target compounds in the solid phase by applying the following equation, for each sampled point:

$$Q_{sol-eq} \left(\frac{mg}{g_{dry\ resin\ or\ CDP}} \right) = \frac{(C_{liq_{initial}} - C_{liq_{sample-eq}}) \times Total\ Volume_{liq}}{Weight_{dry\ solid\ phase}} \quad (3.2)$$

3.5.2 Adsorption Kinetics for CDP

For the CDP-OMW system, 30 g of dry CDP polymer were added to 1L of OMW, and shaken at 140 rpm. Every 10 minutes until 60 minutes a sample of 2mL was taken of the liquid phase, then, every 20 minutes until 120 minutes and finally, every 30 minutes until 180 minutes. The samples were analyzed with the Ty and HTy HPLC method.

Then, with the concentration obtained in the liquid phase the concentration change in the solid phase for Ty and HTy was calculated with the equation 3.2.

3.6 Adsorption Isotherms

3.6.1 Adsorption Isotherms for Amberlite Resins (Phenolic Mixture)

The adsorption isotherms of the total PCs contained in the tested OMW “Imperia 2012” were studied both at 21 and 30°C. Different amounts (0.1, 0.2, 0.5, 1.0 or 2.0 g) of dry resin were introduced into 50 mL glass vials. Two vials were set up for each amount of resin. The resin activation procedure (Section 3.1) was performed inside each vial. After adding 20 mL of OMW were added.

For the other OMW tested, all the estimated resin that was going to be used for isotherm obtaining, was activated (Section 3.1), and then, the equivalent of 5.0g of dry was put in beakers with different OMW quantities (10mL, 25mL, 40mL, 60mL, 90mL, 125mL, 180mL and 270 mL). Then the beakers were placed in a rotatory shaker (140 rpm, at the set temperature) for 2 h. The equilibrium total PC concentration in the liquid phase was evaluated with the HPLC method. The same procedure was applied for the isotherms obtaining with Amberlite IRA 958Cl, the beakers were shaken for 3 h, and the PCs concentration in the liquid phase was evaluated with the Total Phenols HPLC method.

The equilibrium concentration in the solid phase $C_{S,eq}$ was then calculated as:

$$C_{S,eq} = \frac{(C_{L,o} \cdot V_{L,added} - C_{L,eq} \cdot V_{L,final})}{m_s} \quad (3.3)$$

where m_s is the dry resin mass, $C_{L,o}$ and $C_{L,eq}$ are the initial and final concentrations of PCs, in the liquid, whereas $V_{L,added}$ and $V_{L,final}$ are respectively the OMW volume added to the solid and the final liquid volume resulting from the sum of the added OMW and the water initially contained in the activated resin. For Amberlite IRA 958Cl case, $V_{L,final} = V_{L,added}$, because there was not a previous activation procedure. The 95% confidence intervals associated to $C_{S,eq}$ were calculated using standard error propagation rules, on the basis of the 95% confidence intervals associated to the experimental measurements of C_L , V_L and m_s . The 95% confidence interval associated to C_L , was estimated from 15 replicated HPLC analyses of a reference gallic acid standard solution (50 mg/L).

3.6.2 Adsorption Isotherms for CDP (Tyrosol and Hydroxytyrosol)

For the CDP case, 2.0g of dry polymer in beakers with 5mL, 20mL, 50 mL, 150 mL, 250 mL and 350 mL of OMW. The Ty and HTy concentration in the liquid phase were analyzed with the HPLC method for Ty and HTy quantification (Section 3.3.2).

The respective Ty and HTy equilibrium concentrations in the solid phase were estimated with the equation 3.3. For CDP case, $V_{L,final} = V_{L,added}$, because there was not a previous activation procedure.

3.7 OMW pre-treatment

To avoid a gradual pressure drop increase in the adsorption column and eventually the complete clogging of the inlet section, a suitable OMW pre-treatment aimed at suspended solids removal must be performed. For this reason, an OMW 3-step pre-treatment was set up. The first step consisted in centrifugation at 4000 rpm for 30 minutes, using a Thermoscientific SC16R centrifuge (Waltham, Massachusetts). The second and third step consisted in a continuous in-line microfiltration performed respectively with 25 μm and 11 μm GE Healthcare Life Science Whatman filters, placed in plastic filter holders. Filtration was performed at 1.67 cm/min superficial velocity.

For the Ty and HTy adsorption the OMW were centrifugated at 7000 rpm for 20 min and then filtered with the filter holder used in the PCs adsorption system, using the GE Healthcare Life Science Whatman filter paper of 11 μm , in this case the OMW were fed to the filter with a ISMATEC peristaltic pump, at 2.5 cm/min superficial velocity.

3.8 Adsorption column packing

3.8.1 Adsorption Column packing Amberlite Resins

The semicontinuous adsorption / desorption tests were performed in a glass columns of 0.525 m and 2.000 m length with inner diameter 0.020 m. After placing a 10-mm layer of quartz sand at the bottom of the column, the latter was filled with activated XAD16 resin using the Dynamic Axial Compression (DAC) technique, by applying two alternative procedures. The first procedure was based on the use of a

slurry prepared by mixing equal volumes of activated resin (Amberlite XAD 16) and of a 10% solution of acidified ethanol (HCl 0.1 N 0.5%) in water [72]. The slurry resin was then divided into 4 aliquots. After pouring each aliquot, the column was filled with acidified ethanol and the solvent was extracted and recirculated downwards with a Masterflex L/S 0.1HP 1-100 RPM pump (Cole-Parmer, Vernon Hill, Illinois) until the stable settling of the resin. Then, a further aliquot was fed and the procedure was repeated. The second procedure was based on the use of two activated resin slurries, prepared with DI water ($100 \text{ g}_{\text{dry_resin}}/\text{L}_{\text{DI water}}$ and $600 \text{ g}_{\text{dry_resin}}/\text{L}_{\text{DI water}}$, respectively). Each slurry was sonicated for 5 minutes in order to remove the air trapped in the resin beads. Initially, 150 mL of the first slurry were poured on the sand layer and left to natural settling for one hour. Then, after recirculating DI water downwards until the stable settling of the resin, 25 mL of the second slurry were added in three steps, and a further DI water recirculation was applied. As a final step in both column packing procedures, a further 10-mm quartz sand layer was placed at the top of the resin and the column was flushed downwards overnight with DI water.

The packing procedure with demineralized water performed markedly better than that employing acidified ethanol, with: i) a slight increase in the number of theoretical plates (from 93 to 117), a 23-fold reduction in terms of $HETP/d_p$ (from 0.32 to 7.5) and an asymmetry factor significantly closer to 1 (0.82 for the acidified ethanol procedure, 1.1 for the demineralized procedure). The demineralized water procedure was thus utilized for the PCs adsorption/desorption tests object of this work. The same procedure was applied for packing Amberlite IRA 958Cl resin.

3.8.2 Adsorption Column Packing for CDP

For the CDP packing, because of the adsorption system hardware limits and the probable non-sphericity of the particles (powder obtained after grinding with a kitchen crusher), a slurry packing method is not suitable. In this case, $\frac{1}{4}$ at the column bottom and upper part were filled with sand, and $\frac{2}{4}$ with dry CDP. Once the column was closed, demineralized water at 25mL/min (maximum flowrate of the

system) was fed from the top of the column for 1h, then, the procedure was repeated, feeding the demineralized water from the bottom of the column. The water feeding cycles were repeated for another couple of hours, not only for packing the polymer, also for cleaning the CDP of possible residuary substances from its synthesis.

3.9 Fluid dynamic test

3.9.1 Fluid dynamic test Amberlite Resins Packed Bed

To evaluate the packing quality and the fluid dynamic behaviour of the packed bed, a frontal analysis experimental test was carried out after each packing procedure. A 0.04 M NaCl solution was fed from the top of the column at a superficial velocity of 1.22 m/h. At the column outlet, the electrical conductivity (EC) was measured with an EUTECH Instruments 2700 series conductimeter.

The packing quality was evaluated by means of two approaches based on the analysis of the retention times distribution curve (RTD) obtained by calculating point by point the derivative of the sigmoidal experimental curve of normalized EC versus time provided by the fluid-dynamic test [61,73]. The first approach is based on the *Theoretical Plate Model*: the number of theoretical plates N_{tp} can be evaluated as:

$$N_{tp} = 5.54 \cdot (t_R/w_{1/2})^2 \quad (3.4)$$

where t_R indicates the retention time of the RTD curve and $w_{1/2}$ its width at half-height. The height equivalent to a theoretical plate (*HETP*) can then be calculated as L/N_{tp} , where L indicates the column length. A high-quality column packing is characterized by a value of $HETP/d_p < 3$, where d_p indicates the average size of the packing particles [64]. The second approach is based on the *asymmetry factor* (A_s), defined as the ratio between the leading and tailing semi-width of the peak at 10%

of the peak height, and representing the peak deviation from a Gaussian curve. Its value should be as close as possible to 1 [64].

The frontal analysis data were also utilized to estimate the effective porosity (ε) and longitudinal dispersivity (α_L) of the resin packed bed. The former parameter was evaluated directly from the RTD curve according to the procedure proposed by Levenspiel [73], whereas the latter was estimated by best-fit of the experimental outlet concentrations with a 1-D convection-dispersion model:

$$\delta_i \cdot \frac{\partial C_{L,i}}{\partial t} = -v_{int} \cdot \frac{\partial C_{L,i}}{\partial z} + D_L \cdot \frac{\partial^2 C_{L,i}}{\partial z^2} \quad (3.5)$$

In Eq. (3.5) the retardation factor $\bar{\delta}_i$, equal to $1 + K_{eq,i} \rho_b / \varepsilon$, was set to 1 due to the absence of NaCl adsorption, the interstitial velocity v_{int} was calculated as $Q / (S_t \cdot \varepsilon_{resin})$ for the resin bed ($10 \text{ mm} < z < 515 \text{ mm}$) or $Q / (S_t \cdot \varepsilon_{sand})$ for the two sand layers ($z < 10 \text{ mm}$ and $515 \text{ mm} < z < 525 \text{ mm}$ or $1990 \text{ mm} < z < 2000 \text{ mm}$, according to the column length), and the equivalent diffusion coefficient D_L was approximately expressed as $\alpha_{L,resin} \cdot v_{int,resin}$ or $\alpha_{L,sand} \cdot v_{int,sand}$ [47]. The integration of Eq. (3.5) was performed with the time-dependent convection/diffusion module of the finite element PDE solver Comsol Multiphysics 3.5a, using as input values the estimates of ε_{sand} and $\alpha_{L,sand}$ obtained in preliminary tests and the value of ε_{resin} estimated as described above. As for $\alpha_{L,resin}$, its best-fit value and the 95% confidence interval were determined by applying the Gauss-Newton method, following the procedure illustrated by Englezos and Kalogerakis [74] and later adapted to convection-dispersion problems by Zama et al. [75]. In particular, the integration of Eq. (3.5) was repeated for different values of α_L , until the minimization of the sum of the squared residuals between experimental and calculated values at the column outlet. As a convergence criterion, the Gauss-Newton algorithm was stopped when the relative variation in $\alpha_{L,resin}$ resulted $< 10^{-3}$. This procedure was implemented by means of a dedicated MATLAB code.

3.9.2 Fluid dynamic test CDP Packed Bed

For the Ty and HTy adsorption system, the fluid dynamic test performed was the same using the WTW LF 296 conductimeter with a WTW Tetracon 325 electrode, both coupled in the SIMA-tec Allrounder 15 pilot plant, so the pipe at the column exit was connected to the conductimeter system inlet of this second pilot plant. A NaCl 0.01M solution was used as tracer and was fed at the same liquid linear velocity of the adsorption tests (section 3.10).

3.10 Adsorption Process:

3.10.1 Breakthrough tests and simulations for Amberlite Resins

In the case of the Amberlite XAD 16 resin, after packing the column with the second procedure, several adsorption breakthrough tests were performed with the experimental OMW, at different superficial velocities from 0.8 cm/min to 7.6 cm/min and at two different column lengths (0.525 m and 2.000 m). These velocities were selected on the basis of the values typically used in similar studies [37, 38, 76-80]. The breakthrough test were performed at room temperature. The pre-treated OMW was fed downwards with a Masterflex L/S 0.1 HP 1-100 RPM peristaltic pump. Both pressure drop and temperature were measured hourly. The total PCs concentration was measured with the HPLC method in OMW samples taken every hour from the column exit and every 3 hours from the inlet, whereas COD was measured in selected samples at the column inlet and outlet. The average PCs concentration and COD values at the inlet were used to normalize the corresponding outlet values. Continuous-flow dephenolization processes are typically stopped in correspondence with the attainment of a relatively low PCs level at the column outlet, the break-point (e.g., $C_{OUT}/C_{IN} = 0.10-0.20$). However, in the initial experimental tests were continued up to outlet normalized PC concentrations varying between 0.56 (bt 1) and 0.65 (bt 2), in order to increase the extension of the

experimental breakthrough curve, and thus the reliability of the subsequent model simulations. The following adsorption tests were performed until 0.2 – 0.3 of normalized concentrations.

In order to validate the proposed PCs adsorption method, a repeatability test was performed by conducting four adsorption/desorption cycles at the same conditions (same packed bed and liquid linear velocity of 5.0 cm/min), using the procedure described above, with the resin Amberlite XAD 16.

The experimental normalized PCs and COD breakthrough curves were interpreted by means of two types of 1-D convection-dispersion models, in order to study the key controlling phenomena, to evaluate the process efficiency and to set up the basis for a model-based optimization and scale-up of the process. A first set of simulations was performed under the hypothesis of local adsorption equilibrium and linear adsorption isotherm (on the basis of the results of the PC isotherm studies). In these simulations, the normalized PC and COD concentrations were interpreted with Eq. (3.5), with the retardation factors δ_{PCs} or δ_{COD} expressed as $(1+K_{eq,PCs} \cdot \rho_b / \epsilon_{resin})$ or $(1+K_{eq,COD} \cdot \rho_b / \epsilon_{resin})$ for the resin layer ($10 \text{ mm} < z < 515 \text{ mm}$ or 1990 mm , according to the column length used) and set to 1 for the two sand layers. The bulk density ρ_b was calculated as the mass of dry resin introduced during the packing process divided by the volume of the column portion occupied by resin. Using the estimates of ϵ_{resin} and $\alpha_{L,resin}$ obtained from the fluid-dynamic test as input values, the equilibrium constants $K_{eq,PCs}$ and $K_{eq,COD}$ relative to each breakthrough test were estimated by best-fit on the corresponding experimental concentrations following the Gauss-Newton method described in section 3.8. As a convergence criterion, the algorithm was stopped when the average parameter variation resulted $< 10^{-3}$.

In a second set of simulations, conducted under the hypothesis of not negligible mass-transfer resistance and linear isotherm, the normalized outlet PCs and COD were interpreted with the following equation:

$$\frac{\partial C_{L,i}}{\partial t} = -v_{int} \cdot \frac{\partial C_{L,i}}{\partial z} + D_L \cdot \frac{\partial^2 C_{L,i}}{\partial z^2} - k_L a \cdot \left(C_{L,i} - \frac{C_{S,i}}{K_{eq,i}} \right) \quad (3.6)$$

where $C_{L,i}$ indicates the PCs or COD liquid phase concentration, $C_{S,i}$ the corresponding solid-phase concentration (g/g_{dry resin}) and k_La the mass-transfer coefficient. In this model internal and external mass transfer phenomena are expressed by means of an overall volumetric coefficient and an overall driving force [56]. The same k_La value was assumed to be valid for PCs and COD. The presence of a solid-phase concentration independent of the liquid-phase concentration requires the addition of the mass-balance relative to $C_{S,i}$, characterized by the absence of any convection or dispersion:

$$\frac{\rho_b}{\epsilon} \cdot \frac{\partial C_{S,i}}{\partial t} = k_La \cdot \left(C_{L,i} - \frac{C_{S,i}}{K_{eq,i}} \right) \quad (3.7)$$

In these simulations, while k_La_{sand} and $K_{eq,sand}$ (for $z < 10$ mm and 515 mm $< z < 525$ mm or 1900 mm $< z < 2000$ mm according to the column length used) were set equal to zero, both $K_{eq,PCs}$ and k_La_{resin} (for 10 mm $< z < 515$ mm or 1900 mm according to the column length used) were estimated by best-fit on the experimental PC concentrations following the Gauss-Newton method, and the resulting value of $K_{eq,PCs}$ was compared to that obtained from the corresponding PCs isotherm. In the COD simulations, only $K_{eq,COD}$ was estimated by best-fit on the experimental COD concentrations, whereas the k_La_{resin} best estimate obtained from the corresponding PCs breakthrough test was used as an input value. For both sets of simulations, the quality of each best fit was evaluated by means of the correlation coefficient R^2 , defined so as to allow the comparison of models with different numbers of parameters [81]:

$$R^2 = 1 - \frac{\left[\frac{\sum_{j=1}^N (C_{L,measured,j} - C_{L,calculated,j})^2}{N-P-1} \right]}{\left[\frac{\sum_{j=1}^N (C_{L,measured,j} - \bar{C}_{L,measured})^2}{N-1} \right]} \quad (3.8)$$

where N indicates the number of experimental data and P the number of parameters evaluated by best fit on the experimental data (1 or 2, depending on the set of simulations).

For each breakthrough test, the best-fitting simulation was utilized to estimate two types of parameters useful for the evaluation of the adsorption process performance: the PCs and COD adsorption yields $Y_{ads,PCs}$ and $Y_{ads,COD}$, and the resin utilization efficiency (or percent utilization) η_{resin} , complementary to the normalized length of unused bed [56]. Both types of parameters were evaluated relatively to the fraction of breakthrough curve comprised between $C_{PC,OUT}/C_{PC,IN} = 0$ and $C_{PCs,OUT}/C_{PCs,IN} = 0.20$, so as to obtain data representative of a hypothetical industrial process. The adsorption yields $Y_{ads,i}$ were evaluated as $m_{i,sorbed,20\%} / m_{i,fed,20\%}$, where $m_{i,sorbed,20\%}$ indicates the PCs or COD mass adsorbed until the attainment of a 20% outlet normalized PCs concentration, and $m_{i,fed,20\%}$ indicates the corresponding PCs or COD mass fed to the column. $m_{i,sorbed,20\%}$ was estimated as:

$$m_{i,sorbed,20\%} = m_{i,fed,20\%} - m_{i,out,20\%} \quad (3.9)$$

where $m_{i,out,20\%}$ is the mass lost in the outlet up to the 20% breakpoint. Eq. (3.9) neglects the liquid phase PCs content at the 20% breakthrough point, which is generally negligible and whose fate is determined by the process choices on how to move from the adsorption phase to the regeneration step. $m_{i,out,20\%}$ was calculated by integrating the breakthrough curve:

$$m_{i,out,20\%} = Q \cdot \int_0^{t_{20\%}} C_{L,i,OUT} \cdot dt \quad (3.10)$$

A more compact expression for $m_{i,sorbed,20\%}$ can be obtained combining Eqs. (3.9) and (3.10):

$$m_{i,sorbed,20\%} = Q \cdot \int_0^{t_{20\%}} (C_{L,i,IN} - C_{L,i,OUT}) \cdot dt \quad (3.11)$$

The integrals in Eqs. (3.10) and (3.11) were calculated by numerical integration of the best-fitting simulated outlet concentrations.

The resin utilization efficiency η_{resin} represents the fraction of adsorption bed capacity actually utilized. It was evaluated, only for PCs adsorption, as:

$$\eta_{resin} = \frac{m_{PCs,sorbed,20\%}}{m_{PCs,sorbed,sat.}} \quad (3.12)$$

where $m_{PCs,sorbed,sat}$ indicates the PCs mass theoretically adsorbed by the resin upon saturation of the sorption capacity. If the equilibrium constant is known, $m_{PCs,sorbed,sat}$ can be evaluated as $K_{eq,PCs} \cdot C_{L,PCs,IN} \cdot m_{resin}$. Alternatively, by extrapolating the best fitting simulation, it can be estimated as $Q \cdot \int_0^{t_{99.9\%}} (C_{L,i,IN} - C_{L,i,OUT}) \cdot dt$ where $t_{99.9\%}$ indicates the time theoretically corresponding to the attainment of an outlet PCs concentration equal to 99.9% of the inlet value.

For the resin Amberlite IRA 958Cl, two breakthrough tests were performed at 5.0 cm/min and 2.1 cm/min, using the same procedure described for Amberlite XAD 16 above for PCs and for COD adsorption. Simulations were not performed because of the not very good results observed with this resin, which is going to be discussed in the chapter 4.

3.10.2 Breakthrough test for CDP

In the CDP adsorption case, four tests were performed in one column (13.0 cm of length) using the OMW “Imperia 2014”, fed at 0.87 cm/min, 0.58 cm/min and 0.44 cm/min for 1h. Samples at the column outlet were taken every 3 min, and 3 samples of the feed were taken in different moments during the test. Each sample was analysed with the HPLC method for tyrosol and hydroxytyrosol. The average Ty and HTy concentrations at the inlet were used to normalize the corresponding outlet

values. The analysis of the experimental data was done as described for the Amberlite XAD 16 for PCs, the COD adsorption was not studied in this case.

3.11 Desorption-regeneration tests

3.11.1 Desorption-regeneration tests for Phenolic Mixture Recovery

For the phenolics mixture recovery, to desorb and recover the PCs, at the end of each adsorption test acidified ethanol (0.5% v/v HCl 0.1N) was fed from the top of the column with a Masterflex L/S 0.1 HP -1-100 RPM pump. The solvent flow rate was initially set to the OMW flow rate of the corresponding adsorption test. However, due to the increase in solvent viscosity associated to the increase in PCs dissolved concentration, a gradual decrease in solvent flow rate was required in order to maintain the total pressure at the column inlet < 2 bars. Desorption was continued until the attainment of a PC concentration < 5% of the average inlet concentration during the adsorption step. This criterion corresponded to a total desorption time equal to 5 *HRTs* for Amberlite XAD 16. The desorbed extract was submitted to low-pressure distillation in a rotatory evaporator (LABOROTA 4002 Heidolph, Schwabach, Germany), in order to regenerate the solvent and recover the desorbed matter. Temperature was kept at 30°C with a Heizbad WB Heidolph thermostated bath (Schwabach, Germany), and vacuum (0.5 bar of absolute pressure) was applied with a Vacuubrand diaphragm vacuum pump (Wertheim, Germany). Water at 5°C was used as coolant. Preliminary tests indicated that desorption with acidified ethanol is also an effective resin regeneration method for Amberlite XAD 16. On the basis of the integral PCs concentration measured in the ethanol collected from the column outlet, the desorption yield $Y_{des,PCs}$ was evaluated as $m_{PCs,desorbed,total} / m_{PCs,sorbed,total}$.

The same procedure was applied for PCs desorption and bed regeneration in the case of Amberlite IRA 958Cl.

3.11.2 Desorption-regeneration tests for Tyrosol and Hydroxytyrosol Recovery

For desorbing Ty and HTy, a batch test was performed with 7 different organic solvents or their mixtures with water or acidified water (0.5% v/v HCl 0.1N). For this test, 2.0g of CDP were added to 25mL of ethyl acetate, methanol, methanol/water (60%/40%), acidified water (0.5% v/v HCl 0.1N), dicloromethane, methanol/acidified water (20%/80%) and acetonitrile/acidified water (15%/85%). The flasks were shaken at 140 rpm for 2h. According to the results of this experiment, as first approach for continuous desorption, pure methanol fed from the column bottom was used, but the obtaining of elution fractions with low concentrations of Ty and HTy leads to the implementation of a gradient of three mobile phases: acidified water (0.5% v/v HCl 0.1N), acetonitrile and methanol as it is presented in the table 3.3. Samples in the column outlet were taken every 3 minutes, the desorption was stopped when the concentrations of Ty and HTy were not detected by the HPLC. The desorption yields were calculated as $m_{Ty,desorbed,total} / m_{Ty,sorbed,total}$ and $m_{HTy,desorbed,total} / m_{HTy,sorbed,total}$, for Ty and HTy, respectively. After desorption, the column was rinse with demineralized water, no further treatment was necessary before starting a new adsorption cycle.

Time (min)	Solvent
0 min to 15 min	Acidified water
15 min to 30 min	95% Acidified Water + 5% Acetonitrile
30 min to 42 min	85% Acidified Water + 15% Acetonitrile
42min to 72 min	75% Acidified Water + 25% Acetonitrile
72 min to 84 min	80% Acidified Water + 20% Methanol
84 min to 99 min	40% Acidified Water + 60% Methanol
99 min to 159 min	100% Methanol

Table 3.4 Solvent gradient for Ty and HTy desorption.

3.12 Preliminary Economic Analysis for Phenolic Mixture Recovery with Amberlite XAD 16

In order to evaluate the economic feasibility of the proposed adsorption process for the PCs recovery some assumptions for the hypothetical industrial process were considered (table 3.5).

Process Characteristics		
Plant production (OMW treated / year)	10000	m3/y
No. of cycles with the same resin	50	
Column length	2	m
Column diameter	0.42	m
Pump efficiency	0.65	
Ethanol loss per cycle	4	%

Table 3.5 Process assumptions for preliminary economic analysis.

With the results obtained, an evaluation of the factor which impacted significantly the total process cost, was done. Also, a way to calculate the cost resin replacement is presented in the section 4.7.

3.13 Amberlite IRA 958Cl and Amberlite IRA 67Cl Resin Screening

In order to test the performance for PCs adsorption of two ionic-exchange resins some batch experiments were conducted. The resins were tested at different conditions of pH (OMW pH, pH 6 and pH 7, adjusted with a NaOH 10M solution) and with and without VFA presence (acetic acid 2.0 g/L, propionic acid 1.0 g/L, butyric acid 2.0 g/L and valeric acid 1.0 g/L, to mimic the VFAs concentration in an

anaerobically digested OMW). The VFA influence in PCs adsorption was evaluated because the possibility of feeding anaerobically digested OMW to the adsorption columns was considered, as part of an experimental change in the bio-refinery process in which the adsorption column is one of the first steps.

The OMW at each condition were prepared the day before the test, and were left in the fridge overnight at 4°C. Inside microcosms bottles were poured 25 g of each resin (dry weight), and after that, 50 mL of sample of OMW were put inside. The filled bottles were closed and left in a shaker at 140 rpm and at room temperature (24°C). In the initial test, samples were taken at 3h and 24h, because of not concentration change in the liquid, for the following experiments, the total time was fixed at 3h. After 3h, all the liquid phase was taken and the flasks were filled with NaOH 3% (w/v) or acidified ethanol (0.5% v/v with HCl 0.1N), then they were closed. The bottles were shaken at 140 rpm for 3h. Finally, all the liquid phase was collected. The samples were left in the fridge before starting the analysis. The Total Phenols concentration was measured with the HPLC method (section 2.3.1). For the samples in NaOH, the pH was corrected (pH 5) with HCl 1M, before analysis.

COD concentration was measured with the COD Aqualytic COD kit (section 2.3.5). For the samples in NaOH, the pH was corrected (pH 5) with HCl 1M, before analysis. For the samples in acidified ethanol, the ethanol was stripped with nitrogen, and the samples were re-suspended in the same volume of distilled water.

VFA concentration was measured with the HPLC (section 2.3.11). For the samples in NaOH the pH was corrected by diluting the sample 5 times in the HPLC mobile phase, and then 50µL of H₂SO₄ 4N, were added to reach a final pH near to 2 (the pH of the HPLC mobile phase). For the samples in acidified ethanol, the ethanol was stripped with nitrogen, and the samples were re-suspended in the same volume of distilled water, this step was necessary because the ethanol has the same retention time of the isobutyric acid.

CHAPTER 4

RESULTS AND DISCUSSION: RECOVERY OF PHENOLICS MIXTURES

In this chapter the continuous flow solid-liquid extraction of a phenolic mixture from olive mill wastewaters using different commercial resins is discussed. A simulation model is proposed and evaluated with the experimental data. Also a preliminary cost study is done for the process with the resin Amberlite XAD 16.

4.1 Ancillary results: PCs analytical method selection

The HPLC PCs method was studied in order to develop a fast, precise and automatable analytical tool to assess the adsorption performances, whereas it was not meant as a substitute of the Folin-Ciocalteu (FC) method, widely adopted for PCs content assessment. Indeed, neither method guarantees that all and only phenolic compounds will be detected: the HPLC method could in principle sum non-phenolic compounds to the actual PCs and/or fail to detect specific PCs, whereas the FC method can be characterized by an interference due to other organic compounds present in OMW (i.e. proteins and carbohydrates). Both the traditional FC method and the proposed HPLC method treat the PCs mixture as a pseudo component, expressing the total PCs concentration as specific PC equivalent (gallic acid in this case). These methods thus avoid the complexity of taking into account the contribution of each single compound. This approximation is less severe in the case of the FC method, which recognizes the chemical functionality by the selective colorimetric reaction. For that reason, some preliminary cross-checks between the two methods were carried out.

In the first place, the PCs content in the studied Imperia 2012 OMW was measured using both methods (Table 4.1). As expected, the total PCs concentrations measured with the two methods were not equal, and a 36% lower value was

observed with the HPLC method. In order to strengthen the comparison between the two methods, the same type of analysis was applied to a different OMW, characterized by a higher PCs concentration and by a different PCs composition (Gallipoli 2012 OMW, produced in the Apulia Region in Southern Italy, See table 4.2). As shown in Table 4.1, the agreement between the two methods is similar. On the other hand, the low relative errors associated to the HPLC method (equal to about 1/3 of the FC relative errors) indicate that the HPLC method is significantly more precise.

OMW type	Imperia 2012	Gallipoli 2012
Folin-Ciocalteu method (g/L)	1.96 ± 0.37	4.14 ± 0.81
HPLC method (g/L)	1.26 ± 0.09	2.79 ± 0.16
Deviation between the two methods	36%	33%

Table 4.1 PCs concentrations measured in two distinct OMWs with the Folin Ciocalteu colorimetric method and with the HPLC method: average values ± 95% confidence intervals.

Finally, PCs concentration in the samples taken at the column outlet during one of the breakthrough tests performed in this work (Bt2), conducted at 30°C and 2.4 cm/min) was analyzed with both methods. This validation test was aimed at checking the capacity of the HPLC method to mimic the FC results in the characterization of the adsorption process. As different PCs are eluted at different breakthrough times, the outlet composition is continuously changing. Thus, this test is far more severe than the simple comparison of total OMW PCs. The results are shown in Fig. 4.1 in terms of dimensionless outlet PCs concentration versus dimensionless time, defined as time / HRT. The deviation between the two methods ranged between 0.4% and 17%, with an average value (10%) comparable to the relative analytical errors. The scrutiny of Fig. 4.1 confirms the higher precision of the HPLC method. On the basis of these results, the HPLC method was selected as the reference method for this study.

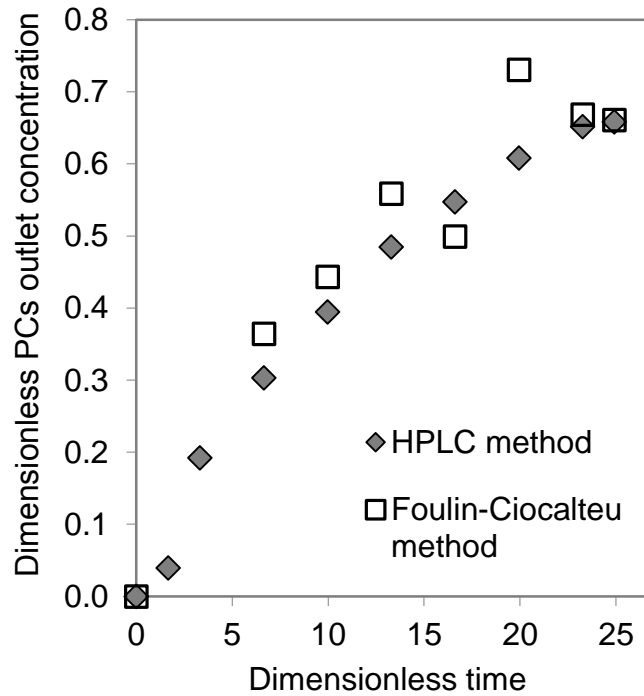


Figure 4.1 Dimensionless outlet PCs concentration versus dimensionless time for breakthrough test n. 2 (30°C, 1.44m/h): comparison between the HPLC method and the Folin-Ciocalteu method.

4.2 Olive Mill Wastewaters (OMW) Characterization

The main characteristics of the different OMW analysed are displayed in Table 4.2. The results presented were obtained with the procedures described in section 3.3 of chapter 3.

OMW	IMPERIA 2012	IMPERIA 2013	IMPERIA 2014	GALLIPOLI 2012
Total phenols Content (g/L)	1.6	0.51	0.8	2.9
Total solids (g/L)	34	13	N.A	77
Suspended solids (g/L)	0.7	4.5	N.A	40
Disolved solids (g/L)	33	8	N.A	37
COD (g/L)	32	21	32	69
Total carbohydrates (g/L)	5.4	23	16.2	16.8
Density (g/mL)	1.01	1.00	1.01	1.02
pH	4.60	4.59	4.96	4.62

Table 4.2 Main characteristics of the tested “Imperia 2012”, “Imperia 2013”, “Imperia 2014” and “Gallipoli 2012” OMW.

All the procedures were applied in triplicated. For the total phenols content was applied the hplc method described in section 3.3.1 to three samples of the inlet OMW before starting each breakthrough test.

4.3 Adsorption Kinetics for Amberlite XAD 16

In order to obtain the time in which the equilibrium of the system is achieved, experiments of adsorption kinetics were performed for all the studied systems.

The adsorption kinetics for the resin *Amberlite XAD 16* were obtained according to the procedure described in the section 3.5. The results achieved with the OMW Imperia 2012 are displayed in the following graph.

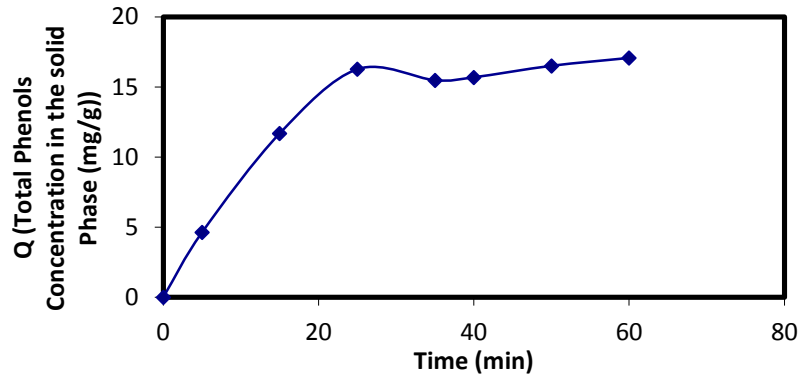


Figure 4.2 Adsorption Kinetics for the Amberlite XAD 16 and the OMW Imperia 2012.

The concentration of total phenols was measured in the liquid phase, so their concentration in the solid phase was obtained indirectly using the expression:

$$Q \left(\frac{mg}{g_{dry\ resin}} \right) = \frac{(C_{Lo} - C_{Li}) \times Vol}{W_{dry\ resin}} \quad (4.1)$$

Where

Q is the mass of total phenols per gram of dry resin

C_{Lo} is the initial concentration of total phenols in the liquid phase

C_{Li} is the total phenols concentration in the sample

Vol is the total volume of the liquid phase

$W_{dry\ resin}$ is the mass of dry resin

According to the results plotted, the dynamic equilibrium is reached at approximately 1 hour.

Similar results were obtained for the OMW Imperia 2013 and Imperia 2014 with the same solid phase (Amberlite XAD 16).

4.4 Adsorption Isotherms for Amberlite XAD 16

The adsorption isotherms describe the equilibrium relation between the liquid and the solid phases that are in contact.

The adsorption isotherms were obtained at different temperatures for all the OMW-resin systems studied.

This resin was the most studied adsorbent phase, so the adsorption isotherms were obtained at different temperatures with the OMW Imperia 2012 and Imperia 2013. All isotherms were achieved using the procedure described in the section 3.6.

4.4.1 OMW Imperia 2012

The isotherms were obtained at 21°C and 35°C. The results obtained are displayed in the following graph.

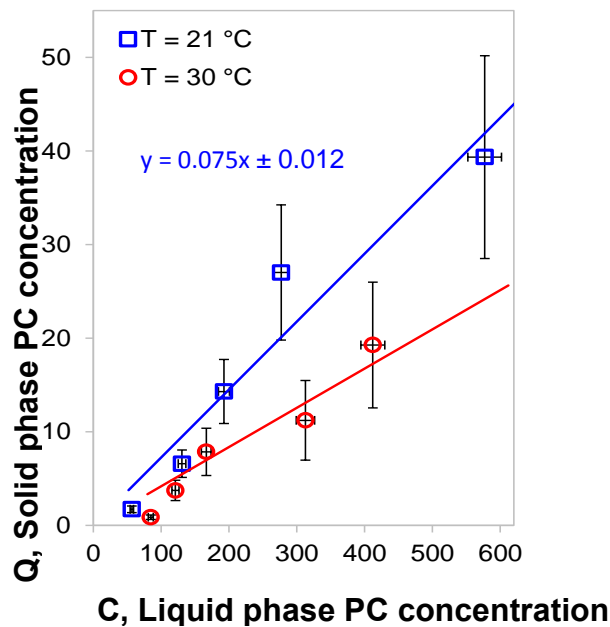


Figure 4.3 Adsorption isotherm for the system OMW Imperia 2012-Amberlite XAD 16 at 21°C and at 35°C.

As it is expected, the adsorption constant is higher when the temperature is lower.

4.4.2 OMW Imperia 2013

The adsorption isotherms for the OMW Imperia 2013 were obtained as it is described in the section 3.6 of the chapter 3.

In this case, to be sure that the isotherm could be considered linear also at high adsorption grade, the OMW Imperia 2013 were concentrated through a rota evaporator system, thus the last two points of the isotherms were concentrated to 1/3 and 2/3 of the initial volume, respectively.

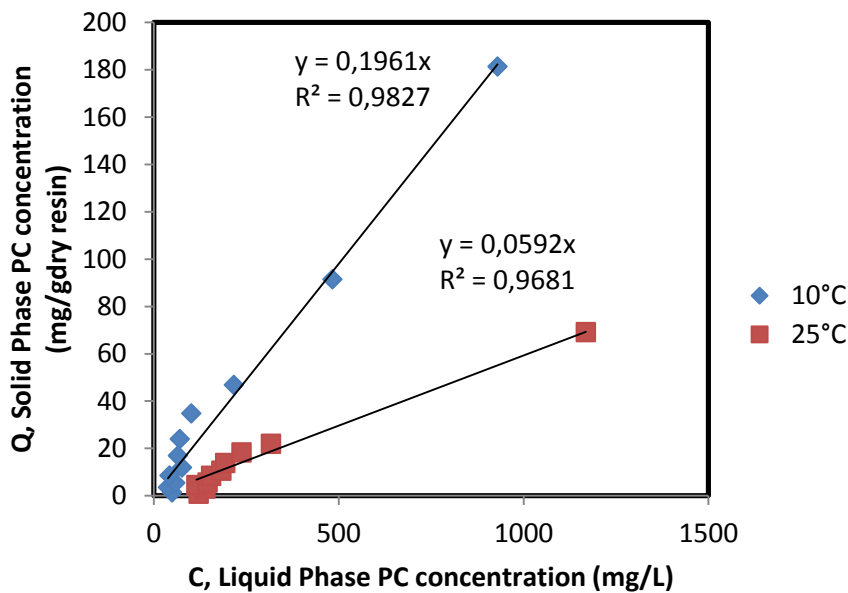


Figure 4.4 Adsorption isotherm for the system OMW Imperia 2013-Amberlite XAD 16 at 10°C and at 25°C.

Despite the quite high data dispersion in the four isotherms, the points seem to follow a slightly pronounced sigmoidal curve that might result from the competitive adsorption of multiple PCs, measured by the selected analytical method as a single equivalent compound. Nevertheless, as shown in Fig. 4.4, at all tested temperatures a linear interpolation – corresponding to the initial linear part of the Langmuir curve – resulted in acceptable R^2 values. Indeed, the almost linear behavior of these isotherms is reasonable considering that the resin adsorption capacity (370 mg/g_{dry resin}, referred to medium molecular weight compounds; Table

3.1) is almost 10 times higher than the maximum concentration of sorbed PCs attained in these tests (47 mg/g_{dry resin}, without considering the last two concentrated points as the OMW Imperia 2013 isotherms). Also, with the concentrated points in the isotherm of the OMW Imperia 2013, still, a linear behaviour is observed. Thus, other types of interpolations were not taken into consideration. The best estimates of $K_{eq,PC}$ obtained from the isotherms of Fig. 4.3 and 4.4 are in agreement with the results of Bertin et al. [28], who tested XAD16 on a different OMW. Although Bertin et al. [28] used both a Langmuir and a Freundlich isotherm, their experimental data correlate very well with a straight line corresponding to an equilibrium constant of 58 L/kg_{dry resin}, versus 42-193 L/kg_{dry-resin} in this study.

4.5 Fluid Dynamic Characterization for Amberlite XAD 16

In order to evaluate the packing procedure and to calculate some important parameters for the adsorption process (bed porosity and residence time) fluid dynamic tests of stimulus/response with step disturbance using NaCl as tracer, as it was described in the section 3.8.

The tests were performed after each packing procedure and during the repeatability test (discussed later), after each adsorption/desorption cycle.

The initial fluid dynamic tests were done to evaluate the packing quality of the bed. The packing was achieved using the first procedure described in the section 3.9, using demineralized water with acidified ethanol as solvent for the resin slurry. Then, for the next tests the second packing procedure explained in the same section, was applied. Before choosing that packing procedure, a comparison of the packing quality was done in order to choose the most reliable and most repeatable procedure. The packing quality and the repeatability of the parameters calculated from it affect directly the adsorption performance of the column, so the selection of the right packing procedure is a crucial step for an adsorption process.

In the figure 4.5 there is shown as a representative example a *Cumulative Retention Time Curve* or *F Curve*, obtained during one of the fluid dynamic tests performed (superficial velocity range 2.0 cm/min to 5.1 cm/min).

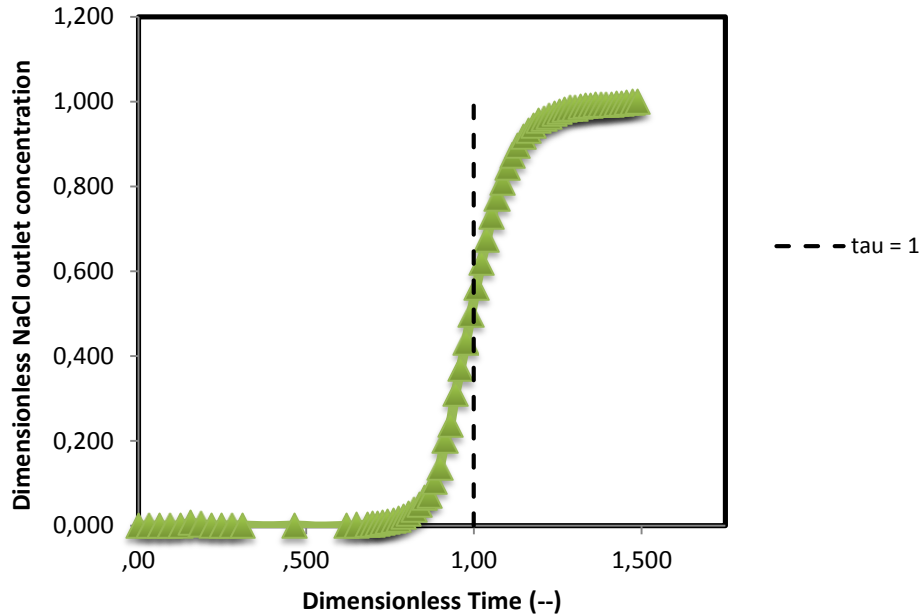


Figure 4.5 *F Curve* after column packing. Liquid superficial velocity of 5.03 cm/min.

The uniformity of the sigmoidal curve means a good packing quality. Deriving the *F* curve it is possible to obtain the *Retention Time Curve* or *E Curve* from which is possible to calculate the different parameters that characterize the packing (*N*, *HETP*, *h* and *A_s*, see section 2.7).

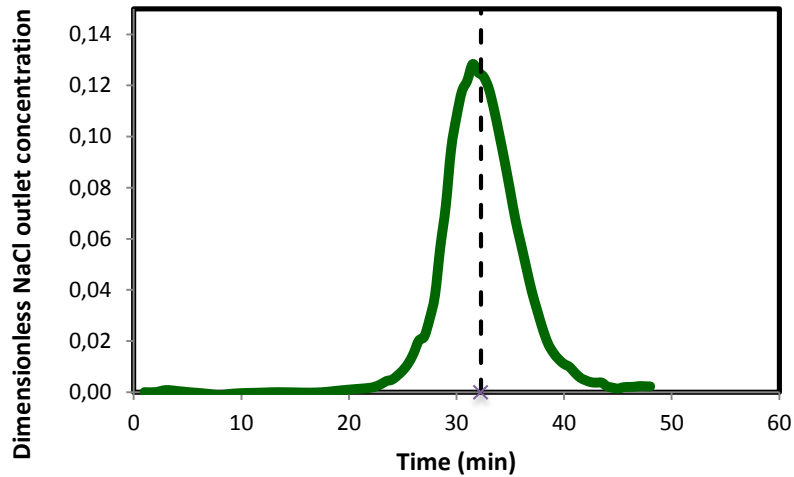


Figure 4.6 *E Curve* obtained by derivation of *F curve*. Liquid superficial velocity of 5.03 cm/min.

As it was said before, two column packing methods were applied in order to decide the best one for our purposes. The obtained results are presented in the table 4.3.

Parameter	First packing procedure (Acidified ethanol)	Second packing procedure (Demineralized water)
No. of theoretical plates (N)	93	117
Height of theoretical plate / d_p (h)	7.5	0.32
Asymmetry factor (As)	0.82	1.10

Table 4.3 Comparison between the two column packing procedures evaluated.

With the second packing procedure, the column has a higher number of plates, a *reduced plate height (h)* minor than 3 [64], and the asymmetry factor is nearer to 1, all of them, characteristics of a very high quality packing. Thus, the second column packing procedure was chosen as the method to pack our adsorption column.

Then, in order to evaluate the stability of the packed bed, a fluid dynamic test was performed after each adsorption cycle during an adsorption repeatability test. After each test the repeatability of the porosity value was evaluated. The obtained results are shown in the table 4.4.

Breakthrough test No.	Superficial Velocity (m/s)	τ (min)	Porosity %
Breakthrough 3	5,03	32,3	83,6
Breakthrough 4	4,88	32,5	81,6
Breakthrough 5	5,13	33,5	88,2
Breakthrough 6	5,07	33,9	89,1

Table 4.4 Porosity values obtained from fluid-dynamic test after each adsorption/desorption cycle during an adsorption repeatability test.

It can be noticed that the porosity values changes slightly, this can be explained for the formation of preferential paths in the packed bed.

Another important factor for the fluid dynamic characterization is the *longitudinal dispersivity* (α_L), which was calculated by best-fit of the experimental data with the equations 2.6 and 2.16. The system was solved by a Gauss-Newton algorithm. With this calculation methodology, also the porosity values are re-evaluated, the simulated values are in agreement with the obtained directly with the experimental data.

Figure 4.7 shows an experimental F curve and the obtained one with the best-fit of the 1D-fluy dynamic model. As it is evident, the best fit of the experimental points is very good, with a R^2 equal to 0.9994.

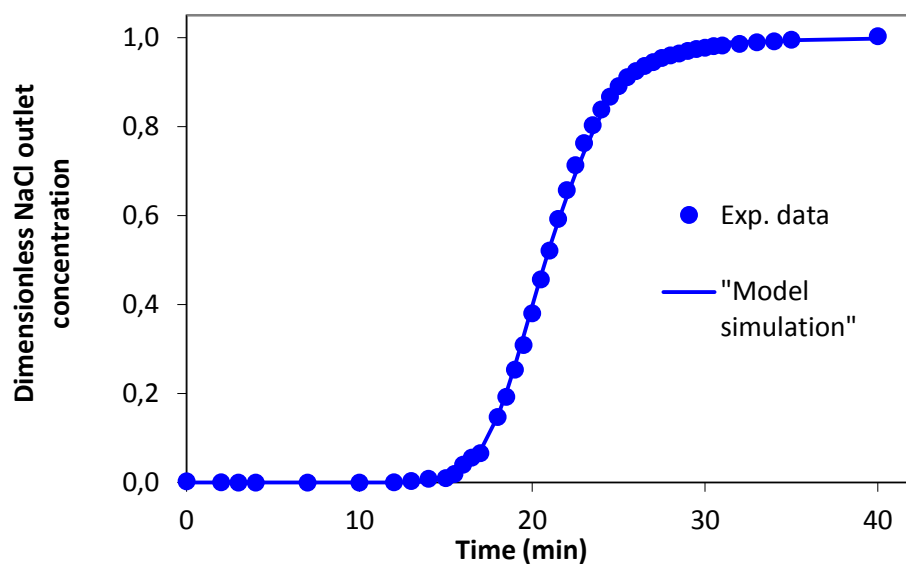


Figure 4.7 Fluid-dynamic test at 2.04 cm/min. Experimental dimensionless NaCl concentration at the column exit and corresponding best-fitting simulation.

The longitudinal dispersivity values obtained for all the fluid dynamic tests performed for the Amberlite XAD 16 are presented in the table 4.5.

Breakthrough Test No.	Longitudinal Dispersivity (m)
1	0,0041 +/- 0,0002
2	0,0040 +/- 0,0002
3	0,0088 +/- 0,0002
4	0,0191 +/- 0,0004
5	0,0290 +/- 0,0004
6	0,0323 +/- 0,0010
7	0,0552 +/- 0,0017
8	0,0620 +/- 0,0020

Table 4.5 Longitudinal dispersivity values obtained for all the fluid dynamic tests performed for the Amberlite XAD 16 with 95% confidence interval.

4.6 OMW pre-treatment

With regards to the OMW pre-treatment required before feeding the adsorption column, the suspended solid removal was equal to 91.5% after the initial centrifugation step (4000 rpm, 30 minutes), and to 98.5% after the entire pre-treatment sequence (centrifugation + 25 μm filtration + 11 μm filtration). Despite the high removal obtained with only centrifugation, preliminary breakthrough tests performed with centrifuged but unfiltered OMW in the Amberlite XAD 16 bed, led to a marked increase in pressure drop across the column (from 0.1 to 1 bar). Conversely, the complete pre-treatment allowed the operation of 36-hour breakthrough tests with modest pressure drop increases (from 0.1 to 0.3 bar, corresponding to a total pressure in the column inlet of 1.1-1.3 bars), that were completely reversed during the subsequent desorption step. The PCs removal associated to the complete pretreatment sequence, measured with the HPLC method, resulted equal to 7-8%.

Because of the good results obtained with the complete pre-treatment of OMW for Amberlite XAD 16 case, the same procedure was applied before feeding OMW at Amberlite IRA 958Cl bed, no pressure problems were observed during the adsorption tests.

Also in the CDP bed the pressure did not present problems during the breakthrough tests after OMW pre-treatment.

4.7 Phenolic compounds and COD Breakthrough tests for Amberlite XAD 16

In order to understand the phenolic and other organic compounds continuous adsorption some breakthrough experiments were performed, monitoring the phenolic compounds and the COD concentration at the column outlet.

The first two breakthrough experiments were done with a 0.52 m length column, at 0.8 cm/min and 2.4 cm/min. Usually, the adsorption is conducted until a limit of 5%-10% of the inlet concentration at the column outlet, but in these cases the

experiment continued until the 56% of breakthrough for the first test and 65% for the second one, in order to have more information to understand the continuous adsorption on the Amberlite XAD 16.

The results obtained are displayed in the figure 4.8, in the Y axis there are the normalized PCs outlet concentration and in the X axis the dimensionless time (t/HTR or t/τ). The Pcs concentration at the column outlet was normalized respect to the PCs concentration in the feed.

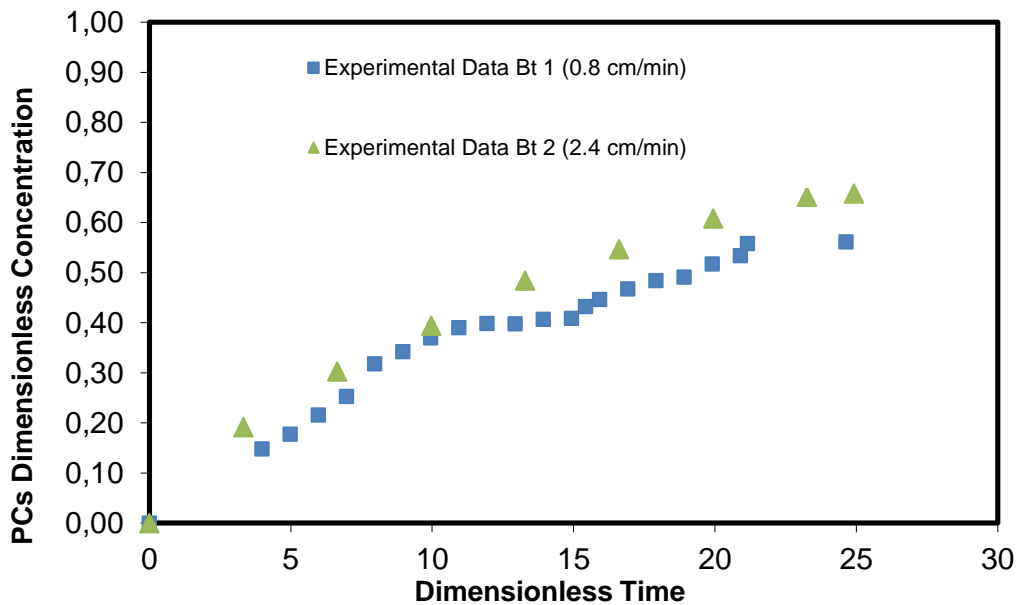


Figure 4.8 Experimental Breakthrough Curves at 0.8 cm/min (Bt1) and 2.4 cm/min (Bt 2) with a 0.52 m length column.

Following the procedure explained in the section 3.10, a set of the simulations was done under the hypothesis of local equilibrium. The best-fitting sigmoidal curves are completely incompatible with the experimental data, as it is presented in the figures 4.9a. and 4.9b.

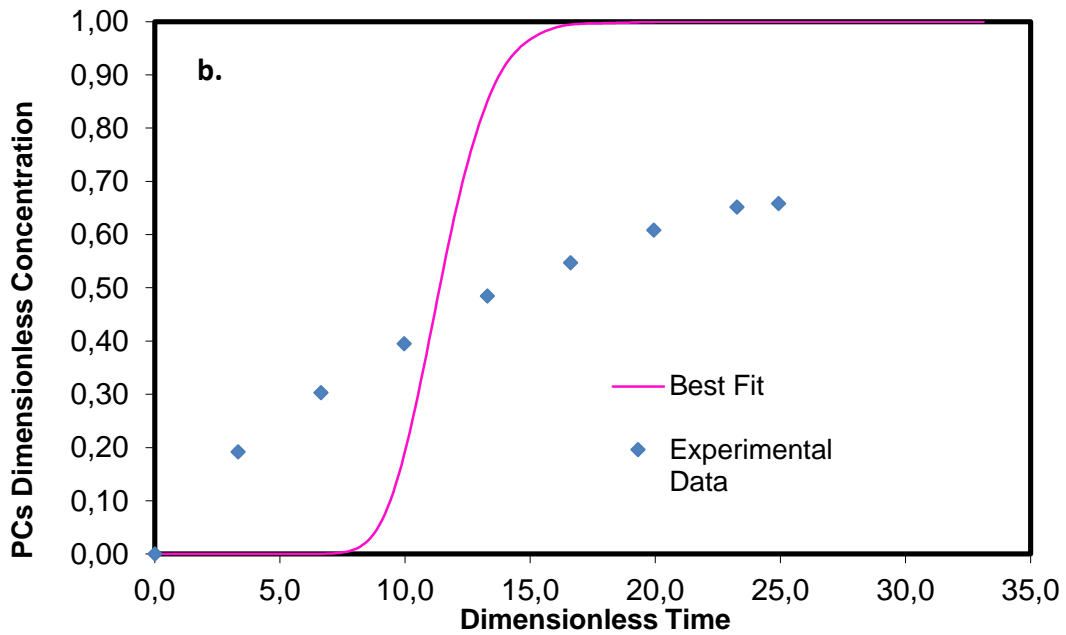
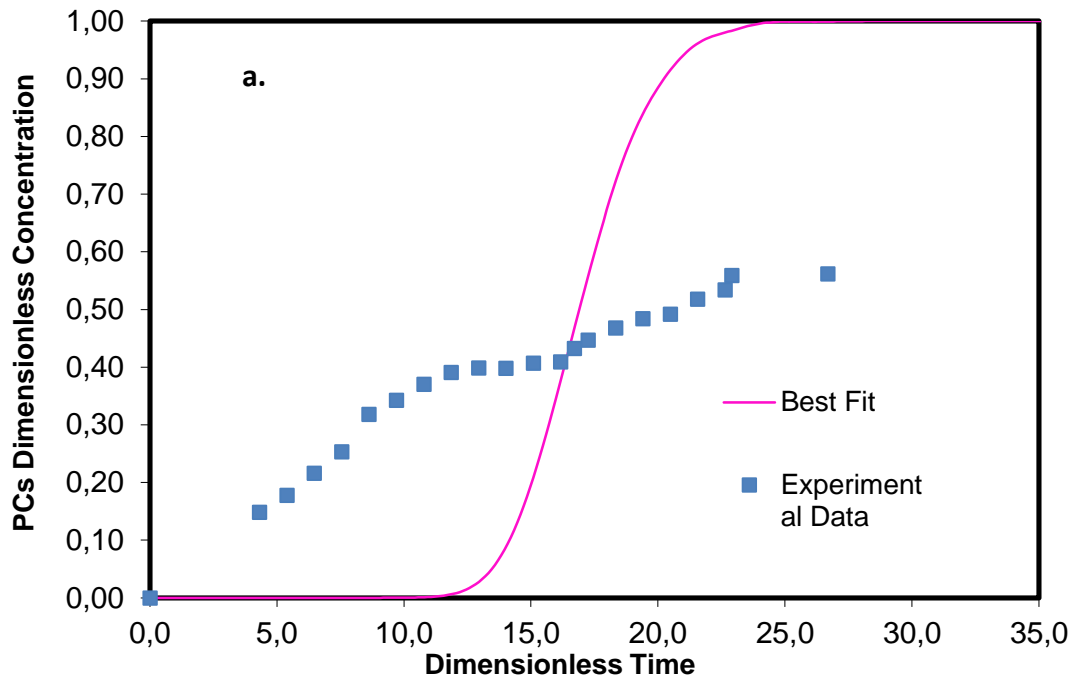


Figure 4.9 a.) Experimental Breakthrough Curve at 0.8 cm/min (Bt 1) and the respective Best Fit Curve obtained with the hypothesis of local equilibrium.

Figure 4.9 b.) Experimental Breakthrough Curve at 2.4 cm/min (Bt 2) and the respective Best Fit Curve obtained with the hypothesis of local equilibrium.

These results make evident that the mass transfer phenomena has to be taken into account in the simulation model. Thus, a second set of simulations were done with the hypothesis of non-negligible mass transfer resistance and linear equilibrium isotherm, using equations 2.27 and 2.28 (section 2.5). This consideration led to satisfactory simulations with R^2 in the 0.95-0.99. The K_{eq} obtained with the linear approximation of the experimental data are lower (28% for 21°C and 50% for 30°C) than the values obtained with the simulation model, this can be explained for the simplifying approximation of treating all the PCs as a single pseudo-component. With this hypothesis all the PCs are assumed to present a single breakthrough curve, whereas the observed experimental trends in the breakthrough experiments result from the combination of different, and possibly competing, adsorption curves. This time-changing adsorption equilibrium is not present in the isotherm experiments, where all the PCs are at equilibrium contemporaneously.

The curves obtained with the non-equilibrium model are displayed on figure 4.10.

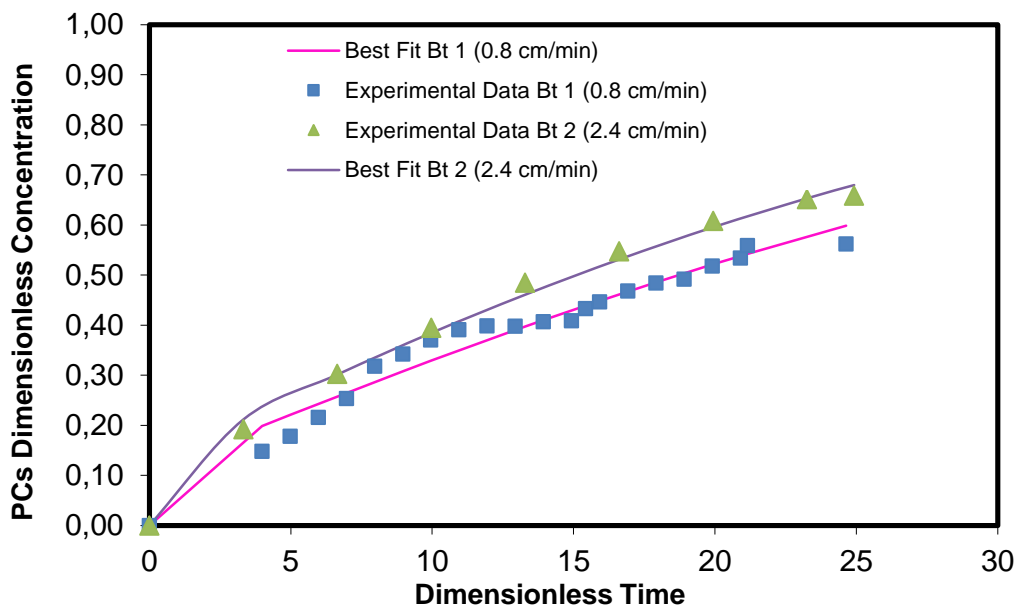


Figure 4.10 Experimental Breakthrough Curve at 0.8 cm/min (Bt 1) and the respective Best Fit Curve obtained with the hypothesis of non-negligible mass transfer resistance and Experimental Breakthrough Curve at 2.4 cm/min (Bt 2) and the respective Best Fit Curve obtained with the hypothesis of non-negligible mass transfer resistance.

With the simulated data, it was possible to calculate the fraction of utilized bed for these tests, and as it was expected (also for the experimental sigmoidal curves shape), just the 16%, approximately, was used (evaluating the data until 20% of breakthrough).

Then, in order to improve the column performance some work was done to identify the optimal column length. As it is explained in the section 2.5.2, an increase in the column efficiency, means an increase in the fraction of used bed (resin utilization efficiency), for this, it is more convenient to increase the column length than reduce the liquid superficial velocity, that can reduce the value of the mass transfer coefficient $k_L a$, lowering the effect in the column efficiency improvement (see equations 2.40 and 2.41 of the section 2.5.2).

For this, the 1-D dispersion, convection and non-equilibrium with mass transfer model best fitting estimates of $K_{ee\ PCs}$, $K_{eq\ COD}$ and $k_L a$ obtained for the Bt 2 (2.4 cm/min, 30°C) were used to simulate the PCs adsorption in columns characterized by different lengths in the 0.5m-10m range. As it is shown in the figure 4.11, the PCs adsorption yield and the resin utilization efficiency increase with the bed length (evaluating at the 20% of breakthrough).

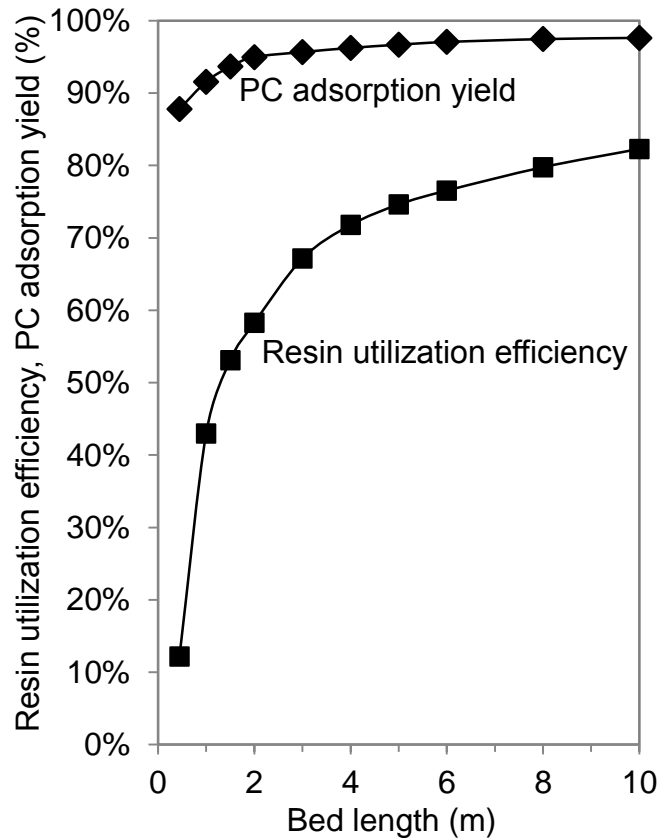


Figure 4.11 PCs adsorption yield and resin utilization efficiency at a 20% breakthrough point evaluated for columns of different lengths, using the best-fitting parameters estimated for Bt 2 (2.4 cm/min 30°C).

The increase in the resin utilization efficiency is related to a lower yearly cost associated to the periodic resin replacement, so finding the optimal column length is also very important from the economic point of view.

To explain this better there are some mathematical expression that can be useful:

The duration of each adsorption step, or the breakthrough time (t_b) can be calculated as:

$$t_{bt} = \frac{m_{PCs,sorbed,bt}/Y_{ads,PCs}}{\dot{m}_{PCs,IN}} = \frac{m_{PCs,sorbed,sat} \cdot \eta_{resin}}{\dot{m}_{PCs,IN} \cdot Y_{ads,PCs}} = \frac{K_{eq,PCs} \cdot \rho_b \cdot S_t \cdot L \cdot C_{PCs,IN} \cdot \eta_{resin}}{Q \cdot C_{PCs,IN} \cdot Y_{ads,PCs}} \quad (4.2)$$

Then, assuming two columns working in parallel which have adsorption and desorption stages of the same length, it is possible to estimate the *resin operational time* (t_{resin}) as:

$$t_{resin} = 2 \cdot t_{bt} \cdot n_{cycles} = 2 \cdot n_{cycles} \cdot \frac{K_{eq,PCs} \cdot \rho_b \cdot S_t \cdot L \cdot \eta_{resin}}{Q \cdot Y_{ads,PCs}} \quad (4.3)$$

Where η_{cycles} is the number of adsorption/desorption cycles that can be performed with one resin load. The last equation is based on the assumption that η_{cycles} is independent from η_{resin} .

Thus, the yearly cost for the resin replacement can be calculated as:

$$C_{resin} = \frac{m_{resin} \cdot SC_{resin}}{t_{resin}} = \frac{2 \cdot \rho_b \cdot S_t \cdot L \cdot SC_{resin}}{t_{resin}} = \frac{Q \cdot SC_{resin} \cdot Y_{ads,PCs}}{n_{cycles} \cdot K_{eq,PCs} \cdot \eta_{resin}} \quad (4.4)$$

As it is evident, the resin yearly cost is inversely proportional to the resin utilization efficiency (η_{resin}).

The identification of the optimal column length requires a deeper study on all these factors. However, the figure 4.11 shows that at column lengths between 2m and 4m the PCs adsorption yield is almost complete and the resin utilization efficiency increases with a lower slope. So, a column with a length in the range of 2.0m-4.0m could be preliminarily identified as a good starting point to continue with the process development and optimization. For this reason, it was decided to work with a 2.0m length column.

The experimental data and the effects of the column length in the PCs adsorption are shown in the figure 4.12.

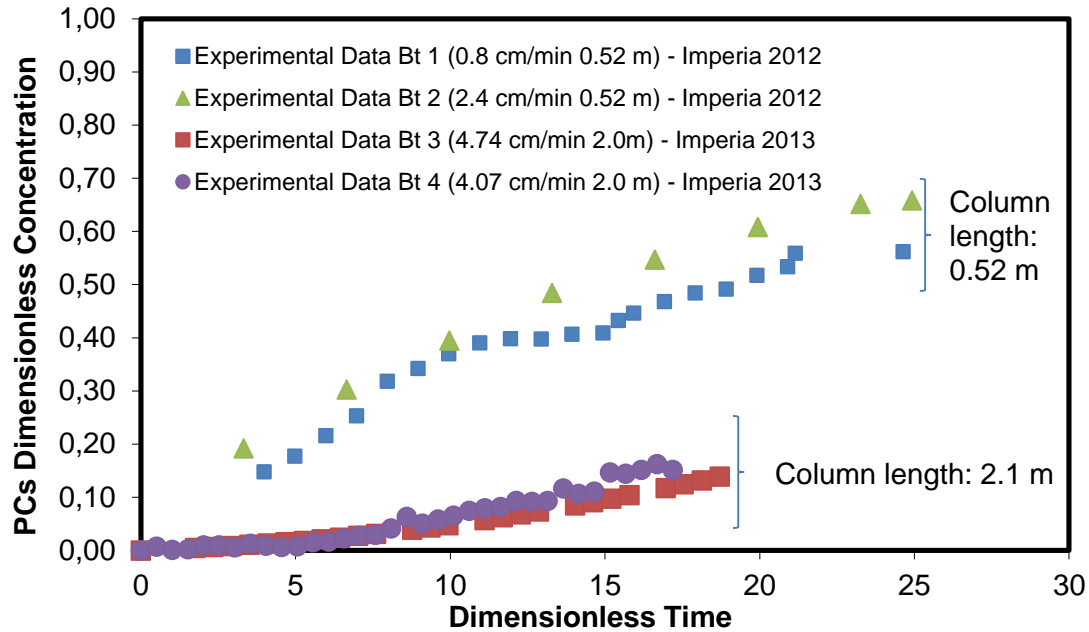


Figure 4.12 Column length effect. Experimental Breakthrough curves at 0.52 m and 2.0 m with OMW Imperia 2012 and Imperia 2013.

The breakthrough curves shape improved by increasing four times the column length. The area corresponding to the *operational capacity of the column* (see section 2.5.1) increased, as well as, the fraction of utilized bed (resin utilization efficiency), that changed from 16% to 50% (evaluating the data until 20% of breakthrough) .

Also the adsorption yield was enhanced, valuating the data until 20% of breakthrough, with a column length of 0.52m the 54% of the PCs fed was adsorbed, while with a column length of 2.0m the 94% of the fed PCs was retained. To calculate these values, the equations of the section 2.5.1 were used. To estimate the mass adsorbed at saturation, simulations were done until the 99.99% of adsorption using the parameters values (α_L , ε , K_{eq} and K_{La}) evaluated with the experimental data best fit, using the non-equilibrium mass transfer model.

With the good results obtained for the 2.0m length, then the liquid superficial velocity effect was valuated using this column length. For this, breakthrough tests

were conducted at three different liquid linear velocities (2.2 cm/min, 4.6 cm/min and 7.6 cm/min). The dimensionless plot is presented is the figure 4.13.

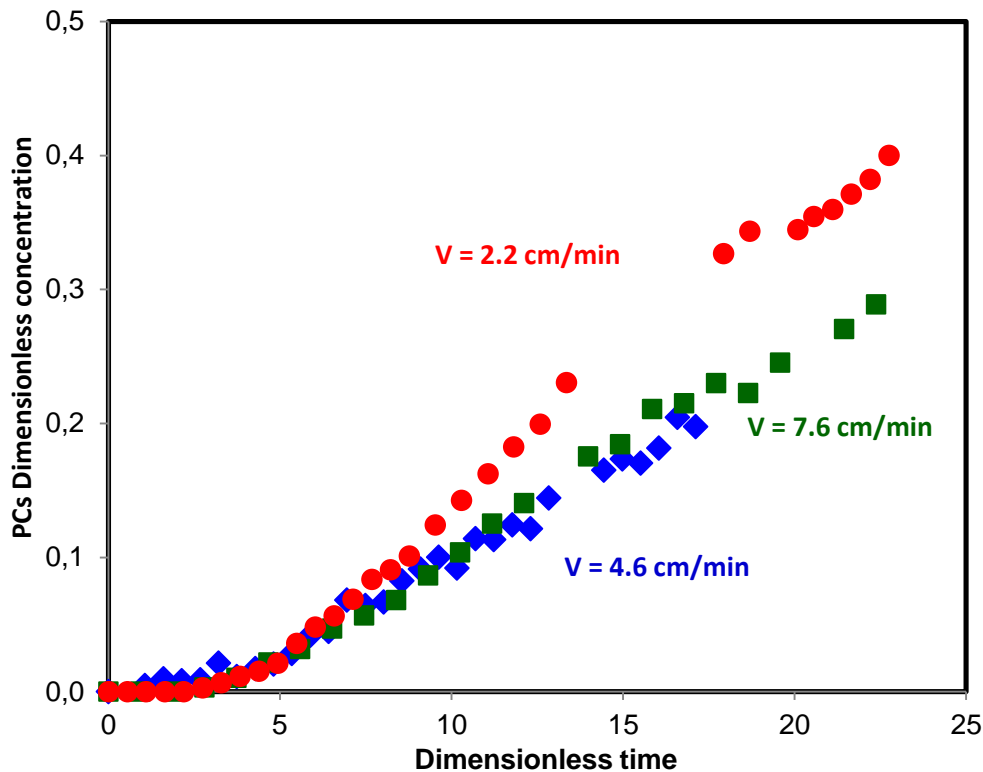


Figure 4.13 Liquid superficial velocity effect. Experimental Breakthrough curves at 2.2cm/min, 4.6 cm/min and 7.6 cm/min with OMW Imperia 2013.

As the plotted results are making evident, there is not a significant liquid superficial velocity effect, there is just a slight decrease in the adsorption efficiency at 2.2 cm/min, and there is not an important improvement above 4.6 cm/min. This means that for the industrial scale up of the process, the optimal liquid linear velocity has to be higher than 4.6 cm/min. The optimal value depends on several economic factors, because using high velocities (if the column length does not change) leads to a smaller column diameters, so smaller quantities of resin, which means a lower investment cost, but the pressure drop increases, then, also the operational costs. So an overall economic analysis of the process is needed to find the optimal liquid superficial velocity value.

Once the effects of the column length and liquid linear velocity were studied and in order to validate the adsorption method proposed for the PCs mixture recovery, a repeatability test of four breakthrough experiments at 2.0m column length and at the same liquid superficial velocity (5.0cm/min approximately), was performed, using the OMW Imperia 2013.

The results are displayed in the figure 4.14.

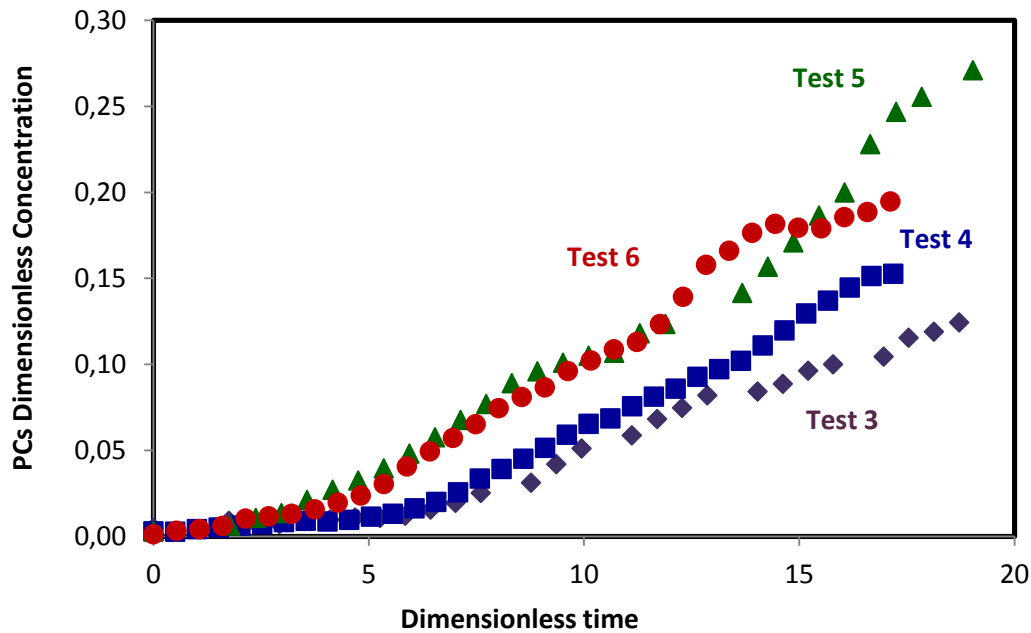


Figure 4.14 Repeatability test breakthrough curves at 5.0 cm/min approx. and 2.0m column length with OMW Imperia 2013.

If we take a look at the same dimensionless time value, in the last tests the content of PCs at the column outlet is higher, this means that the column efficiency is reducing (slightly), which is expected due to the previous desorption stages in which the recovery of the adsorbed PCs is less than 100%, so in each new cycle the active sites available for adsorption are less, decreasing the adsorption efficiency. Despite of the reduction in the column efficiency, it is important to make evident that after five adsorption/desorption cycles, the efficiency decreased by less than 5%, then, it is possible to say that the adsorption step is stable.

With a good repeatability test and with different experimental breakthrough curves obtained, the mass transfer coefficient k_{La} was evaluated through the best fit of the experimental data using the non-equilibrium mass transfer model. A representative plot is displayed in the figure 4.15.

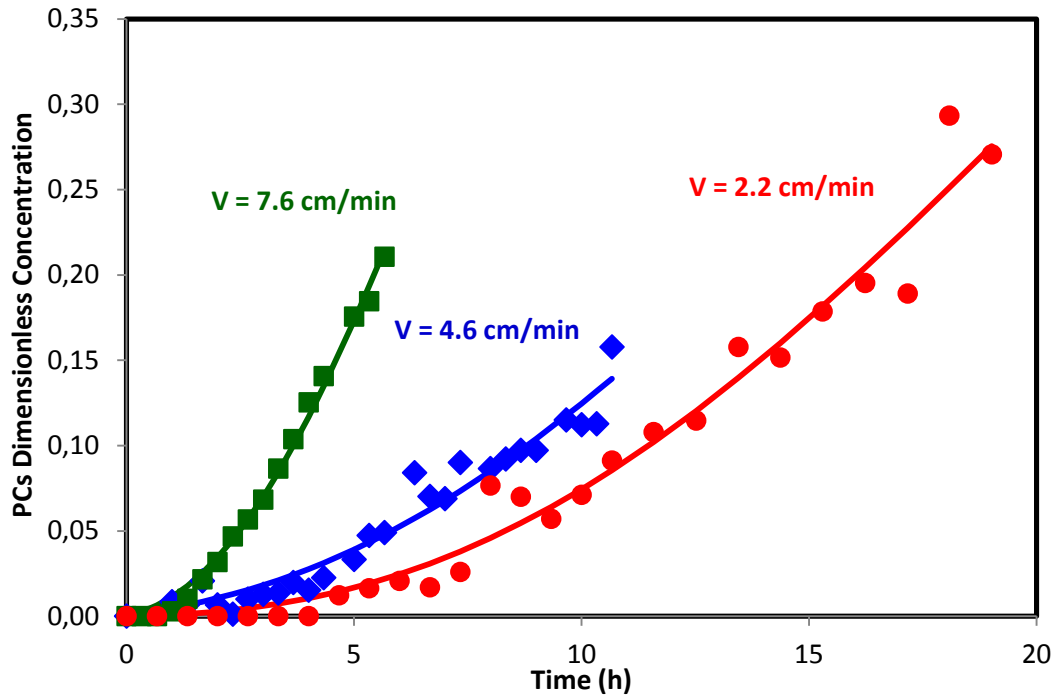


Figure 4.15 Experimental breakthrough curves with their respective simulation curves used for the calculation of the mass transfer coefficient (k_{La}) at different liquid superficial velocities.

The different points correspond to the experimental data and the continuous lines to the respective best fit curves.

The values for the mass transfer coefficient k_{La} obtained for the presented curves are:

Liquid Superficial Velocity (cm/min)	k_{La} (s ⁻¹)
2.2	0.9 +/- 0.1
4.6	3.0 +/- 0.3
7.6	4.6 +/- 0.6

Table 4.6 Values of the mass transfer coefficient k_{La} obtained with the best fit of the experimental data using the non-equilibrium mass transfer model, at different liquid superficial velocities (OMW Imperia 2013).

The non-equilibrium model with mass transfer with the independently estimated parameters (ε , α_L , K_{eq} and k_{La}) allows a satisfactory fit of the experimental curves obtained at different liquid linear velocities.

The value of the mass transfer coefficient increases when the velocity increases. This behaviour is in reasonable agreement with the Wilson and Geankopoli's model (equation 4.5), valid in our Reynolds number range (0.1-0.2).

$$Sh = \frac{1.09}{\varepsilon} \cdot Re^{0.33} \cdot Sc^{0.33} \quad (4.5)$$

Where,

Sh is the Sherwood number

Re is the Reynolds number

Sc is the Schmidt number

ε is the porosity of the packed bed

Then, in order to assess the selectivity of the resin during the breakthrough tests at both column lengths (0.52m and 2.0m) the adsorption of the COD (organic matter) was monitored. The figure 4.16 presents, as representative case, the breakthrough curves for PCs and COD at a superficial velocity of 4.6 cm/min using the 2.0m length column.

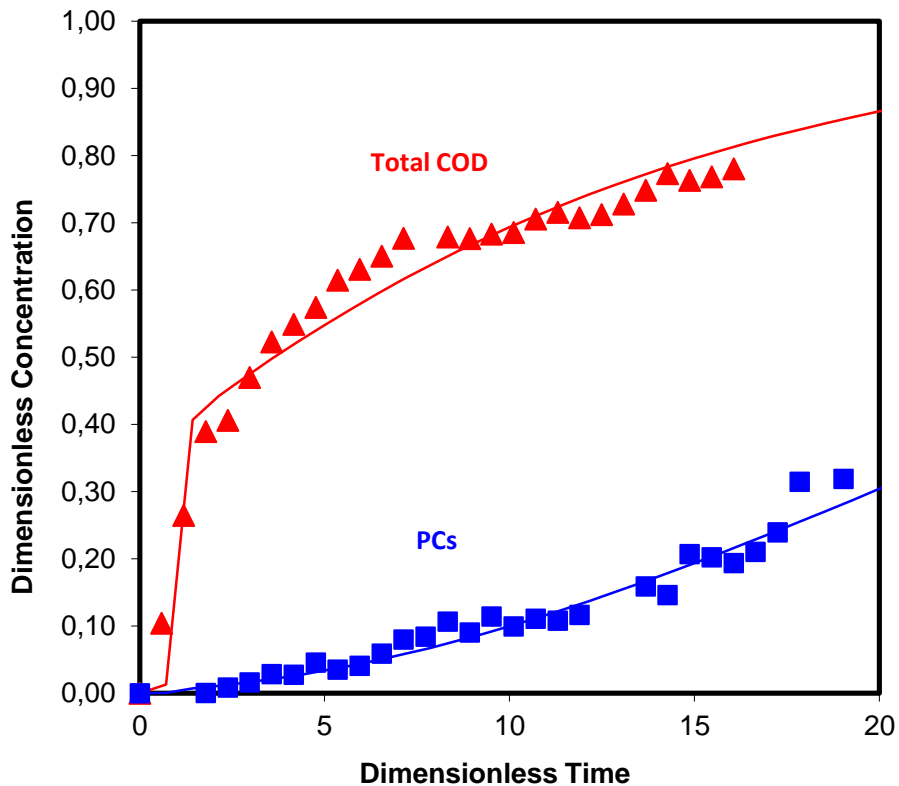


Figure 4.16 PCs and COD experimental breakthrough curves (4.6 cm/min, 2.0m column length, OMW imperia 2013) with their respective simulation curves.

It is evident that the total COD is reaching the saturation faster than the PCs, this means that there is a high selectivity of the resin for the PCs. However, if we consider the adsorption until the 20% of PCs breakthrough, nearly the 32% of non-phenolic COD has been adsorbed, and it was found that this COD is almost completely release (95%) in the desorption step, so we have a final product with more than 30% of non-phenolic substances. This situation leads to two important considerations, the first is the effect that this “contamination” can have during a subsequent purification step of the product and the second is the effect that the presence of non-phenolic COD can have in the utilization of a phenolic mixture as an antioxidant, without any further purification. In other words, the influence on this COD has to be evaluated according to the final use of the product.

A more detailed analysis has been done with the breakthrough curves obtained for PCs and COD for the tests Bt 1 (0.8 cm/min) and Bt 2 (2.4 cm/min), using the column of 0.52m length.

Besides the experimental data obtained for both PCs and COD, also best fit simulations were done for the COD breakthrough curves. The simulations were done under the hypothesis of non-negligible mass transfer resistance and linear equilibrium isotherm, as for the PCs. For these set of simulations the volumetric mass transfer coefficient k_{La} estimated for PCs was used as input data for the calculation of the COD equilibrium constant $K_{eq,COD}$. This approximation was done considering that k_L (individual mass transfer coefficient), which depends on the diffusion coefficient and the fluid dynamic conditions, is not very different for PCs and carbohydrates (main compounds of the COD studied), while the interfacial area a is the same for both cases (PCs and COD). This assumption leads to COD best fit curves with good correlation coefficients R^2 , in the range of 0.83 – 0.96. The values obtained for $K_{eq,COD}$ are 11 +/- 1 L/Kg_{dry resin} and 11 +/- 2 L/Kg_{dry resin} for Bt 1 and Bt 2, respectively.

The Gauss-Newton method used by the MatLab code converged after 6-7 iterations, and provided 95% confidence intervals varying between 2% and 18% of the corresponding best estimates. The low $K_{eq,COD} / K_{eq,PC}$ ratio, equal to 0.11-0.13, confirms the quite high selectivity of the tested resin for PCs. The experimental and simulated breakthrough curves obtained are displayed on figures 4.17a and 4.17b. for Bt 1 and Bt 2, respectively.

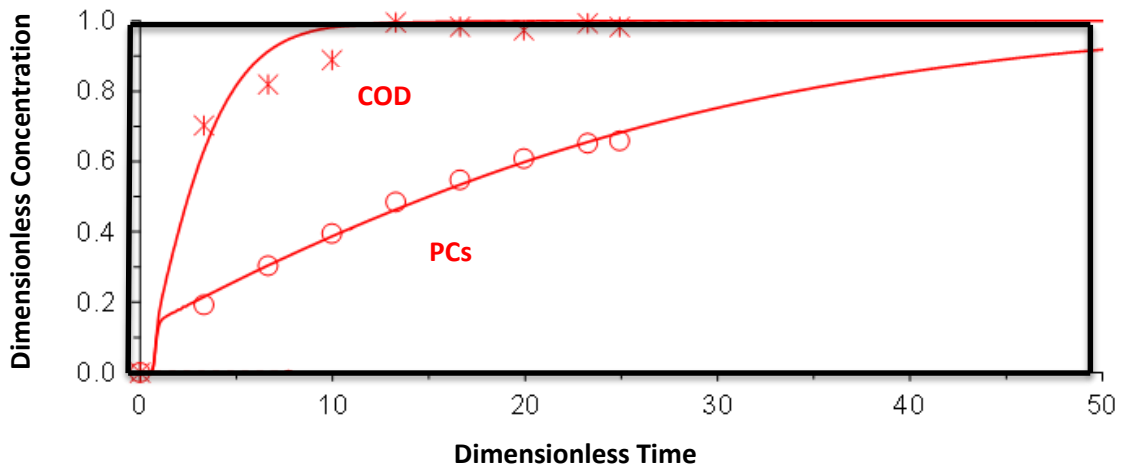
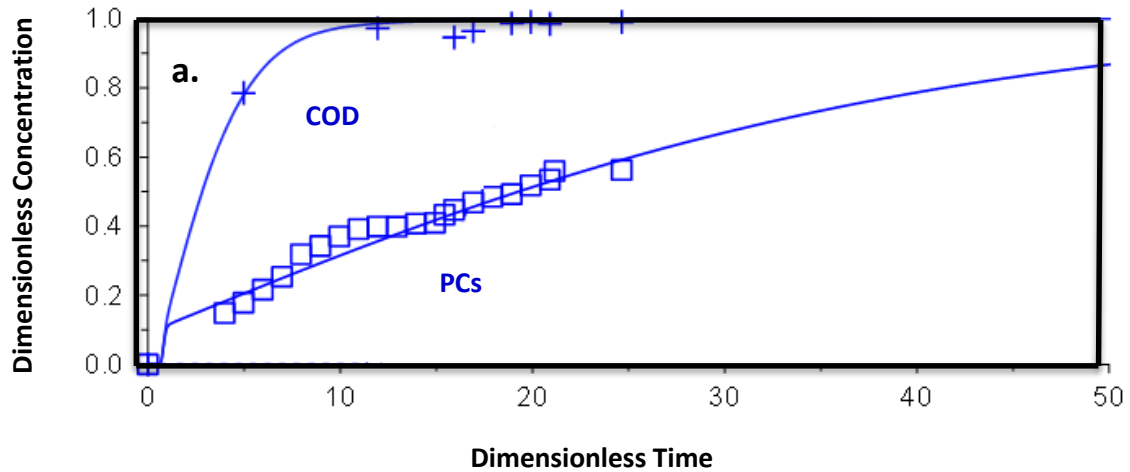


Figure 4.17 a). Experimental PCs and COD breakthrough curves for Bt 1 (0.8 cm/min, 0.5m column length, OMW Imperia 2012) and their respective simulation curves.

Figure 4.17 b). Experimental PCs and COD breakthrough curves for Bt 2 (2.4cm/min, 0.5m column length, OMW Imperia 2012) and their respective simulation curves.

The best-fitting PCs and COD simulations were used to calculate the PCs and COD adsorption yields ($Y_{ads,PCs}$ and $Y_{ads,COD}$) and the resin utilization efficiency (η_{resin} , see equation 2.38) at the selected 20% breakpoint (Table 4.7). $Y_{ads,PCs}$ resulted close to 90%, independently of temperature and superficial velocity. From the same simulated data, the PCs adsorption yield and the PCs mass fraction in the adsorbed matter (phenolic COD / total COD) were evaluated against dimensionless time (Figure 4.18). The resulting plots show that, as the adsorption time (and therefore

the breakthrough concentration) increases, the PCs adsorption yield decreases but the selectivity in PCs against COD increases, and a more pure product is thus obtained.

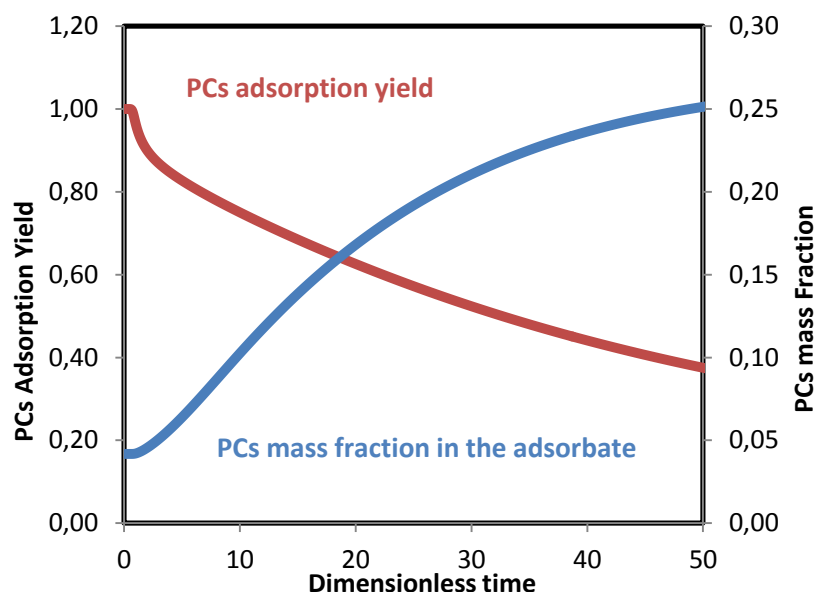


Figure 4.18 Model-based evaluation of the PCs adsorption yield and PCs mass fraction in the adsorbate relative to test Bt 2 (2.4 cm/min, 30°C).

Despite the good selectivity of resin Amberlite XAD16 for PCs, as a result of the lower content of OMWs in PCs with respect to total COD (the phenolic COD / total COD ratio is typically very low, 7% for the studied OMW in this case, Imperia 2012) even at very high dimensionless times the purity of the final product is low (< 30%). Indeed, if a process strategy to maximize $Y_{ads,PCs}$ is chosen, only a modest concentration of PCs in the COD of the final product is achieved; on the contrary, if the maximization of PCs in the desorbed product is privileged (with a considerable PCs loss in the treated OMW) the selectivity of Amberlite XAD16 for PCs allows to obtain a 4-fold increase of the PCs/COD ratio.

Some work was done to characterize the COD in both the desorbed product and the treated OMW obtained in test Bt 2. The analyses showed that carbohydrate concentration in the treated OMW was reduced from 23 g/L to 7 g/L (in good agreement with the 70% adsorption yield calculated from the experimental data

model simulation), whereas proteins were completely adsorbed. The residual carbohydrate concentration in the treated OMW did not lead to any observable inhibition effect in the subsequent anaerobic digestion process [24] of the biorefinery process in which the proposed adsorption process is the initial step. With regard to the desorbed product, the analyses showed that the non-phenolic COD was composed by carbohydrates (84%) and proteins (16%).

4.8 Desorption step and Antioxidant Activity of the Obtained Product (Amberlite XAD 16)

After each adsorption stage a desorption step was executed using acidified ethanol (0.5% HCl 0.1N) as solvent. The desorption procedure is described in section 3.11. The samples in ethanol were analysed with the total phenols HPLC method explained in section 3.3.1, which have been used for the quantification on the total phenols concentration in all the samples taken during the study of the adsorption/desorption process proposed.

As it was mentioned in the section 3.11, due to the high viscosity of the richest fractions in phenolic compounds, during the elution step, sometimes, it was necessary to adjust manually the flow rate, in order to keep the total pressure at the column inlet into a safe limit (< 2bar), because the adsorption columns are made of glass. The desorption main space velocities were in the range of 0.29 cm/min to 0.51 cm/min).

A representative desorption profile is presented in figure 4.19.

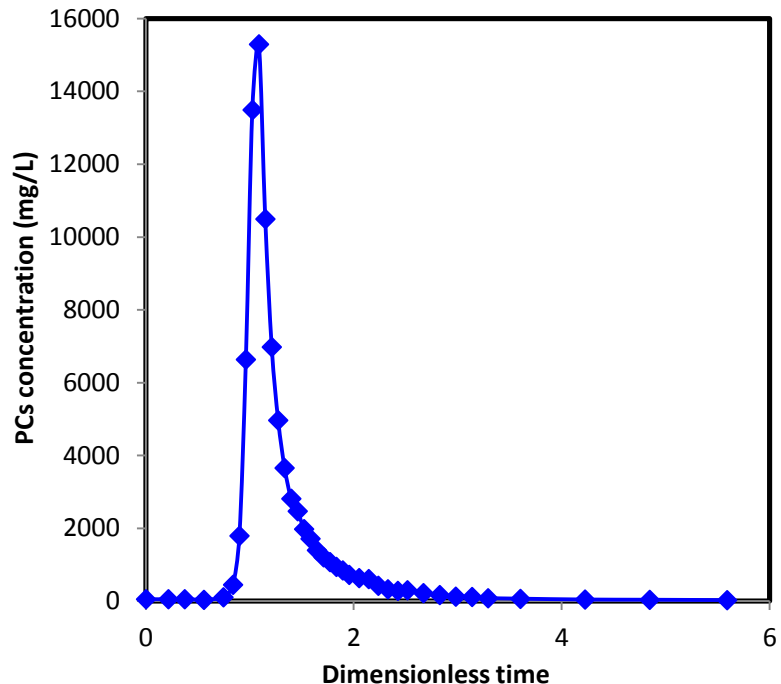


Figure 4.19 Experimental desorption profile (0.43 cm/min approx. PCs from OMW Imperia 2013, desorption solvent: acidified ethanol 0.5%v/v HCl 0.1N).

The desorption step is faster than the adsorption one, the complete elution of the adsorbed PCs takes less than 6 HTR (or tau) while the adsorption takes between 20 HTR - 30 HTR. This characteristic is very important for a future industrial process.

Then, in order to evaluate the repeatability of the desorption step the different desorption profiles obtained during different adsorption/desorption cycles were plotted together (Figure 4.20). The obtained graph shows the high stability of this stage, so, it is possible to say that the complete adsorption/desorption process proposed is stable.

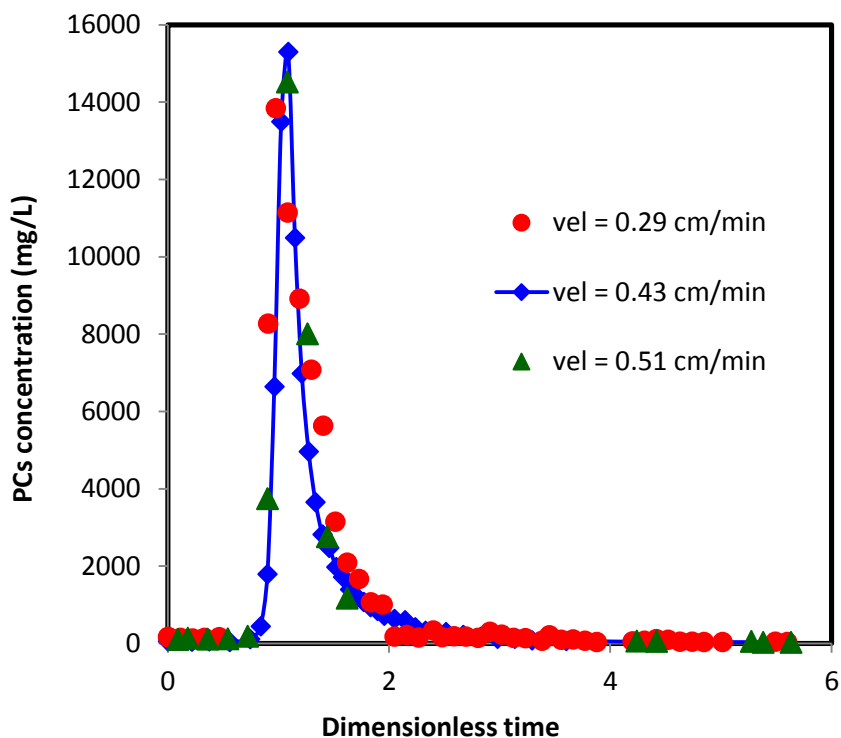


Figure 4.20 Experimental desorption profiles at 0.20 cm/min, 0.43 cm/min and 0.51 cm/min (PCs from OMW Imperia 2013, desorption solvent: acidified ethanol 0.5%v/v HCl 0.1N).

The PCs desorption yield was between 65% and 74% during the adsorption/desorption cycles performed. In an earlier batch experiment, the desorption yield was lower (53%), other authors obtained complete desorption of PCs from different adsorbents using different ethanol/water mixtures [76, 82]. Agalias et al. [37] worked with an actual OMW and with the Amberlite XAD 16 resin, and reported a successful PCs desorption using an ethanol/isopropanol mixture. These works showed that an almost quantitative recovery of PCs from Amberlite XAD16 is possible and that an optimization of the desorption step in the continuous-flow process is needed. The optimization need of PCs desorption is supported also by the overall process yield that is between 50% and 68%, (the adsorption yield is near to 90%). With the information given by other authors, the optimization of desorption should have different alternatives to be successful.

Another important issue is the non-phenolic COD desorption, that was discussed previously on section 4.7, supporting the conclusion that an optimization of the desorption step is needed.

Once the desorption product was collected, the ethanol was recovered by low pressure distillation and the separated product was re-suspended in demineralized water, as it was described on section 3.21. The product antioxidant activity was evaluated by the ABTS assay explained on section 3.3.9. According to the results obtained, the final product (in which between the 8% and 10% of the mass corresponds to the phenolic compounds, and the rest to the non-phenolic COD desorbed) has an antioxidant activity of nearly 25mM of ascorbic acid equivalent, which is a value almost five times higher than the antioxidant activity reported in literature (M.I. Gil et al. 2000 [86]) with the same method for the green tea and red wine, to agro industrial products widely known for their antioxidant properties.

This characteristic of the final mixture is very interesting and lets its utilization in different fields, for example, as an antioxidant additive in plastics.

4.9 Preliminary Cost Evaluation for Amberlite XAD 16

In order to evaluate the economic feasibility of the proposed process a preliminary cost evaluation was done.

The characteristics of the studied plant are listed on table 3.5.

According to the considerations done for the plant production and all the involved expenses, the yearly cost, which includes the operational cost and the amortization of capital cost, would be around 375000 €/year or 37.5€/m³.

The yearly revenues are around 400000€/year - 500000€/year from sales of a phenolic mixture [83]. The value could increase for sales of purified phenolic compounds.

The figure 4.21 shows the contribution of all the factors involved in the process.

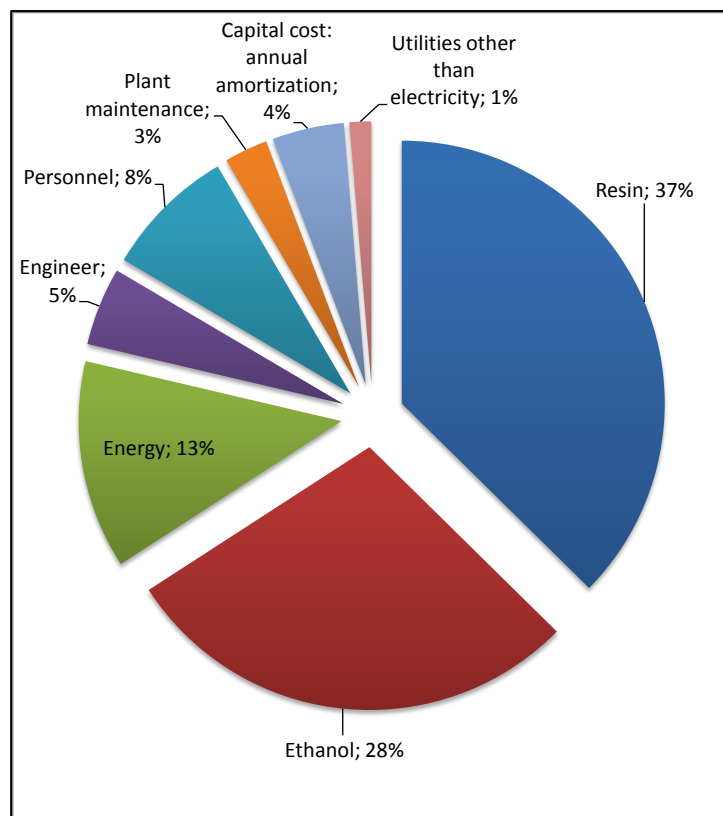


Figure 4.21 Cake diagram of the contribution of each process factor in the total process cost for the preliminary economic evaluation.

As the graph makes evident, the highest cost is the resin periodic replacement, so there are two ways to affront this situation, the first one is to increase the number of cycles performed with the same resin charge and the second way is to find a new and cheaper solid phase that can be used for the phenolic compounds adsorption, even if its efficiency is slightly lower than the adsorption efficiency of the Amberlite XAD 16.

In this project, the way chosen was the second one, and for this two anionic exchange resins which cost six times less than the Amberlite XAD 16, were tested. The results obtained during the screening and the different experiments performed are going to be discussed in the next sections.

4.10 Amberlite IRA 958Cl and Amberlite IRA 67Cl Screening

The screening tests were performed following the procedure described in the section 3.13. The condition of 50 mL of OMW with 25g of dry resin corresponds to a low concentration point in the isotherms obtained for Amberlite XAD 16. The chosen point corresponds to dimensionless concentration of about 0.1, a reasonable value at the column outlet, commonly used to stop the adsorption step in an actual industrial process, it is the breakpoint.

As it was described in the section 3.13, the resins performances were studied at different conditions, at the OMW pH (around 4.9), pH 6 and pH 7, being ion-exchange resins, the pH can have an important effect in the adsorption of acidic compounds like PCs.

Also the presence of VFAs (volatile fat acids) was investigated, because the possibility of feeding OMW anaerobically digested was considered, in order to possibly change the digestion step of the biorefinery process in which the PCs adsorption is participating.

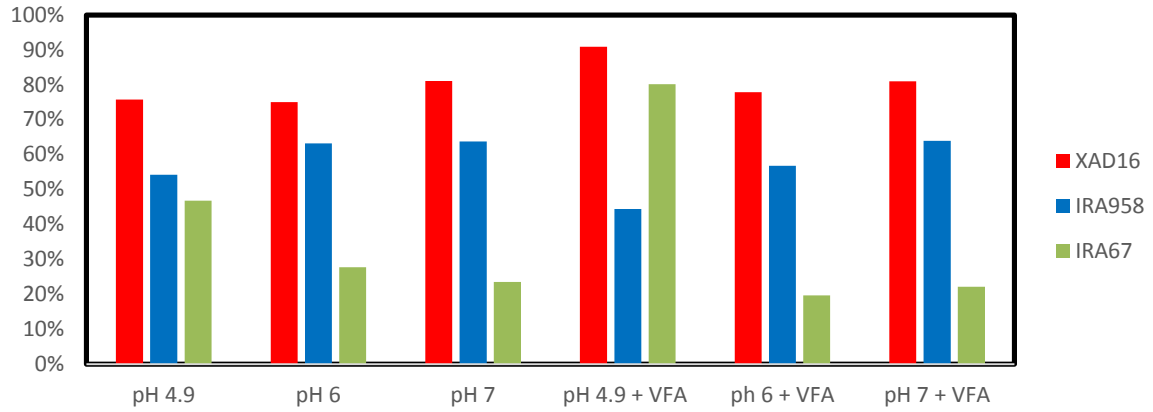
Also the Amberlite XAD 16 was tested in the same conditions for direct comparison purposes.

For all three resins the adsorption performances for PCs, COD and VFAs were evaluated by the comparison of the respective adsorption yields $Y_{ads,i}$ calculated as $m_{i,adsorbed} / m_{i,fed}$ and the adsorption selectivities, estimated as PCs/COD and PCs/VFAs yields ratios.

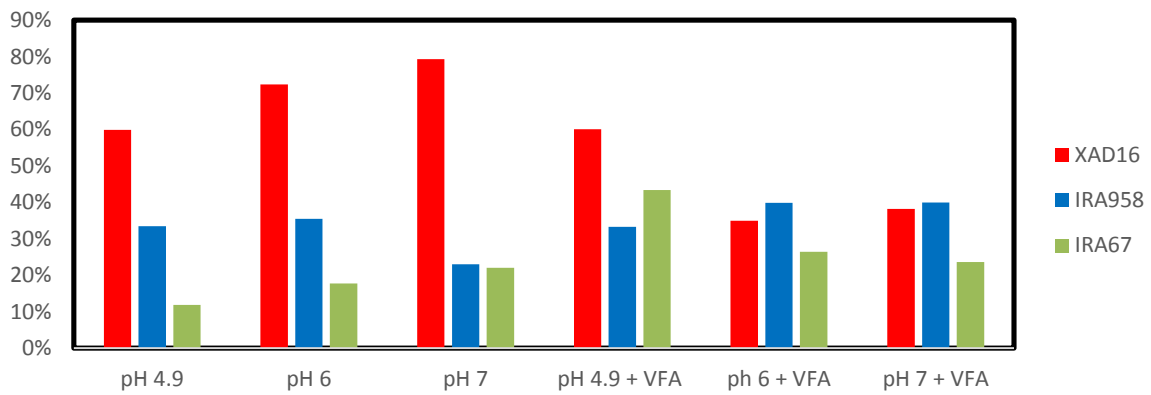
The results are displayed on figures 4.22a. and 4.22b. The calculations are presented in table 4.7.

a. Yields

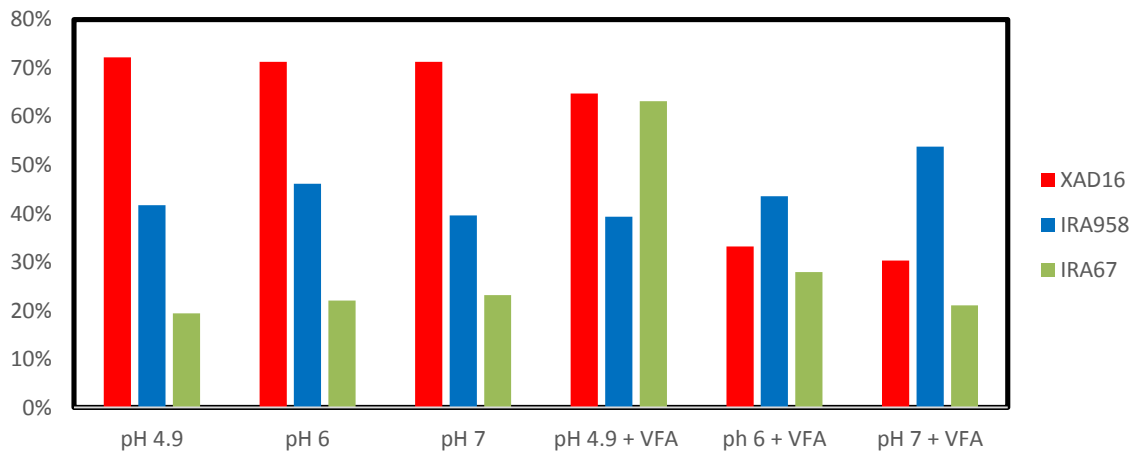
PCs Yield



COD Yield



VFAs Yield



b. Selectivities

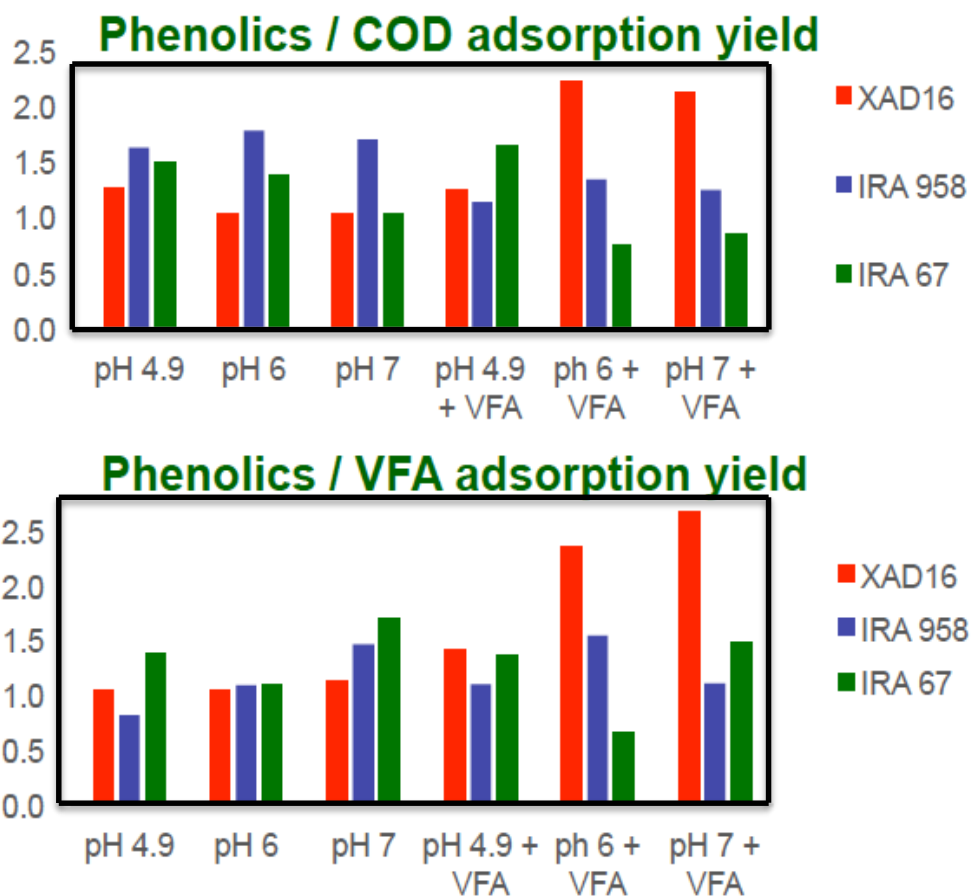


Figure 4.22 a.) Amberlite XAD 16, Amberlite IRA 958CI and Amberlite IRA 67CI PCS and COD adsorption yields at different pH and VFAs content.

Figure 4.22 b). Amberlite XAD 16, Amberlite IRA 958CI and Amberlite IRA 67CI PCs adsorption selectivities respect to COD and VFAs.

		PC s	CO D	VFA s	Selectivity as Yield ratio		PCs	CO D	VFA s
		Y ad s	Y ads	Y ads	PCs/CO D	PCs/VF As	g_a ds	g_a ds	g_a ds
XAD16	no VFAs addition	77 %	71%	72%	1.1	1.1	0.7	18.4	1.8
	with VFA addition	83 %	44%	43%	1.9	1.9	0.7	19.5	5.7
IRA 958CI	no VFAs addition	60 %	31%	43%	2.0	1.4	0.5	9.4	0.4
	with VFA addition	55 %	38%	46%	1.5	1.2	0.4	16.2	3.3
IRA 67CI	no VFAs addition	33 %	17%	22%	1.9	1.5	0.3	5.6	0.2
	with VFA addition	41 %	31%	37%	1.3	1.1	0.3	13.2	2.7

Table 4.7 Adsorption yields for PCS, COD and VFAs, PCs adsorption selectivities as yield ratio and PCs, COD and VFAs mass adsorbed for Amberlite XAD 16, Amberlite IRA 958CI and Amberlite IRA 67CI.

The experimental data has a wide dispersion, although that it is possible to conclude that:

- In all conditions Amberlite XAD 16 has a better performance than the two anionic exchange resins. It has a PCs yield between 75% and 90%, while Amberlite IRA 958CI, the best of the ionic resins, has values between 45% and 65%.
- With pH 4.9 with the addition of VFAs, the Amberlite IRA 67CI has an adsorption yield of 80%, a value comparable with the performance of the Amberlite XAD 16.

- The pH variation seems to have no effects on the Amberlite XAD 16 performance, with and without VFAs addition, while for Amberlite IRA 958CI the pH increase improves the performance, whereas for Amberlite IRA 67CI the effect is the opposite. In general, the pH is not influencing the selectivity of the process in any case.
- The VFAs presence seems to have a non-significant influence in the performance of all resins.
- In terms of PCs adsorption capacity, Amberlite XAD 16 confirms to be the best option, but talking about selectivity this resin is not the best, the average PCs, COD and VFAs yields are very similar (77%, 71% and 72%, respectively, see table 4.8).
- Both Amberlite IRA resins have a poor PCs capacities, but higher selectivities, for example, the Amberlite IRA 958CI in absence of VFAs adsorbs 60% PCs, but just the 31% of COD and 43% of VFAs.
- The samples with VFAs presence showed that Amberlite IRA resins have a low VFAs adsorption capacities (just 46%).
- The Amberlite XAD 16 selectivity seems to improve significantly when the VFAs are present: the PCs/COD and PCs/VFAs yield ratios are almost the double (from 1.1 to 1.9 for both cases).

The performance of the Amberlite IRA resins is lower than for Amberlite XAD 16 in terms of adsorption capacity, but they have a better efficiency talking about selectivity. An important characteristic for Amberlite IRA 958CI is its low affinity for VFAs, which make it suitable for a process in which the fed OMWs be anaerobically digested. Knowing this and on the basis of the lower Amberlite IRA 958CI cost, it was selected for further investigation (isotherm obtaining, see section 4.12), and breakthrough experiments, see section 4.14).

4.11 Adsorption Kinetics for Amberlite IRA 958CI

For the anionic resin Amberlite IRA 958CI the time in which the equilibrium is reached was obtained during the screening step by taking samples after 3 hours and 18 hours of experiment. According to the results obtained, it was observed that there is not a significant difference in the total phenols concentrations between the samples taken at 3 hours and at 18 hours, so for the further experiments, the equilibrium time used was 3 hours.

4.12 Adsorption Isotherms for Amberlite IRA 958CI

The isotherm of the system Amberlite IRA 958CI – OMW Imperia 2014 was obtained at 30°C, the same temperature of one of the isotherms obtained for the Amberlite XAD 16. The data of both isotherms obtained at 30°C with both solid phases is displayed in the following figure.

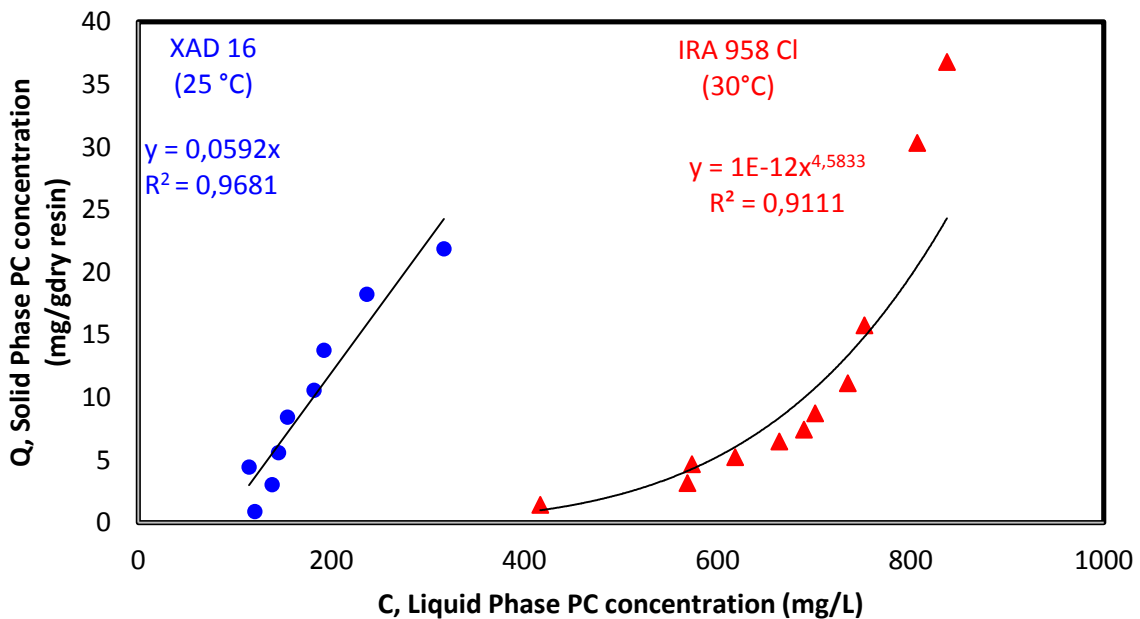


Figure 4.23 Adsorption isotherms for the systems OMW Imperia 2013-Amberlite XAD 16 at 25°C and OMW Imperia 2014-Amberlite IRA 958CI at 30°C.

In the case of XAD 16, we have experimental equilibrium points that describe a type linear trend which can be envisaged as the initial linear part of a conventional Langmuir isotherm; this last hypothesis is supported by the theoretical XAD 16 capacity declared by the producer (370 mg/g_{dryresin}, referred to medium molecular weight compounds) that is several times higher than the maximum solid concentration measured, as it was said before.

On the other hand, IRA958CI experimental points show only an unfavourable behaviour with a trend that can be interpreted by a power-low curve (Freundlich type isotherm) with an exponent higher than 1. It cannot be excluded that the IRA 958CI behaviour at higher PCs concentration would become about linear as in the case of XAD16. Those higher concentration values could not be investigated due to the relative low PCs content in the untreated OMW, and for this same reason are less interesting from an industrial point of view.

Regardless of the different isotherm type and the slight difference in the temperature, the comparison of the experimental data clearly shows that the IRA 958CI adsorption performance is significantly worse than that of XAD 16, at least at the low PCs concentration typical of the OMWs. Nevertheless, the characterization of IRA 958CI and the comparison with XAD were completed carrying out breakthrough tests in the 2.0m adsorption column designed to optimize the adsorption/desorption with XAD 16, and that is going to be further explained.

4.13 Fluid dynamic Characterization for Amberlite IRA 958CI Bed

The 2.0m column was packed with Amberlite IRA 958CI with the second procedure described on section 3.8, and once the column was packed, and after each adsorption/desorption cycle, a fluid dynamic test was performed as it was explained on section 3.9.

For the resin IRA 958CI, as representative case of *F curves (Cumulative Retention Time Curves)*, the figure 4.24 shows the data obtained before the breakthrough test

at 5cm/min (Bt 7) and after a second breakthrough test at 2.1 cm/min (Bt 8), with the fluid dynamic information of the breakthrough test Bt 4 (experimental data and simulation).

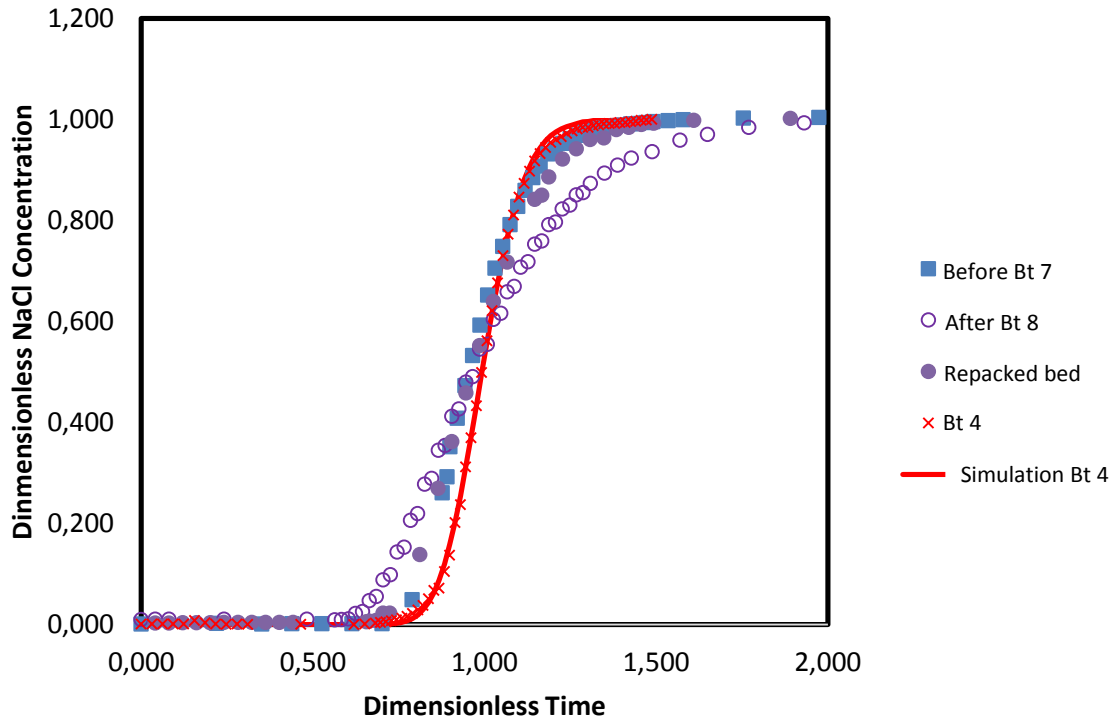


Figure 4.24 *F* curves before Bt 4, before Bt 7 and Bt 8 and after Bt 8 (repacked bed) with the simulation *F* curve of Bt 4.

After Bt 8 a partial and limited collapse of the packed bed was observed after the desorption step in the last of the four columns that compound the adsorption system, and a less important collapse was observed in the other three columns. The fluid dynamic test record this incident showing a large change in the slope of the experimental *F* Curve suggesting a decrease in the number of plates (N) increasing also the longitudinal dispersivity (α_L), worsen the adsorption performance.

The quality packing evaluation confirmed this (see table 4.8), the number of plates (N) decreases and the asymmetry factor is very far from 1, indicating a pronounced tail in the retention time curve (*E* curve), which could mean mixing/stagnant zone.

Thus, the adsorption bed was re-packed, pouring new fresh resin in the upper part of the column to fill the gap formed during the collapse in the desorption step.

Test	N	HETP (m)	HETP/dp	As	Packing Quality
Desirable values	<i>high</i>	<i>low</i>	<i>low</i>	<i>near 1</i>	
XAD 16 Bt 3 new	121	0.017	27	1.3	very good
XAD 16 Bt 4 used	57	0.037	58	1.0	very good
IRA 958CI Bt 7	46	0.045	61	1.3	very good
IRA 958CI Bt 8 / 4th col. collapsed	19	0.112	151	2.8	poor
IRA 958CI Bt 8 re- packing	29	0.073	99	1.8	good

Table 4.8 Fluid dynamic parameters comparison to evaluate column packing quality between Amberlite XAD 16 and Amberlite IRA 958CI packed beds.

4.14 Phenolic compounds and COD Breakthrough tests for Amberlite IRA 958CI

A breakthrough test (Bt 7) was carried out after packing the column with the resin *Amberlite IRA 958CI*. The liquid linear velocity was set at around 5.0 cm/min, as the tests conducted for the repeatability study of the adsorption step for *Amberlite XAD 16*. In this cases (Bt 3- Bt 6 and Bt 7), the column length was 2.0m.

A comparison between the experimental breakthrough curves for *Amberlite XAD 16* and *Amberlite IRA 958CI* is presented in figure 4.25. The performance for the Pcs adsorption of the resin *Amberlite IRA 958CI* is far worse than the resin *Amberlite XAD 16*, an important presence of PCs at the column outlet started at around 1

HTR for *Amberlite IRA 958CI* while for the hydrophobic resin *Amberlite XAD 16* this situation started at near 5 HTR.

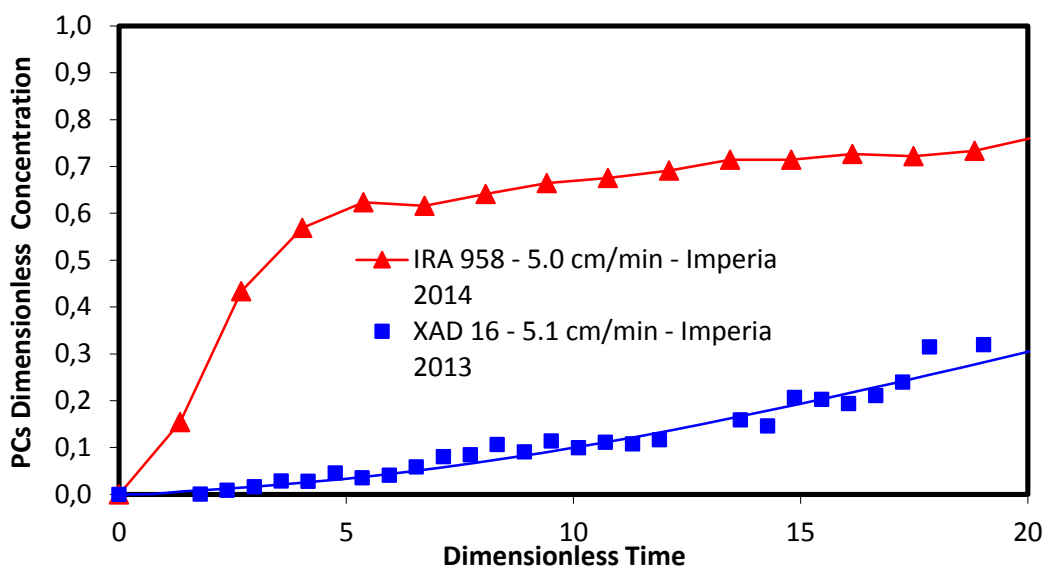


Figure 4.25 PCs experimental breakthrough curves for Amberlite XAD 16 (5.1 cm/min, 2.0m column length, OMW Imperia 2013) and Amberlite IRA 958CI (5.0 cm/min, 2.0m column length, OMW Imperia 2014).

During the PCs breakthrough test Bt 7, as for the case of *Amberlite XAD 16*, the COD adsorption was also monitored, the experimental data is displayed in the figure 4.26.

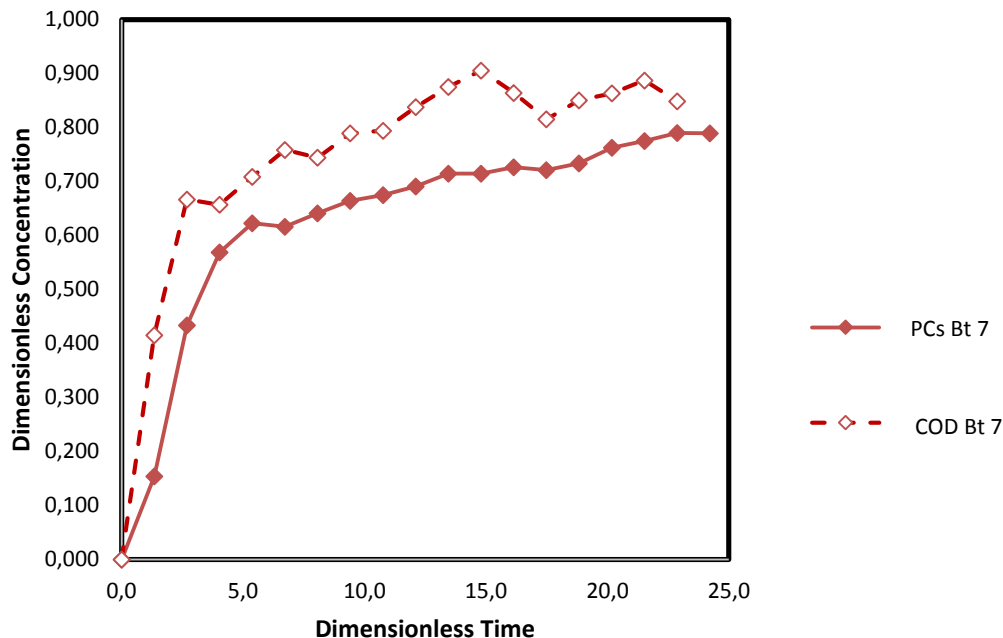


Figure 4.26 PCs and COD experimental breakthrough curves at 5.0 cm/min (2.0m column length OMW Imperia 2014) for Amberlite IRA 958CI).

The COD and PCs breakthrough curve have a similar trend, even if the COD one is a bit faster is closer to the PCs curve than in the case of *Amberlite XAD 16* (see section 4.7). This means that *Amberlite IRA 958CI* has a poorer selectivity for PCs, and this leads to a lower concentration of these compounds in the final solid extract. Although simulation of this data was not done, with the experimental data was possible to estimate PCs and COD yields, and the resin utilization efficiency. This information is presented on the table 4.9. Even if the PCs yield could be considered reasonably good, the COD yield is very near and the resin utilization efficiency is very low.

Parameter	Bt2	Bt5	Bt7	Bt8
Resin	XAD16	XAD16	IRA958Cl	IRA958Cl
Column length (m)	0.5	2.0	2.0	2.0
Bulk density (ρ_b , kg _{dry resin} /L)	0.870	0.870	0.654	0.654
T (°C)	30	24	29.4	26.4
Vs (cm/min)	2.4	5.1	5.0	2.1
OMW (Imperia)	2012	2013	2014	2014
$\alpha_{L,resin}$ (m)	0.004	0.029	N.A.	N.A
Resin porosity (ϵ_{resin})	0.830	0.894	0.532	0.554
PCs adsorption yield ($Y_{ads,PC}$, -) ^a	88%	92%	87%	97%
COD adsorption yield ($Y_{ads,COD}$, -) ^a	75%	37%	95%	96%
Resin utilization efficiency (η_{resin} , -) ^a	12%	42.4%	9%	30%
PCs desorption yield ($Y_{des,PC}$, -)	74%	75%	60%	51%
gPCs,OMW/gCOD,OMW	3.7%	3.8%	2.4%	2.7%
gPCs,ads/gCOD,ads	4.3%	9.7%	2.2%	2.7%
Productivity (g _{sorbed PC} / kg _{resin})	3.4	7.6	2.1	0.9

Table 4.9 Bt 2, Bt 5, Bt 7 and Bt 8 adsorption and fluid dynamic parameters and process productivity comparison.

Due to the low performance of the *Amberlite IRA 958Cl*, but in order to try to have better results, a second test was conducted at around 2.0 cm/min (Bt 8). This can double the residence time influencing positively in the resin utilization efficiency, but can reduce the liquid linear velocity, affecting negatively the mass transfer coefficient performance, if mass transfer is the key phenomenon, as in the case of

Amberlite XAD 16. The results obtained for Bt 7 and Bt 8 with the respective COD curves, are presented in figure 4.27.

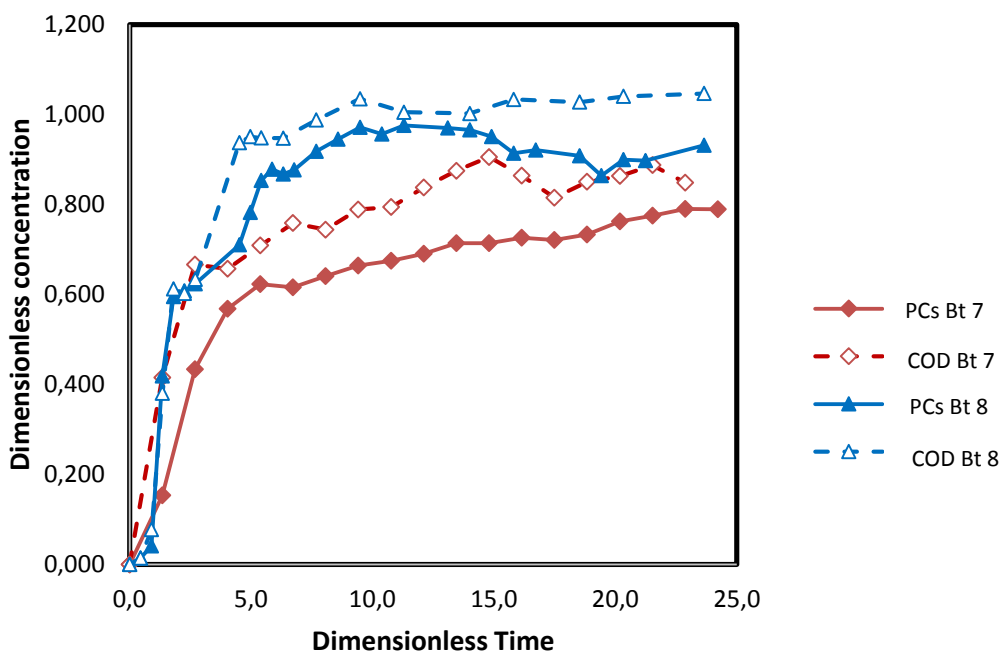


Figure 4.27 PCs and COD experimental breakthrough curves at 5.0 cm/min and 2.1 cm/min (2.0m column length, OMW Imperia 2014) for Amberlite IRA 958CI.

These results show that an important improvement of the PCs adsorption was not reached by reducing the liquid superficial velocity. This suggests that for PCs adsorption, although its high price, it is more convenient to use the hydrophobic resin *Amberlite XAD 16*.

4.15 Desorption-regeneration tests and productivity for Amberlite IRA 958CI

As for the *Amberlite XAD 16* case, after each adsorption step, the desorption stage was performed using acidified ethanol (0.5% v/v HCl 0.1N) and the subsequent rinsing with demineralized water, as it was described in the *Materials and Methods* chapter.

The desorption profiles are not shown because of the frequent manual changes in the ethanol flow rate in order to keep the total pressure at the column inlet below 2 bars (glass columns).

The obtained extract was analyzed to estimate the PCs desorption yield. In the case of *Amberlite XAD 16*, the desorption yield is around 75% while for *Amberlite IRA 958Cl* was very low for both tests, between 50%-60%. Also the rinsing water was analyzed, and 1/3 and half of the desorbed PCs was there. So, the desorption procedure for *Amberlite IRA 958Cl* has to be changed. Studies regarding to the desorption step improvement for the ionic resin were not conducted because of the not very good results obtained also for the adsorption stage.

From the economical point of view, it was important to evaluate the productivity (g of PCs/ Kg dry resin) in one adsorption/desorption cycle, in order to compare the performances of both types of resin (*Amberlite XAD 16* and *Amberlite IRA 958Cl*), taking into account the difference of bulk density that exists between them.

The experimental values are presented in the table 4.9.

For *Amberlite XAD 16* the productivity was enhanced by increasing the column length. In the case of *Amberlite IRA 958Cl*, considering the case with higher liquid linear velocity, the productivity is just three times lower than for *Amberlite XAD 16* in the same conditions. Even if the productivity of *Amberlite IRA 958Cl* increases, the cost of this improvement is seen in a lower resin utilization efficiency.

CHAPTER 5

RESULTS AND DISCUSSION: RECOVERY OF PURE POLYPHENOLS

The continuous flow selective extraction of tyrosol and hydroxytyrosol from olive mill wastewaters using a cyclodextrin-based polyurethane is discussed in this chapter.

5.1 Cyclodextrin based Polymers (CDP) for single phenolic compounds Recovery: Tyrosol (Ty) and Hydroxytyrosol (HTy)

In order to recover tyrosol and hydroxytyrosol from OMWs, the nanoscience research group of the FHNW (Fachhochschule Nordwestschweiz) at Basel, Switzerland, produced a cyclodextrin based polymer made of methylated β -cyclodextrin (Me β CD) and of 4,4'-methylene diphenyl diisocyanate (MCI), produced with the methodology described in the section 3.2.

5.2 Adsorption Kinetics for CDP

To obtain the adsorption kinetics of tyrosol and hydroxytyrosol the procedure described in the section 3.5 was applied, using the OMW Imperia 2014. The concentration of these phenolic compounds were measured in the liquid phase through the hplc method for the identification and quantification of these substances, presented in the section 3.3.2. The concentration of tyrosol (Ty) and hydroxytyrosol (HTy) in the solid phase were calculated with the equation 4.1.

The results are displayed in the following graph.

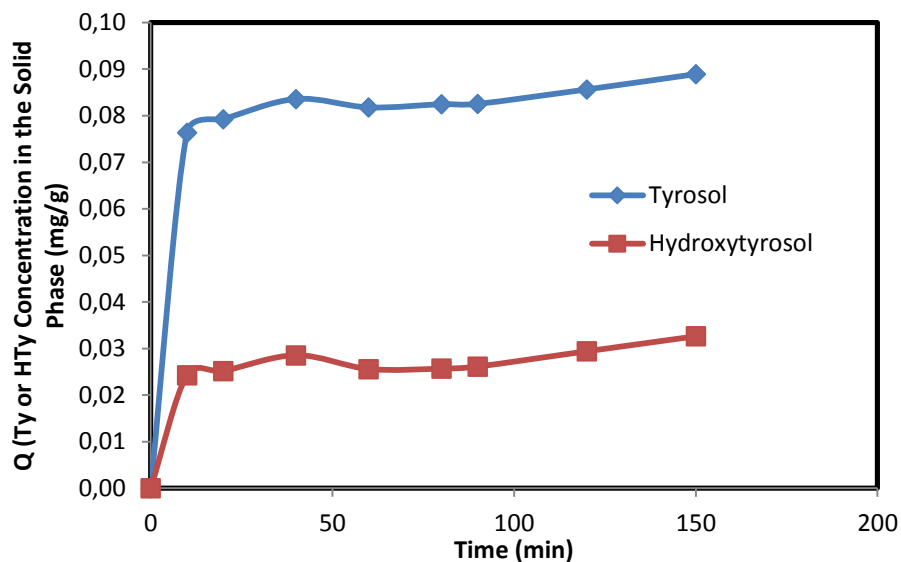


Figure 5.1 Adsorption Kinetics for the CDP and the OMW Imperia 2014.

The dynamic equilibrium is reached after 150 minutes.

The equilibrium information was used to perform the experiments for the adsorption isotherms obtaining.

5.3 Adsorption Isotherms for Tyrosol and Hydroxytyrosol with CDP

For the CDP solid phase, the isotherms were obtained for tyrosol and hydroxytyrosol, using the OMW Imperia 2014, using the procedure described in the section 3.5 and applying the Ty and HTy hplc method of section 3.3.2.

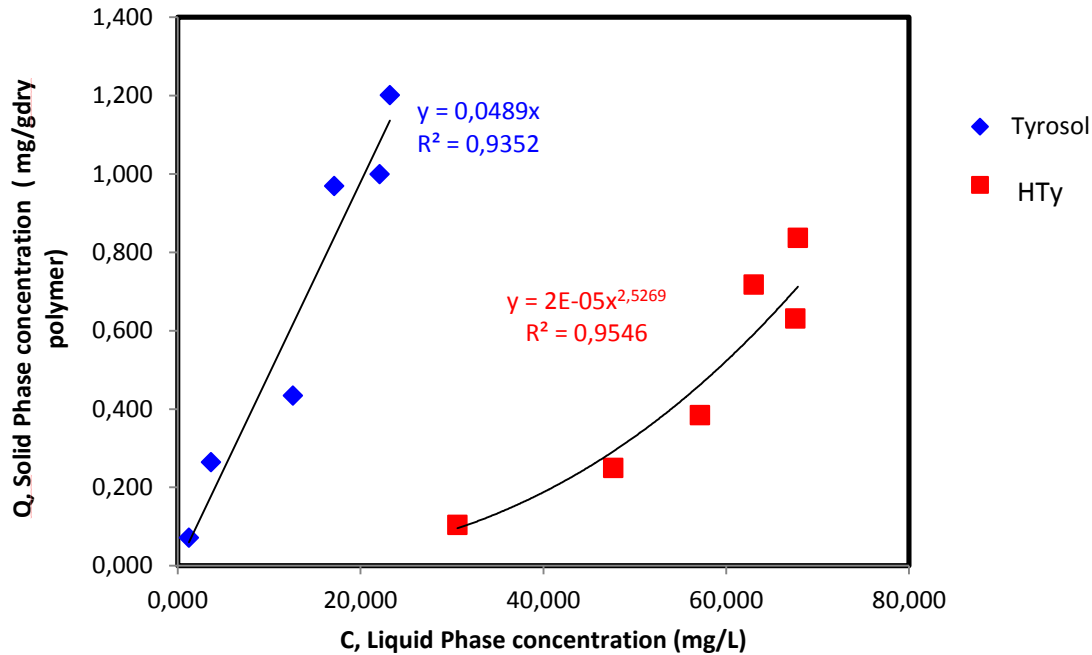


Figure 5.2 Adsorption isotherms for the systems Ty-CDP and HTy-CDP at 30°C (Ty and HTy from OMW Imperia 2014).

The isotherm for tyrosol has a linear trend with an acceptable R^2 , this behaviour maybe be due to the not very high concentration of this phenol (around 5.6mg/L) in the OMW Imperia 2014. This result shows the affinity of the solid phase for this substance.

In the other hand, the isotherm of the hydroxytyrosol can be described for a power law function, so it is a Freundlich type isotherm, with an exponent higher than 1, so the curve shape is unfavourable, indicating a low affinity of the CDP polymer for this phenolic compound. Although this result, the hydroxytyrosol adsorption was monitored during the breakthrough test to evaluate the tyrosol recovery.

The cyclodextrin based polyurethane was packed following the dry-packing procedure described on chapter 3 in the adsorption system of the figure 3.2 of the section 3.4.

5.4 Fluid Dynamic Characterization of the CDP Bed

Once the bed was packed with fresh CDP a fluid dynamic test was performed following the method of the section 3.9 with a liquid superficial velocity of 0.87 cm/min.

The *cumulative retention time curve* (*F curve*) obtained is display in the figure 5.3.

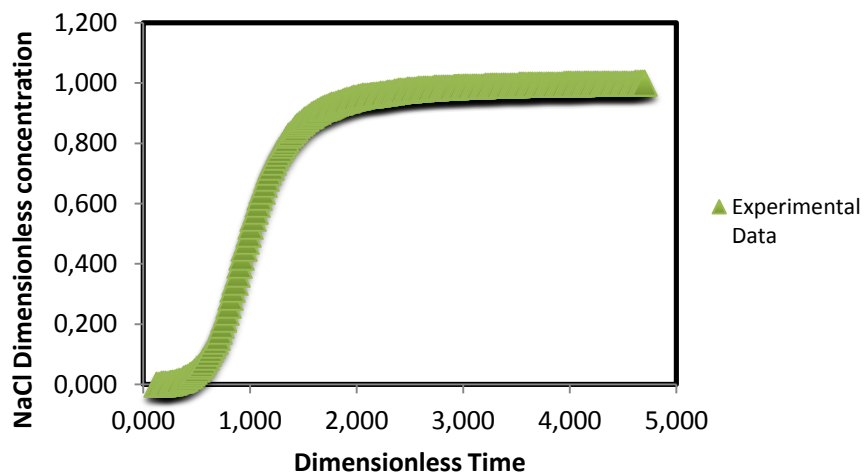


Figure 5.3 *F curve* obtained for CDP packed bed before breakthrough tests.

The parameters calculated from the derivation of the *F curve* are listed in the table 5.1.

Parameter	Value
Porosity	0.29
Number of Plates (N)	12.05
Height Equivalent Theoretical Plate (m) (HETP)	0.11
Asymmetry Factor	1.47

Table 5.1 Fluid dynamic parameters for CDP packed bed.

According to this results and with the uniformity of the sigmoid that describes the F curve, the packing was consider of enough quality and some breakthrough tests were conducted.

5.5 Tyrosol and Hydroxytyrosol Breakthrough tests for CDP

With the packed bed were conducted four breakthrough tests at different liquid linear velocities and the outlet concentrations of tyrosol and hydroxytyrosol were estimated with the hplc method described in the section 3.3.2.

Before feeding the OMW Imperia 2014 in the adsorption system, the OMWs were treated as described on section 3.7.

During the first adsorption test (0.87 cm/min) all the tyrosol fed with the OMW Imperia 2014 was adsorbed while hydroxytyrosol was detected at the column outlet, so the CDP has more affinity for Ty than for HTy, confirming the results previously obtained with the adsorption isotherms in the section 5.3.

After the fourth adsorption/desorption cycle (0.44 cm/min), the tyrosol adsorption yield was still high (86%).

The breakthrough curves obtained for both compounds in the first and in the fourth tests are shown in figure 5.4.

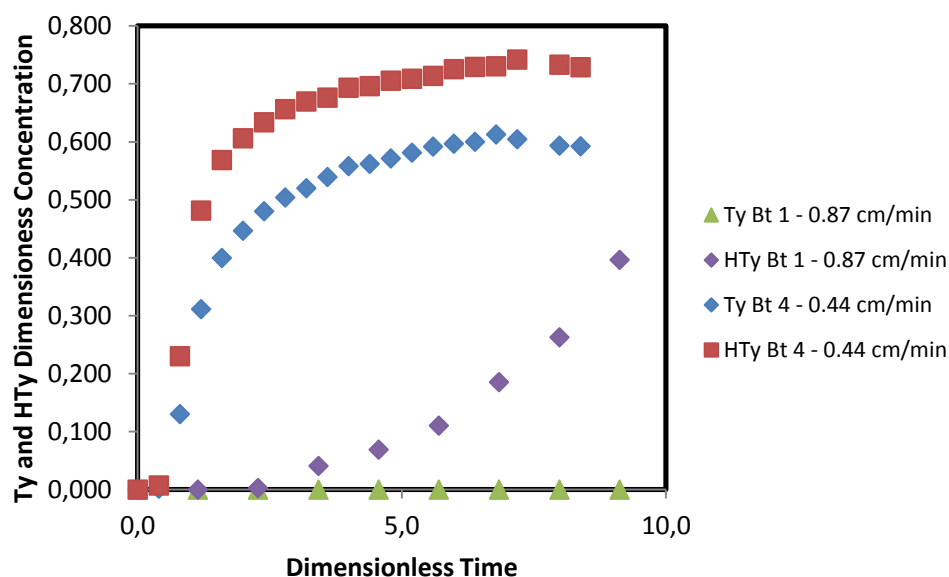


Figure 5.4 Tyrosol and hydroxytyrosol experimental breakthrough curves at 0.87 am/min and 0.44 cm/min (OMW Imperia 2014) for CDP.

The complete adsorption of tyrosol was observed also in the second test (0.87 cm/min), the tyrosol adsorption yield reduces from the third test (0.58cm/min – 86%) and was stable in the fourth cycle (86%). Also a reduction in the hydroxytyrosol was observed from 71% in the first test to 55% in the fourth one.

The decrease in the tyrosol and hydroxytyrosol adsorption yields could be due to the reduction in the number of available sites, which is normal because with the desorption less than the 100% of the molecules adsorbed are released. Also, this situation can be worsened by instability of the packed bed, one of the disadvantages of the dry-packing method is that the bed stability cannot be kept for a long term [60], however, because of the CDP very small particle size and because of the adsorption system hardware and its liquid flow settings it was not possible to use another packing method, for the industrial process this step could be enhanced using a more suitable hardware which can apply higher pressures that could pack better the polymer inside the column.

5.6 Desorption Solvent Selection: Batch tests

In order to find the most suitable solvent for the extraction of tyrosol and hydroxytyrosol, seven different organic solvents were tested, the results are presented in the table 5.2.

Solvent	% Des Ty	% Des HTy
Ethyl Acetate	63,54	59,33
Methanol	81,43	100,38
Methanol/ water 60%/40%	72,08	99,49
Acidified Water	41,43	51,08
Dicloromethane	20,53	0
MetOH/ Acid. Water (20%/80%)	81,97	62,44
ACN/ Acid. Water (15%/85%)	100	73,69

Table 5.2 Organic solvent tested in batch experiments for tyrosol and hydroxytyrosol desorption from CDP.

The acidified water contained 0.5% v/v of HCl 0.1N.

The pure methanol presented the best results. Good results were presented also for the mixtures methanol/acidified water (20%/80%) and acetonitrile/ acidified water (15%/85%), so, it was decided to build a solvent gradient with methanol, acetonitrile and acidified water.

Pure methanol and the solvent gradient were tested in the pilot plant. The description of the solvent gradient is in table 3.3 in chapter 3.

5.7 Desorption-regeneration tests for CDP

With pure methanol it was possible to recover the 92% and the 59% of the Ty and HTy adsorbed, respectively. At around 10 HTR no more desorption of these compounds was detected. An analysis of the desorbed product reveals that the 27% of it was composed by Ty (20%) and HTy (7%).

The desorption profiles are presented in figures 5.5a. and 5.5b.

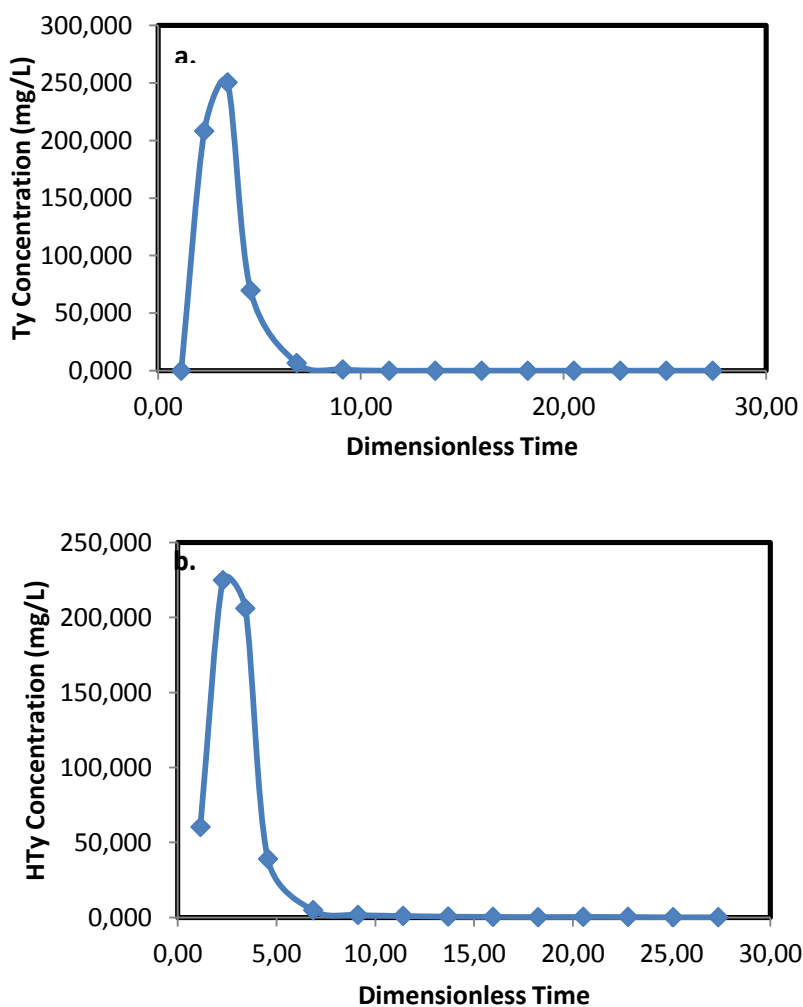


Figure 5.5 a). Tyrosol desorption profile using methanol as extraction solvent.

Figure 5.5 b). Hydroxytyrosol desorption profile using methanol as extraction solvent.

With the desorption with the solvent gradient, it was possible to recover the 90% and the 86% of the adsorbed TY and HTy, respectively. The desorption profiles are displayed in figures 5.6a. (Ty) and 5.6b. (HTy).

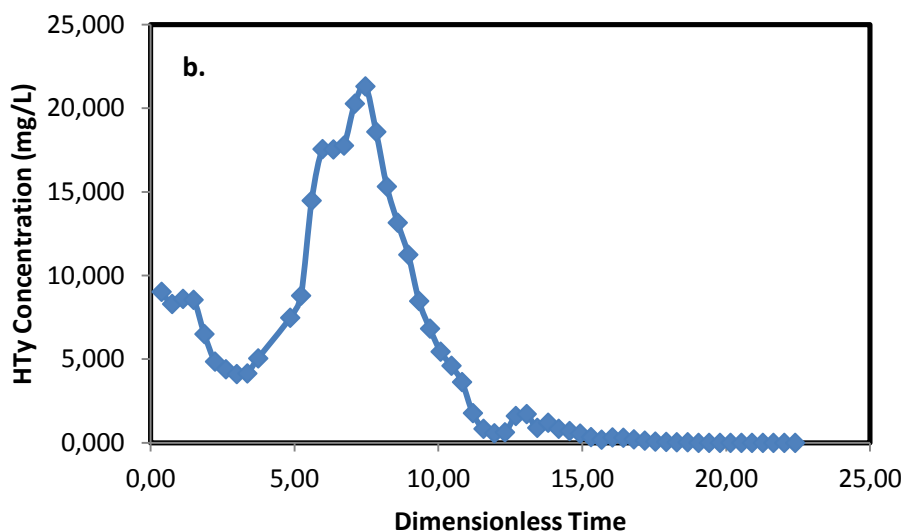
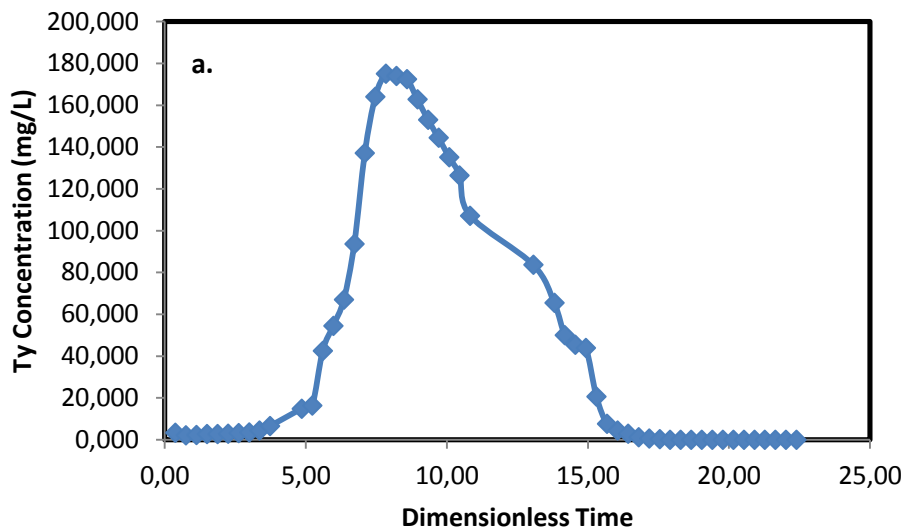


Figure 5.6 a). Tyrosol desorption profile using the organic solvent gradient as elution solvent.

Figure 5.6 b). Hydroxytyrosol desorption profile using the organic solvent gradient as elution solvent.

The desorption finishes at around 15 HTR, more than in the methanol case, but it was possible to recover almost the same percentage of Ty and to increase the

percentage of HTy desorbed. And according to the hplc analysis of the desorbed product, 61% is composed by Ty and 11% by HTy, so it was possible to have a final product that is composed mainly of Ty and HTy.

The approach of using a gradient solvent to desorb the target compounds could be very interesting but it is necessary to think about a separation method which lets the obtaining of the extracted product without the solvent mixture.

CHAPTER 6

CONCLUSIONS

The work performed with the different solid phases and the diverse adsorption systems leads to the following conclusions.

For the Recovery of Phenolics Mixtures:

- As first developments of this work, an effective OMW pre-treatment was settled and an analytical HPLC method more precise and less time-consuming than the traditional FC method was set up and validated.
- A good packing method was found for *Amberlite XAD 16*, the calculation of different parameters like the number of plates (N), the asymmetry factor (A_s) and the porosity of the bed, had demonstrated that the packing procedure is repeatable and leads to packed beds of good quality and high stability, enhancing the column performance, and letting the use of the same bed during several adsorption/desorption cycles.
- The experimental tests conducted with an adsorption bed of 0.52m, led to the development of a reliable model of the process, based on the assumption of non-equilibrium adsorption and characterized by an overall mass transfer resistance. The model parameters were estimated with a high accuracy and fitting quality. The model was utilized to estimate the process performances and to accomplish a preliminary evaluation of the optimal column length for a pilot plant. The column length estimated with the model (2.0m) was utilized successfully for the adsorption process optimization study and for a more robust assessment of the process performances.
- The non-equilibrium model with mass transfer resistance was suitable to interpret, fit and predict the experimental information obtained with the 2.0m column.
- The increase in the column length improve considerably the PCs adsorption yield, the resin utilization efficiency and the process productivity.

- The adsorption step was validated by means of a repeatability test, which demonstrated that this stages is reliable and stable.
- The repeatability of the desorption profiles shown that also this step is stable. However, further research is needed to optimize the desorption step, to evaluate the number of adsorption/desorption cycles that can be performed with the same resin, and to perform an overall and more robust economic optimization of the process.
- The continuous-flow PCs adsorption, desorption and recovery proposed process with the *Amberlite XAD 16* proved to be feasible, reliable and effective. Despite the high selectivity of this resin for PCs, the PCs purity in the finale product resulted < 30% as a result of the very low (phenolic COD / total COD) ratio of the tested OMW. However the non-phenolic COD presence, the product obtained has a very high antioxidant activity, which lets the use of the phenolic mixture in other fields, like the plastics production, where it can be used as surfactant. So the obtained product with interesting characteristics, so its economic value could increase.
- The preliminary cost analysis showed that the factor that is affecting considerably the process cost is the frequent change of the resin bed. So, two ion exchange resins were tested as alternative.
- Two ion exchange resins were tested in batch experiments for the PCs adsorption, as less expensive solid phases, and the *Amberlite IRA 958Cl* proved to have a good enough performance to be well worth testing in a breakthrough test experiment.
- With the selected *Amberlite IRA 958Cl* two breakthrough tests were performed at different liquid superficial velocities, the performances, in terms of resin bed utilization efficiency and PCs selectivity on COD, were just acceptable. So, for PCs recovery the *Amberlite XAD 16* is still the best option for this process, and even its cost the process is economically feasible.
- Another resins should be tested in order to find a good agreement between the solid phase price, and its performance, including the number on cycles that can be done with each resin load.

For the Recovery of Pure Polyphenols:

- The cyclodextrine based polyurethanes (CDP) demonstrated to be a promising approach for the selective recovery of target phenolic compounds from the OMW. It was possible the selective adsorption of tyrosol and hydroxytyrosol, two of the phenolic compounds with the highest added value for their interesting properties.
- A more suitable packing procedure should be found for the CDP bed in order to improve the performance of the column and the number of cycles that can be done with one CDP load.
- The desorption with a solvent gradient leads to the obtaining of a product that in a 72% is composed by tyrosol and hydroxytyrosol, so the product is of high interest and very high quality. However, the desorption step has to be studied deeply in order to find a suitable separation process that lets the obtaining of a Ty and HTy extract free of the solvent mixture, and maybe this process could give also the option to separate the solvents, so it would be possible to recover and re-utilize them in a next adsorption/desorption cycle.
- An economic analysis should be done to evaluate the CDP process feasibility, the solid phase is very expensive, but the product obtained is of very high quality, so the costs could be compensated, but the real possibilities of the process can be understood only with a costs study.
- Overall, this study represents an important step towards the development, modeling and preliminary optimization of a continuous flow adsorption/desorption process aimed at the separation of PCs mixtures or single PCs from OMW.

LIST OF SYMBOLS

A_s	Asymmetry factor (-)
$C_{L,i}$	Liquid phase concentration of compound i (mg/L)
$\bar{C}_{L,measured}$	Average liquid phase concentration measured during a given experiment (mg/L)
$C_{L,PCs,0}$	Initial and final (equilibrium) PCs concentration in the liquid phase (OMW) during the isotherm tests (mg _{PC} /L)
$C_{L,PCs,eq}$	
C_{resin}	Yearly cost for the periodic resin replacement (€/y)
$C_{S,i}$	Solid phase (resin) concentration of compound i (mg/ g _{dry resin})
$C_{S,PCs,eq}$	Final (equilibrium) PCs concentration in the solid phase (resin) during the isotherm tests (mg _{PC} /g _{dry resin})
D_{eq}	Equivalent diffusion coefficient, calculated as $\alpha_L \cdot v_{int}$
d_p	Average size of the packing particles (m)
$HETP$	Height equivalent to a theoretical plate, in the packed column (m)
HRT	Hydraulic residence time in the column, calculated as $V_{resin} \cdot \epsilon_{resin} / Q + V_{sand} \cdot \epsilon_{sand} / Q$ (s)
$K_{eq,i}$	Adsorption constant of compound i , defined as the slope of the linear portion of the isotherm (L _{pore volume} / kg _{dry resin}). A further subscript, if present, indicates the temperature.
$k_L a$	Mass transfer coefficient (1/s)
L	Column length (m)
$\dot{m}_{PCs,IN}$	PCs mass flow rate entering the column (mg/s)
$m_{PCs,sorbed,bt}$	PCs mass adsorbed by the resin at time t_{bt} (mg)
$m_{PCs,sorbed,sat}$	PCs mass theoretically adsorbed by the resin upon saturation of the

	sorption capacity (mg)
m_s	Mass of dry resin in the isotherm studies ($g_{\text{dry resin}}$)
N	Number of experimental data used to calculate each R^2 value (-)
n_{cycles}	Number of adsorption and desorption cycles that can be performed with one resin load (-)
N_{tp}	Number of theoretical plates in the column packing (-)
P	Number of parameters estimated in each model calibration (-)
Q	Volumetric flow rate through the column (m^3/s)
SC_{resin}	Resin specific cost ($\text{€}/\text{kg}$)
S_t	Column section (m^2)
t_{bt}	Breakthrough time (s)
t_R	Retention time of the RTD curve, in the fluid-dynamic tests (s)
t_{resin}	Resin operational time (s)
V_{sup}	Superficial velocity (m/s)
V_{int}	Interstitial velocity (m/s)
$W_{1/2}$	Width of the RTD curve at half-height, in the fluid-dynamic tests (s)
$Y_{\text{ads},i}$	Adsorption yield of compound i in a breakthrough test, calculated as $m_{i,\text{sorbed},20\%} / m_{i,\text{fed},20\%}$ (-)
α_L	Longitudinal dispersivity (m)
δ_i	Retardation factor \square_i , calculated as $1 + K_{\text{eq},i} \rho_b / \varepsilon$ (-)
ε	Effective porosity (-)
η_{resin}	Resin utilization efficiency, calculated as $m_{\text{PC},\text{sorbed},20\%} / m_{\text{PC},\text{sorbed},\text{sat}}$ (-)
ρ_b	Resin bulk density (kg/m^3)

INDEX OF TABLES

Table 1.1 Olive Oil Production in the year 2014/2015 [1].....	14
Table 1.2 Chemical Characteristics of the Olive Mill Wastewaters [16].....	25
Table 3.1 Technical characteristics of adsorption resin Amberlite XAD 16	60
Table 3.2 a). Technical characteristics of adsorption ionic resin Amberlite IRA 958CI	61
Table 3.2 b). Technical characteristics of adsorption ionic resin Amberlite IRA 67CI	61
Table 3.3 Flow rate ramp for HPLC method for VFA quantification.....	65
Table 3.4 Solvent gradient for Ty and HTy desorption.....	82
Table 3.5 Process assumptions for preliminary economic analysis.....	83
Table 4.1 PCs concentrations measured in two distinct OMWs with the Folin Ciocalteu colorimetric method and with the HPLC method: average values \pm 95% confidence intervals.....	86
Table 4.2 Main characteristics of the tested "Imperia 2012", "Imperia 2013", "Imperia 2014" and "Gallipoli 2012" OMW.....	88
Table 4.3 Comparison between the two column packing procedures evaluated...	94
Table 4.4 Porosity values obtained from fluid-dynamic test after each adsorption/desorption cycle during an adsorption repeatability test.....	95
Table 4.5 Longitudinal dispersivity values obtained for all the fluid dynamic tests performed for the Amberlite XAD 16 with 95% confidence interval.....	96

Table 4.6 Values of the mass transfer coefficient k_{La} obtained with the best fit of the experimental data using the non-equilibrium mass transfer model, at different liquid superficial velocities (OMW Imperia 2013).....	108
Table 4.7 Adsorption yields for PCS, COD and VFAs, PCs adsorption selectivities as yield ratio and PCs, COD and VFAs mass adsorbed for Amberlite XAD 16, Amberlite IRA 958Cl and Amberlite IRA 67Cl.....	121
Table 4.8 Fluid dynamic parameters comparison to evaluate column packing quality between Amberlite XAD 16 and Amberlite IRA 958Cl packed beds.....	126
Table 4.9 Bt 2, Bt 5, Bt 7 and Bt 8 adsorption and fluid dynamic parameters and process productivity comparison.....	129
Table 5.1 Fluid dynamic parameters for CDP packed bed.....	136
Table 5.2 Organic solvent tested in batch experiments for Tyrosol and Hydroxytyrosol desorption from CDP.....	138

INDEX OF FIGURES

Figure 1.1 Olive oil production with the two and three phases systems based on [6]	20
Figure 2.1 Isotherms shape classification according to <i>Brunauer, Deming, Deming and Teller</i> [49]	43
Figure 2.2 Adsorption breakthrough curve [54]	48
Figure 2.3 Response of a pulse injection test [61]	54
Figure 2.4 Response of a step injection test [61]	55
Figure 2.5 <i>E curve (for pulse or step injection) or C curve (for pulse injection)</i> analysis for packing quality and column efficiency testing. Modified from [64]	57
Figure 3.1 a). PCs adsorption system	66
Figure 3.1 b). Process flow diagram of the PCs adsorption system	67
Figure 3.2 a). "Laboratory-Phenols-Adsorption-Reactor" of SIMA-tec GmbH (Schwalmtal, Germany), for Ty and HTy adsorption (SIMA-tec)	68
Figure 3.2 b). Process flow diagram of the "Laboratory-Phenols-Adsorption-Reactor" of SIMA-tec GmbH (Schwalmtal, Germany), for Ty and HTy adsorption (SIMA-tec)	69
Figure 4.1 Dimensionless outlet PC concentration versus dimensionless time for breakthrough test n. 2 (30°C, 1.44m/h): comparison between the HPLC method and the Folin-Ciocalteu method	87
Figure 4.2 Adsorption Kinetics for the Amberlite XAD 16 and the OMW Imperia 2012	89

Figure 4.3 Adsorption isotherm for the system OMW Imperia 2012-Amberlite XAD 16 at 21°C and at 35°C.....	90
Figure 4.4 Adsorption isotherm for the system OMW Imperia 2013-Amberlite XAD 16 at 10°C and at 25°C.....	91
Figure 4.5 <i>F Curve</i> after column packing. Liquid superficial velocity of 5.03 cm/min	93
Figure 4.6 <i>E Curve</i> obtained by derivation of F curve. Liquid superficial velocity of 5.03 cm/min.....	94
Figure 4.7 Fluid-dynamic test at 2.04 cm/min. Experimental dimensionless NaCl concentration at the column exit and corresponding best-fitting simulation.....	96
Figure 4.8 Experimental Breakthrough Curves at 0.8 cm/min (Bt1) and 2.4 cm/min (Bt 2) with a 0.52 m length column.....	98
Figure 4.9 a.) Experimental Breakthrough Curve at 0.8 cm/min (Bt 1) and the respective Best Fit Curve obtained with the hypothesis of local equilibrium.....	99
Figure 4.9 b.) Experimental Breakthrough Curve at 2.4 cm/min (Bt 2) and the respective Best Fit Curve obtained with the hypothesis of local equilibrium.....	99
Figure 4.10 Experimental Breakthrough Curve at 0.8 cm/min (Bt 1) and the respective Best Fit Curve obtained with the hypothesis of non-negligible mass transfer resistance and Experimental Breakthrough Curve at 2.4 cm/min (Bt 2) and the respective Best Fit Curve obtained with the hypothesis of non-negligible mass transfer resistance.....	100
Figure 4.11 PCs adsorption yield and resin utilization efficiency at a 20% breakthrough point evaluated for columns of different lengths, using the best-fitting parameters estimated for Bt 2 (2.4 cm/min 30°C).....	102
Figure 4.12 Column length effect. Experimental Breakthrough curves at 0.52 m and 2.0 m with OMW Imperia 2012 and Imperia 2013.....	104

Figure 4.13 Liquid superficial velocity effect. Experimental Breakthrough curves at 2.2cm/min, 4.6 cm/min and 7.6 cm/min with OMW Imperia 2013.....	105
Figure 4.14 Repeatability test breakthrough curves at 5.0 cm/min approx. and 2.0m column length with OMW Imperia 2013.....	106
Figure 4.15 Experimental breakthrough curves with their respective simulation curves used for the calculation of the mass transfer coefficient (K_{La}) at different liquid superficial velocities.....	107
Figure 4.16 PCs and COD experimental breakthrough curves (4.6 cm/min, 2.0m column length, OMW imperia 2013) with their respective simulation curves.....	109
Figure 4.17 a). Experimental PCs and COD breakthrough curves for Bt 1 (0.8 cm/min, 0.5m column length, OMW Imperia 2012) and their respective simulation curves.....	111
Figure 4.17 b). Experimental PCs and COD breakthrough curves for Bt 2 (2.4cm/min, 0.5m column length, OMW Imperia 2012) and their respective simulation curves.....	111
Figure 4.18 Model-based evaluation of the PCs adsorption yield and PCs mass fraction in the adsorbate relative to test Bt 2 (2.4 cm/min, 30°C).....	112
Figure 4.19 Experimental desorption profile (0.43 cm/min approx. PCs from OMW Imperia 2013, desorption solvent: acidified ethanol 0.5%v/v HCl 0.1N).....	114
Figure 4.20 Experimental desorption profiles at 0.20 cm/min, 0.43 cm/min and 0,51 cm/min (PCs from OMW Imperia 2013, desorption solvent: acidified ethanol 0.5%v/v HCl 0.1N).....	115
Figure 4.21 Cake diagram of the contribution of each process factor in the total process cost for the preliminary economic evaluation.....	117
Figure 4.22 a.) Amberlite XAD 16, Amberlite IRA 958Cl and Amberlite IRA 67Cl PCS and COD adsorption yields at different pH and VFAs content.....	120

Figure 4.22 b). Amberlite XAD 16, Amberlite IRA 958CI and Amberlite IRA 67CI PCs adsorption selectivities respect to COD and VFAs.....	120
Figure 4.23 Adsorption isotherms for the systems OMW Imperia 2013-Amberlite XAD 16 at 25°C and OMW Imperia 2014-Amberlite IRA 958CI at 30°C.....	123
Figure 4.24 <i>F curves</i> before Bt 4, before Bt 7 and Bt 8 and after Bt 8 (repacked bed) with the simulation <i>F curve</i> of Bt 4.....	125
Figure 4.25 PCs experimental breakthrough curves for Amberlite XAD 16 (5.1 cm/min, 2.0m column length, OMW Imperia 2013) and Amberlite IRA 958CI (5.0 cm/min, 2.0m column length, OMW Imperia 2014).....	127
Figure 4.26 PCs and COD experimental breakthrough curves at 5.0 cm/min (2.0m column length OMW Imperia 2014) for Amberlite IRA 958CI).....	128
Figure 4.27 PCs and COD experimental breakthrough curves at 5.0 cm/min and 2.1 cm/min (2.0m column legth, OMW Imperia 2014) for Amberlite IRA 958CI.....	130
Figure 5.1 Adsorption Kinetics for the CDP and the OMW Imperia 2014.....	133
Figure 5.2 Adsorption isotherms for the systems Ty-CDP and HTy-CDP at 30°C (Ty and HTy from OMW Imperia 2014).....	134
Figure 5.3 <i>F curve</i> obtained for CDP packed bed before breakthrough tests.....	135
Figure 5.4 Tyrosol and hydroxytyrosol experimental breathrough curves at 0.87 am/min and 0.44 cm/min (OMW Imperia 2014) for CDP.....	137
Figure 5.5 a). Tyrosol desorption profile using methanol as extraction solvent.....	139
Figure 5.5 b). Hydroxytyrosol desorption profile using methanol as extraction solvent.....	139
Figure 5.6 a). Tyrosol desorption profile using the organic solvent gradient as elution solvent.....	140

Figure 5.6 b). Hydroxytyrosol desorption profile using the organic solvent gradient
as elution solvent.....140

BIBLIOGRAPHY

- [1] International Olive Council, 2015.
<http://www.internationaloliveoil.org/estaticos/view/131-world-olive-oil-figures>
(accessed on February 10, 2016).
- [2] D. Frascari, A.E. Molina Bacca, F. Zama, L. Bertin, F. Fava, D. Pinelli, Olive mill wastewater valorisation through phenolic compounds adsorption in a continuous column, Chemical Eng. Journal 283 (2016) 293-303.
- [3] D. Topi, I. Beqiraj, B. Seiti, E. Halimi, Environmental Impact from Olive Mills Waste Disposal, Chemical analysis of solid wastes and wastewaters, Journal of Hygienic Engineering and Design 7 (2014) 44-48.
- [4] European Comission, Environment, Urban Waste Water Directive Overview.
http://ec.europa.eu/environment/water/water-urbanwaste/index_en.html
(accessed on February 10 2016).
- [5] European Comission, Environment, Directive 2008/98/EC on waste (Waste Framework Directive). <http://ec.europa.eu/environment/waste/framework/>
(accessed on February 10 2016).
- [6] J. Tardáguila, F. Montero, M. Olmeda, J. Alba, R. Bernabéu, Análisis del Sector del Aceite de Oliva, Alimentación, Equipos y Tecnología (1996).
<http://www.ujaen.es/huesped/aceite/articulos/paper.htm> (Accessed on February 22 2016).
- [7] Obtención del Aceite de Oliva. <http://www.aceitedeoliva.com/aceite-de-oliva/obtencion-aceite-de-oliva/> (Accessed on February 25 2016).

- [8] Aceite de Oliva. Información y Noticias sobre el Aceite de Oliva. Elaboración del Aceite de Oliva. http://www.aceitedeoliva.net/elaboracion_del_aceite_de_oliva.php (Accessed on February 23 2016).
- [9] Aceite de Las Valdesas. Preguntas Frecuentes sobre el Aceite de Oliva. <http://www.aceitedelasvaldesas.com/preguntas-frecuentes/detalle/refinado> (Accessed on February 26 2016).
- [10] Interempresas. Industria del Aceite. Cómo producir aceite de oliva y aprovechar todo lo que genera. Comas. V. (2012) <http://www.interempresas.net/Produccion-Aceite/Articulos/101786-Como-producir-aceite-de-oliva-y-aprovechar-todo-lo-que-genera.html> (Accessed on February 26 2016).
- [11] J.A. Albuquerque, J. González, D. García, J. Cegarra, Agrochemical characterization of “alperujo”, a solid by-product of the two-phase centrifugation method for olive oil extraction, *Bioresource Technology* 91 (2004) 195-200.
- [12] A. Fernández-Hernández, A. Roig, N. Serraniá, C. García-Ortiz Civantos, M.A. Sánchez-Monedero, Application of compost of two-phase olive mill waste on olive grove: Effects on soil, olive fruit and olive oil quality, *Waste Management* 34 (2014) 1139-1147.
- [13] D. Hernández, L. Astudillo, M. Gutiérrez, C. Tenreiro, C. Retamal, C. Rojas, Biodiesel production from an industrial residue: Alperujo, *Industrial Crops and Products* 52 (2014) 495-498.

- [14] A. Lama-Muñoz, P. Álvarez-Mateos, G. Rodríguez-Gutiérrez, M. Montaña Durán-Barrantes, J. Fernández-Bolaños, Biodiesel production from olive-pomace oil of steam-treated alperujo, *Biomass and Bioenergy* 67 (2014) 443-450.
- [15] F. Rubio-Senent, G. Rodríguez-Gutiérrez, A. Lama-Muñoz, J. Fernández-Bolaños, Pectin extracted from thermally treated olive oil by-products: Characterization, physico-chemical properties, *in vitro* bile acid and glucose binding, *Food Hydrocolloids* 43 (2015) 311-321.
- [16] S. Dermeche, M. Nadour, C. Larroche, F. Moulti-Mati, P. Michaud, Olive mill wastes: biochemical characterizations and valorization strategies, *Process Biochem.* 48 (2013) 1532–1552.
- [17] A. Y. Gebreyohannes, R. Mazzei, L. Giomo, Trends and current practices of olive mill wastewater treatment: Application of integrated membrane process and its future perspective. Review. *Separation and Purification Technology* 162 (2016) 45-60.
- [18] V. Nogueira, I. Lopes, A.C. Freitas, T.A.P. Rocha-Santos, F. Goncalves, A.C. Duarte, R. Pereira, Biological treatment with fungi of olive mill wastewater pre-treated by photocatalytic oxidation with nanomaterials, *Ecotoxicology and Environmental Safety* 115 (2015) 234-242.
- [19] A.Y. Gebreyohannes, E. Curcio, T. Poerio, R. Mazzei, G. Di Profio, E. Drioli, L. Giorno, Treatment of Olive Mill Wastewater by Forward Osmosis, *Separation and Purification Technology* 147 (2015) 292-302.

- [20] A. Casanovas, A. Galvis, J. Llorca, Catalytic steam reforming of olive mill wastewater for hydrogen production, *International Journal of Hydrogen Energy* 40 (2015) 7539-7545.
- [21] S. Tosti, C. Cavezza, M. Fabbricino, L. Pontoni, V. Palma, C. Ruocco, Production of hydrogen in a Pd-membrane reactor via catalytic reforming of olive mill wastewater, *Chemical Engineering Journal* 275 (2015) 366-373.
- [22] F. Masi, R. Bresciani, G. Munz, L. Lubello, Evaporation-condensation of olive mill wastewater: Evaluation of condensate treatability through SBR and constructed Wetlands. *Ecological Engineering* 80 (2015) 156-161.
- [23] A. Scoma, F. Varela-Corredor, L. Bertin, C. Gostoli, S. Bandini, Recovery of VFAs from anaerobic digestion of dephenolized Olive Mill Wastewaters by Electrodialysis, *Separation and Purification Technology* 159 (2016) 81-91.
- [24] G.A. Martinez, L. Bertin, A. Scoma, S. Rebecchi, G. Braunegg, F. Fava, Production of polyhydroxyalkanoates from dephenolised and fermented olive mill wastewaters by employing a pure culture of *Cupriavidus necator*. *Biochem. Eng. J.* 97 (2015) 92-100.
- [25] K. Gerasopoulos, D. Stagos, S. Kokkas, K. Petrotos, D. Kantas, P. Goulas, D. Kouretas, Feed supplemented with byproducts from olive oil mill wastewater processing increases antioxidant capacity in broiler chickens, *Food and Chemical Toxicology* 82 (2015) 42-49.
- [26] NeoMundo (2010). Comer frutas es más saludable de lo que hasta ahora pensaban los nutricionistas.
<http://web.archive.org/web/20100912023642/espanol.news.yahoo.com/s/0809>

2010/93/comer-fruta-mas-saludable-ahora-pensaban.html (Accessed on March 10 2016).

- [27] P.S. Rodis, V. T. Karathanos, A. Mantzavinou, Partitioning of olive oil antioxidants between oil and water phases, *J. Agric. Food Chem.* 50 (2002) 596–601.
- [28] L. Bertin, F. Ferri, A. Scoma, L. Marchetti, F. Fava, Recovery of high added value natural polyphenols from actual olive mill wastewater through solid phase extraction, *Chem. Eng. J.* 171 (2011) 1287– 1293.
- [29] T. Yangui, S. Sayadi, A. Gargoubi, A. Dhouib, Fungicidal effect of hydroxytyrosol-rich preparations from olive mill wastewater against *Verticillium dahlia*, *Crop Protection* 29 (2010) 1208-1213.
- [30] L.C. Davies, A.M. Vilhena, J.M. Novais, S. Martins-Dias, Olive mill wastewater characteristics: modelling and statistical analysis, *Grasas Aceites* 55 (2004) 233-241.
- [31] F. Pouci, A. Scoma, G. Cirillo, L. Bertin, F. Fava, N. Picci, Selective extraction and purification of gallic acid from actual site olive mill wastewaters by means of molecularly imprinted microparticles, *Chemical Engineering Journal* 198-199 (2012) 529-535.
- [32] N. Kalogerakis, M. Politi, S. Foteinis, E. Chatzisyneon, D. Mantzavinos, Recovery of antioxidants from olive mill wastewaters: a viable solution that promotes their overall sustainable management, *J. Environ. Manage.* 128 (2013) 749-758.
- [33] L. Tuck, P.J. Hayball, Major phenolic compounds in olive oil: metabolism and health effects, *J. Nutr. Biochem.* 13 (2002) 636-644.

- [34] C. Fortes, J.A. García-Vilas, A.R. Quesada, M.A. Medina, Evaluation of the anti-angiogenic potential of hydroxytyrosol and tyrosol, two bio-active phenolic compounds of extra virgin olive oil, in endothelial cell cultures, *Food Chem.* 134 (2012) 134-140.
- [35] A. El-Abbassi, H. Kiai, J. Raiti, A. Hafidi, Application of ultrafiltration for olive processing wastewaters treatment, *J. Cleaner Prod.* 65 (2014) 432-438.
- [36] O. Gortzi, S. Lalas, A. Chatzilazarou, E. Katsoyannos, S. Papaconstandinou, E. Dourtoglou, Recovery of natural antioxidants from olive mill wastewater using Genapol-X080, *J. Am. Oil Chem. Soc.* 85 (2008) 133-140.
- [37] A. Agalias, P. Magiatis, A-L. Skaltsounis, E. Mikros, A. Tzarbopoulos, E. Gikas, I. Spanos, T. Manios, A new process for the management of olive oil mill waste water and recovery of natural antioxidants, *J. Agric. Food Chem.* 55 (2007) 2671-2676.
- [38] D. R. Kammerer, R. Carle, R.A. Stanley, Z.S. Saleh, Pilot-scale resin adsorption as a means to recover and fractionate apple polyphenols, *J. Agric. Food Chem.* 58 (2010) 6787–6796.
- [39] E. Miró-Casas, M.-I. Covas, M. Fitó, M. Farré-Albadalejo, J., Marrugat, R. De la Torre, Tyrosol and Hydroxytyrosol are absorbed from moderate and sustained doses of virgin olive oil in humans, *European Journal of Clinical Nutrition* 57 (2003) 186-190.
- [40] Fitoquímicos. <http://www.fitoquimicos.com/Hidroxitirosol.html> (Accessed on March 2 2016)

- [41] M.A.S. Alem, M.D.Y., Oteef., T. H. Flowers, L. J., Douglas, Production of Tyrosol by *Candida albicans* Biofilms and Its Role in Quorum Sensing and Biofilm Development, *Eukariotic Cell* (2006) 5 (10) 1770-1779.
- [42] F. Sannino, A. De Martino, R. Capasso, I. El Hadrami, Valorisation of organic matter in olive mill wastewaters: Recovery of highly pure hydroxytyrosol, *Journal of Geochemical Exploration* 129 (2013) 34-39.
- [43] Z. Kaleh, S.U. Geißen, Selective isolation of valuable biophenols from olive mill wastewater. *Journal of Environmental Chemical Engineering* 4 (2016) 373-384.
- [44] C. Michailof, P. Manesiotis, C. Panayiotou, Synthesis of caffeic acid and p-hydroxybenzoic acid molecularly imprinted polymers and their application for the selective extraction of polyphenols from olive mill waste waters, *Journal of Chromatography A*, 1182 (2008) 25-33.
- [45] R. E. Treybal,., *Operaciones de Transferencia de Masa*, second ed., McGrawHill, Mexico D.F. 1982.
- [46] R.G. Harrison, P. Todd, S. R. Rudge, D.P. Petrides, *Bioseparation Science and Engineering*, first ed., Oxford University Press, New York - Oxford 2003.
- [47] C.W. Fetter, *Applied Hydrogeology*, fourth ed., Prentice Hall, Upper Saddle River, New Jersey, 2001.
- [48] Adsorption Kinetics – The Rate of Adsorption. http://www.chem.qmul.ac.uk/surfaces/scc/scat2_3.htm (Accessed on November 13 2015).
- [49] Coulson & Richardson, *Chemical Engineering: Particle Technology and Separation Processes*, Vol. 2, fifth ed., Butterworth Heinemann, Bath 2002.

- [50] C.P. Bergmann & M. Jung de Andrade, *Nanostructured Materials for Engineering Applications*, Springer, Verlag Berlin Heidelberg 2011.
- [51] K. S. W. Sing, Adsorption methods for the characterization of porous materials, *Advances in Colloid and Interface Science* (1998) 76-77 3-11.
- [52] Pinelli, Davide. “Adsorbimento”, *Impianti Chimici-LT Chimica Industriale*, Università di Bologna. Lecture Notes.
- [53] Mass Transfer Zone and Breakthrough. http://www.separationprocesses.com/Adsorption/AD_Ch02c.htm (Accessed on November 5 2015).
- [54] Boi, Cristiana. “Teoria delle Separazioni Cromatografiche”, *Bioseparazioni*, Università di Bologna. Lecture Notes.
- [55] D.O. Cooney, *Adsorption Design for Wastewater Treatment*, Lewis Publishers, United States of America 1999.
- [56] W.L. McCabe, J.C. Smith, P. Harriott, *Unit Operations of Chemical Engineering*, sixth ed., McGraw-Hill, New Ork, 2001.
- [57] I. Bemberis, A. Noyes, V. Natarajan. Column Packing for Process-Scale Chromatography: Guidelines for Reproducibility. *BioPharm International* July 2003 23-30.
- [58] S. Millar 2012. *Tips and Tricks for the Lab: Column Packing* .Wiley-VCH Verlag GmbH & Co. KGaA. Weinheim. http://www.chemistryviews.org/details/education/2040151/Tips_and_Tricks_for_the_Lab_Column_Packing.html (Accessed on November 3 2015).
- [59] R.D. Davies, The dry-packing of columns in liquid chromatography, *Journal of High Resolution Chromatography* (1981) 4 270-275.

- [60] T. Braun & G. Ghersini, *Extraction Chromatography*, Elsevier Scientific Publishing Company (1975).
- [61] S.H. Fogler & M.N. Gürmen, *Elements of Chemical Reaction Engineering*, forth ed., Pearson, Michigan, 2008.
- [62] H.W. Blanch & D.S. Clark, *Biochemical Engineering*, second ed., Marcel Dekker, Inc., New York - Basel 1997.
- [63] A. Malavasi (2009). Comparison between two different chromatographic technologies (Undergraduate Thesis). University of Bologna, Bologna, Italy.
- [64] GE Healthcare Bio-Sciences AB, Column efficiency testing - Application note 28-9372-07 AA, Uppsala, Sweden, 2010.
https://www.gelifesciences.com/gehcls_images/GELS/Related%20Content/Files/1352880951136/litdoc28937207_20141127221416.pdf (accessed on May 20, 2015).
- [65] PALL Life Sciences. MEP HyperCel™ Mixed-Mode Chromatography Sorbent. Packing Protocol for Conventional Column From 9 cm to 45 cm I.D.
<http://www.pall.com/main/biopharmaceuticals/literature-library-details.page?id=20120215154709> (Accessed on December 2013).
- [66] A. Scoma, C. Pintucci, L. Bertin, P. Carlozzi, F. Fava, Increasing the large scale feasibility of a solid phase extraction procedure for the recovery of natural antioxidants from olive mill wastewaters, *Chem. Eng. J.* 198-199 (2012) 103–109.
- [67] O. Folin, V. Ciocalteu, On tyrosine and tryptofan determinations in protein, *J. Biol. Chem.* 73 (1927) 627–650.

- [68] M.F. Chaplin, Monosaccharides. In: Chaplin MF, Kennedy JF, editors. Carbohydrate analysis-a practical approach. 2nd ed, New York: Oxford University Press, Inc; 1994. 1–41.
- [69] C.S. Frings, T.W. Fendley, R.T. Dunn, C.A. Queen, Improved determination of total serum lipids by the sulfo-phospho-vanillin reaction, *Clinical Chem.* 18 (1972) 673–674.
- [70] M.M. Bradford, A rapid and sensitive method for the quantitation of microgram quantities of protein utilizing the principle of protein-dye binding, *Anal. Biochem.* 72 (1976) 248–254.
- [71] M. Ferri, A. Gianotti, A. Tassoni, Optimisation of assay conditions for the determination of antioxidant capacity and polyphenols in cereal food components, *J. Food Composition Analysis* 30 (2013) 94-101.
- [72] A.S. Rathore, R.M. Kennedy, J.K. O'Donnell, I. Bemberis, O. Kaltenbrunner, Qualification of a chromatographic column. Why and how to do it, *BioPharm International* 16 (2003) 30-40.
- [73] O. Levenspiel, *Chemical Reaction Engineering*, third ed., Wiley, New York, 1999.
- [74] P. Englezos, N. Kalogerakis, *Applied parameter estimation for chemical engineers*, Marcel Dekker, New York – Basel, 2001.
- [75] F. Zama, R. Ciavarelli, D. Frascari, D. Pinelli, Numerical parameter estimation in models of pollutant transport with chemical reaction, in: *IFIP Advances in Information and Communication Technology*, vol. 391, D. Homberg, F. Troltsch (Eds.), *System Modeling and Optimization*, Springer, Heidelberg, 2013, pp. 547 – 556.

- [76] T.J. Buran, A.K. Sandhu, Z. Li, C.R. Rock, W.W. Yang, L. Gu, Adsorption/desorption characteristics and separation of anthocyanins and polyphenols from blueberries using macroporous adsorbent resins, *J. Food Eng.* 128 (2014) 167–173.
- [77] M. Otero, M. Zabkova, A.E. Rodrigues, Phenolic wastewaters purification by thermal parametric pumping: modeling and pilot-scale experiments, *Water Res.* 39 (2005) 3467–3478.
- [78] J. Kim, M. Yoon, H. Yang, J. Jo, D. Han, Y.J. Jeon, S. Cho, Enrichment and purification of marine polyphenol phlorotannins using macroporous adsorption resins, *Food Chem.* 162 (2014) 135–142.
- [79] K. Chen, H. Lyu, S. Hao, G. Luo, S. Zhang, J. Chen, Separation of phenolic compounds with modified adsorption resin from aqueous phase products of hydrothermal liquefaction of rice straw, *Biores. Technol.* 182 (2015) 160–168.
- [80] Y. Liu, Q. Bai, Y. Liu, D. Di, M. Guo, L. Zhao, J. Li, Simultaneous purification of tea polyphenols and caffeine from discarded green tea by macroporous adsorption resins, *Eur. Food Res. Technol.* (2014) 238:59–69.
- [81] D. Frascari, S. Fraraccio, M. Nocentini, D. Pinelli, Trichloroethylene aerobic cometabolism by suspended and immobilized butane-growing microbial consortia: a kinetic study. *Biores. Technol.* 1244 (2013) 529-538.
- [82] X. Wang, P.D. Patil, C. He, J. Huang, Y.N. Liu, Acetamide-modified hyper-cross-linked resin: synthesis, characterization, and adsorption performance to phenol from aqueous solution. *J. Appl. Polym. Sci.* 132 (2015) 4197.
- [83] Integratori e Coadiuvanti: ricerca prezzi integratori alimentare duocist. http://www.trovaprezzi.it/prezzo_integratori-

[coadiuvanti integratore alimentare duocist.aspx](#) (Accessed on September 15 2015).

- [84] H. Ritter, Superstructures with cyclodextrins: Chemistry and applications. *Journal of Organic Chemistry* 8 (2012) 1303-1304.
- [85] American Chemistry Council. Introduction to Polyurethanes. <https://polyurethane.americanchemistry.com/Introduction-to-Polyurethanes> (Accessed on March 11 2016).
- [86] M.I. Gil, F.A. Tomás-Barberán, B. Hess-Pierce, D. M. Holcroft, A.A. Kader, Antioxidant Activity of Pomegranate Juice and Its Relationship with Phenolic Composition and Processing. *J. Agric. Food Chem.* 48 (2000) 4581-4589.